



National Library
of Canada

Bibliothèque nationale
du Canada

Canadian Theses Service

Service des thèses canadiennes

Ottawa, Canada
K1A 0N4

NOTICE

The quality of this microform is heavily dependent upon the quality of the original thesis submitted for microfilming. Every effort has been made to ensure the highest quality of reproduction possible.

If pages are missing, contact the university which granted the degree.

Some pages may have indistinct print especially if the original pages were typed with a poor typewriter ribbon or if the university sent us an inferior photocopy.

Reproduction in full or in part of this microform is governed by the Canadian Copyright Act, R.S.C. 1970, c. C-30, and subsequent amendments.

AVIS

La qualité de cette microforme dépend grandement de la qualité de la thèse soumise au microfilmage. Nous avons tout fait pour assurer une qualité supérieure de reproduction.

S'il manque des pages, veuillez communiquer avec l'université qui a conféré le grade.

La qualité d'impression de certaines pages peut laisser à désirer, surtout si les pages originales ont été dactylographiées à l'aide d'un ruban usé ou si l'université nous a fait parvenir une photocopie de qualité inférieure.

La reproduction, même partielle, de cette microforme est soumise à la Loi canadienne sur le droit d'auteur, SRC 1970, c. C-30, et ses amendements subséquents.

UNIVERSITY OF ALBERTA
TOPOGRAPHIC DE-PHASING AND AMPLITUDE MODULATION
OF ROSSBY WAVE TRIAD PACKETS



BY
WARREN CREE

A THESIS
SUBMITTED TO THE FACULTY OF GRADUATE STUDIES AND RESEARCH
IN PARTIAL FULFILMENT OF THE REQUIREMENTS FOR THE DEGREE
OF MASTER OF SCIENCE
IN
METEOROLOGY

DEPARTMENT OF GEOGRAPHY

EDMONTON, ALBERTA

SPRING 1990



National Library
of Canada

Bibliothèque nationale
du Canada

Canadian Theses Service

Service des thèses canadiennes

Ottawa, Canada
K1A 0N4

NOTICE

The quality of this microform is heavily dependent upon the quality of the original thesis submitted for microfilming. Every effort has been made to ensure the highest quality of reproduction possible.

If pages are missing, contact the university which granted the degree.

Some pages may have indistinct print especially if the original pages were typed with a poor typewriter ribbon or if the university sent us an inferior photocopy.

Reproduction in full or in part of this microform is governed by the Canadian Copyright Act, R.S.C. 1970, c. C-30, and subsequent amendments.

AVIS

La qualité de cette microforme dépend grandement de la qualité de la thèse soumise au microfilmage. Nous avons tout fait pour assurer une qualité supérieure de reproduction.

S'il manque des pages, veuillez communiquer avec l'université qui a conféré le grade.

La qualité d'impression de certaines pages peut laisser à désirer, surtout si les pages originales ont été dactylographiées à l'aide d'un ruban usé ou si l'université nous a fait parvenir une photocopie de qualité inférieure.

La reproduction, même partielle, de cette microforme est soumise à la Loi canadienne sur le droit d'auteur, SRC 1970, c. C-30, et ses amendements subséquents.

ISBN 0-315-60270-8

micro.

UNIVERSITY OF ALBERTA

RELEASE FORM

Name of Author Warren Cree
TITLE OF THESIS Topographic De-phasing and Amplitude Modulation of Rossby
 Wave Triad Packets
DEGREE FOR WHICH THESIS WAS PRESENTED Master of Science
YEAR OF DEGREE GRANTED SPRING, 1990

Permission is hereby granted to the UNIVERSITY OF ALBERTA LIBRARY to reproduce single copies of this thesis and to lend or sell such copies for private, scholarly or scientific research purposes only.

The author reserves other publication rights, and neither the thesis nor extensive extracts from it may be printed or otherwise reproduced without the author's written permission.

(Signed) Warren Cree

Permanent Address:

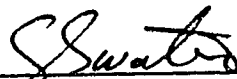
6315 - 129 Street
Edmonton, Alberta, Canada
T6H 3X9

DATED December 1, 1989

THE UNIVERSITY OF ALBERTA
FACULTY OF GRADUATE STUDIES AND RESEARCH

The undersigned certify that they have read, and recommend to the Faculty of Graduate Studies and Research, for acceptance, a thesis entitled Topographic De-Phasing and Amplitude Modulation of Rossby Wave Triad Packets submitted by Warren Cree in partial fulfilment of the requirements for the degree of Master of Science in Meteorology.

G. Swaters



Supervisor

R.B. Charlton



E.R. Reinelt



Date October 27, 1989

ABSTRACT

A theory is developed to describe the topographic de-phasing and amplitude modulation of Rossby wave triads. The model equations are derived via a formal asymptotic expansion in which the topographic gradients have the same assumed small order of magnitude as the non-linear advective interaction terms in the quasi-geostrophic potential vorticity equation. For piecewise linear topographic configurations the perturbed steady-state interaction equations may be solved exactly. The theory developed in this thesis demonstrates that, in the presence of topographic forcing, the nonlinear triad interactions induces a permanent zonal wave number mismatch in the sense that the wave resonance conditions are no longer completely satisfied. The size of this mismatch is dependent on the initial amplitudes, wavelengths and frequencies of the individual Rossby wave packets and the magnitude of the topographic slope. The permanent zonal wave number mismatch that is created will mean that even after the Rossby wave packets have traversed a topographic feature of finite horizontal extent, the energy exchange between the wave packets is no longer maximized. This process is examined in this thesis for different topographic configurations.

ACKNOWLEDGEMENTS

The author would like to thank Dr. G.E. Swaters for his initiation of this project, his detailed review of this work and for his many constructive comments throughout this project. Preparation of this thesis was supported in part by a Science Subvention from the Atmospheric Environment Service of Canada and an Operating Grant from the Natural Sciences and Engineering Research Council of Canada awarded to Dr. G.E. Swaters.

TABLE OF CONTENTS

CHAPTER	PAGE
1. Introduction	1
2. Derivation of the Governing Equations	9
2.1 Derivation of the Quasigeostrophic Potential Vorticity Equation	9
2.2 Derivation of the Amplitude Equations	16
2.3 Conversion of the Amplitude Equations to Standard Form ..	21
3. Conservation Theorems	22
3.1 Conservation of Energy	22
3.2 Conservation of Enstrophy	25
3.3 The Manley-Rowe Relations	26
4. Solutions to the Amplitude Equations	27
4.1 The Pump-Wave Approximation	27
4.2 Solutions Using the Method of Inverse Scattering.	30
4.3. The Steady State Solution in the Absence of Topography and Friction	32
4.4 The Steady State Solution in the Presence of Linear Topography	34
5. Results of the Theory	39
5.1 Calculation of Wave Numbers	39
5.2 Rossby Wave Triad over Piecewise Linear Topographic Configurations	46
5.3 Solutions to the Rossby Wave Triad over Piecewise Symmetric Linear Topographic Configurations	50
5.4 Solutions to the Rossby Wave Triad over non-Symmetric Piecewise Linear Topographic Configurations ...	94
6. Conclusions	105
Bibliography	108
Appendix 1: Derivation of Equation (2.2.15)	111
Appendix 2: Proof of (3.1.10a)	112
Appendix 3: Proof of (4.4.10)	113
Appendix 4: Fortran Program	114

LIST OF TABLES

	PAGE
Table 1. Wave numbers which form a resonant triad	41
Table 2. Wave numbers which form a resonant triad.	42

LIST OF FIGURES

		PAGE
Figure 1.	Geometry of the inviscid shallow-water model.	11
Figure 2.	Cross section of the piecewise linear topographic configuration used in this thesis.	47
Figure 3.	Plot of b_j versus X for initial amplitudes (5.3.2) and topography given by (5.2.1) and (5.3.1) with $H_0 = 0.0$. . .	56
Figure 4.	Plots for initial amplitudes (5.3.2) and topography given by (5.2.1) and (5.3.1) with $H_0 = 10.0$.	
	(A) b_j versus X	57
	(B) Φ versus X	58
	(C) Phase 2 Derivative versus X	59
	(D) Phase 2 versus X	60
	(E) $b_j \cos(\text{phase } 2)$ versus X	61
Figure 5.	Plots for initial amplitudes (5.3.2) and topography given by (5.2.1) and (5.3.1) with $H_0 = 30.0$.	
	(A) b_j versus X	62
	(B) Φ versus X	63
	(C) Phase 2 Derivative versus X	64
	(D) Phase 2 versus X	65
	(E) $b_j \cos(\text{phase } 2)$ versus X	66
Figure 6.	Plots for initial amplitudes (5.3.2) and topography given by (5.2.1) and (5.3.1) with $H_0 = 50.0$.	
	(A) b_j versus X	67
	(B) Φ versus X	68
	(C) Phase 2 Derivative versus X	69
	(D) Phase 2 versus X	70
	(E) $b_j \cos(\text{phase } 2)$ versus X	71
Figure 7.	Plot of b_j versus X for initial amplitudes (5.3.3) and topography given by (5.2.1) and (5.3.1) with $H_0 = 0.0$. . .	72
Figure 8.	Plots for initial amplitudes (5.3.3) and topography given by (5.2.1) and (5.3.1) with $H_0 = 10.0$.	
	(A) b_j versus X	73
	(B) Φ versus X	74
	(C) Phase 2 Derivative versus X	75
	(D) Phase 2 versus X	76
	(E) $b_j \cos(\text{phase } 2)$ versus X	77

Figure 9.	Plots for initial amplitudes (5.3.3) and topography given by (5.2.1) and (5.3.1) with $H_0 = 50.0$.	
(A)	b_j versus X .	78
(B)	Φ versus X .	79
(C)	Phase 2 Derivative versus X .	80
(D)	Phase 2 versus X .	81
(E)	$b_j \cos(\text{phase } 2)$ versus X .	82
Figure 10.	Plot of b_j versus X for initial amplitudes (5.3.4) and topography given by (5.2.1) and (5.3.1) with $H_0 = 0.0$.	83
Figure 11.	Plots for initial amplitudes (5.3.4) and topography given by (5.2.1) and (5.3.1) with $H_0 = 10.0$.	
(A)	b_j versus X .	84
(B)	Φ versus X .	85
(C)	Phase 2 Derivative versus X .	86
(D)	Phase 2 versus X .	87
(E)	$b_j \cos(\text{phase } 2)$ versus X .	88
Figure 12.	Plots for initial amplitudes (5.3.4) and topography given by (5.2.1) and (5.3.1) with $H_0 = 50.0$.	
(A)	b_j versus X .	89
(B)	Φ versus X .	90
(C)	Phase 2 Derivative versus X .	91
(D)	Phase 2 versus X .	92
(E)	$b_j \cos(\text{phase } 2)$ versus X .	93
Figure 13.	Plots for initial amplitudes (5.3.2) and topography given by (5.2.1) and (5.4.1) with $H_0 = 10.0$.	
(A)	b_j versus X .	95
(B)	Φ versus X .	96
(C)	Phase 2 Derivative versus X .	97
(D)	Phase 2 versus X .	98
(E)	$b_j \cos(\text{phase } 2)$ versus X .	99
Figure 14.	Plots for initial amplitudes (5.3.2) and topography given by (5.4.2) and (5.4.3) with $H_0 = 10.0$.	
(A)	b_j versus X .	100
(B)	Φ versus X .	101
(C)	Phase 2 Derivative versus X .	102
(D)	Phase 2 versus X .	103
(E)	$b_j \cos(\text{phase } 2)$ versus X .	104

CHAPTER 1

INTRODUCTION

The north-south undulations of the upper flows, known as ridges and troughs, constitute the planetary or long waves which typically have a meridional amplitude ranging from 45 to 90 degrees of latitude, and have a vertical wave length of roughly the depth of the troposphere. The planetary waves are known as Rossby waves after C.G. Rossby who first discussed their origin in a barotropic atmosphere (Rossby, 1939). Rossby waves owe their existence to the meridional gradient in the radially-outward component of the planetary angular frequency vector which acts as a restoring force when fluid parcels are meridionally displaced from their mean position (Rossby, 1939).

Time averaged maps of the atmosphere at various pressure levels, where the averaging time is many years, show certain characteristic features such as well defined troughs and ridges. These features must be of a stationary nature, otherwise they would be lost in the averaging process. These maps are often used to represent the stationary flow of the atmosphere. Synoptic experience has shown that the atmosphere has other structural entities which are of shorter duration, but which are also quasi-stationary in nature, and have a timespan exceeding that of a travelling disturbance.

Many of these quasi-stationary disturbances are seasonally dependent, such as the monsoon circulation. These structures can be seen on time-averaged maps for the month or season in which they occur, because they are more closely associated with a season than the general circulation in an annual sense.

On still a shorter time scale, it is observed that the atmosphere, from time to time, creates features which have a typical structure, and exist for a certain period in essentially an unchanged form.

Perhaps one of the most interesting and noticeable short-term features is the formation of "blocks". In the Northern Hemisphere, atmospheric blocking is a large-amplitude synoptic-scale phenomenon embedded in the westerlies, that

diminishes or retards the predominantly zonal flow in a limited sector of the hemisphere. The westerlies are split into two distinct meridional flows, one heading southward and the other northward, thus the predominantly zonal flow is "blocked".

An extensive climatology of blocking was carried out by Rex (1950), who provided a detailed description of blocking from a synoptic point of view, as well as an analysis of the climatological aspects of blocking. The definition of blocking provided by Rex (1950) is that blocking must exhibit the following characteristics:

1. The basic current in the upper atmosphere must be split into two streams.
2. Each stream must transport an appreciable mass.
3. The double stream system must extend over 45 degrees of latitude.
4. A sharp transition from zonal to meridional flow must exist in the region of the split.
5. The pattern must persist with recognizable continuity for at least ten days.

Austin (1980) provided a less stringent definition of the blocking phenomenon. A distinction between the synoptician's point of view and that of the theoretical meteorologists is made. The first view is that blocking is a spatially isolated phenomenon consisting of a stationary high pressure cell, cold in the stratosphere and warm in the troposphere, persisting in a region where westerly winds are normally found. The persistence requirement is substantially longer than three days. Austin (1980) also stated that blocking is any stationary wave of large amplitude, meaning that blocking is also seen as a global phenomenon.

A split in the two streams is not made part of the definition, but it is nevertheless mentioned that it occurs particularly in cases where the high pressure cell is at sixty degrees north, and is located to the north of a low pressure cell at forty degrees north. Both these definitions recognize the connection between the split of the two streams upstream and the location of the high pressure cell downstream.

On the basis of these definitions, statistical analyses of blocking have led to three preferred geographical areas where blocking frequently occurs in the northern hemisphere: over the eastern North Atlantic, extending to the southeast of Greenland; over the northern Soviet Union, extending northeast to the Arctic Ocean; over the north Pacific, extending to south of the Aleutians (Austin, 1908; Rex, 1950; Dole and Gordon, 1983). Blocking in the southern hemisphere is less well documented, but it is not infrequent (Trenberth and Mo, 1985). Van Loon (1956) found that sometimes two or three "blocks" may occur simultaneously in the southern hemisphere. By contrast double or triple "blocks" are rare and short lived in the northern hemisphere. A review of blocking in the northern hemisphere is given by Knox (1982).

The effects of blocking on the regional weather are quite dramatic. For example, Atlantic blocking strongly affects the weather in Europe. Below the high pressure ridge, the precipitation is below normal, while above normal precipitation is observed over the east-central Atlantic, and over the two belts over Scandinavia and the Mediterranean under the jet streams.

In 1959 a blocking high formed in late January and persisted into late fall, with only a few short interruptions. Central Europe suffered a severe drought in that summer. In the fall of 1960 a blocking high persisted over northern Europe. Rainfall along the west coast of Norway was less than half of the normal amount, and many coastal stations had the driest autumn on record (Chang, 1972).

In January 1977 the extremely cold winter in the continental interior, and unusually warm temperatures on the west coast of North America, were due to a persistent high pressure ridge over Alaska (Miyakoda et al., 1983).

Blocking can occur in two distinct patterns. The first is a ridge pattern which diverts the mean westerlies northward. The second pattern is a dipole block which takes the form of a meridionally aligned vortex pair with the anti-cyclone north of the cyclone.

The reasons for the development and maintenance of blocking patterns has been debated for over 50 years, and a satisfactory theoretical explanation is still

missing. A good theory must describe the features in the definitions put forth by Rex (1950) and Austin (1980), i.e., the splitting of the two streams upstream of the high, the persistence of the pattern, the preference for certain localities in the Atlantic and Pacific, and the strong seasonal dependence.

Many theories have been proposed to explain the formation and persistence of "blocks". The connection between quasi-stationary blocking ridges, and the forcing due to the earth's topography and surface thermal contrasts, and whether blocking is a regional or global phenomenon, has yet to be understood.

A review of present blocking theories is given by Benzi et al. (1986). Regional theories have centered around work by McWilliams (1980) who suggested that atmospheric blocks could be produced by internal dynamics alone, due to a balance between nonlinear and dispersive effects.

Warn and Brasnett (1983) showed that for baroclinic waves in a shear flow interacting with topography, the quasi-geostrophic potential vorticity equation can be reduced to a non-homogeneous Korteweg-deVries equation, and that Rossby solitons could be simultaneously amplified and stalled by topography, a process they interpret as a transition to a regional blocking configuration.

Pierrehumbert and Malguzzi (1984) showed that a high amplitude equilibrium state could be maintained by a local nonlinear resonance phenomenon. Synoptic observations supporting the regional theory of blocking has been provided by Dole and Gordon (1983).

On a global scale, much interest has been generated by the work of Charney and DeVore (1979) and Hart (1979), which suggested that for given forcing parameters, multiple steady states of the zonal mean wind and planetary wave amplitude were possible, due to orographically induced instability in the barotropic model. Charney and DeVore's (1979) results were obtained by means of barotropic quasi-geostrophic nonlinear spectral models truncated to a few harmonics to allow analytical treatment. Other work has illustrated similar possibilities in baroclinic models (e.g. Pedlosky, 1981; Charney and Strauss, 1980).

In these models, one stable steady state corresponds to a relatively strong zonal flow, while another corresponds to a weak zonal flow, and a wave pattern characteristic of blocking. Charney and DeVore (1979) identified an equilibrium solution, one with a large amplitude perturbation of the zonal flow, which is locked near resonance by the nonlinearity with a blocking configuration. Blocking may be considered as the product of resonant forcing and nonlinearity.

Tung and Lindzen (1979) suggested that linear resonance in response to topographic forcing is responsible for rapid growth of long planetary waves observed both in blocking and with stratospheric warmings. In the case of a zonal wind having realistic vertical shear, Tung and Lindzen (1979) focused on the vertical profiles of the zonal wind and the resonant wave amplitude at equilibrium, but no resonant growth rates were calculated.

Nonlinear mechanisms have also been used to try to explain blocking. Perhaps the first was proposed by Rossby (1950) who recognized that blocking action follows the split of the jet stream in time, and suggested that blocking can be explained at least partly by comparing it with a hydraulic jump. He derived some criteria for the onset of blocking.

Rossby's theory was found to be far from satisfactory by (Benzi et al., 1986; Egger, 1978), because the stationary character of the flow in a blocking high makes it unlikely that the violent, turbulent motion in a hydraulic jump can serve as an analogue for the blocking high. More recently Egger (1978, 1979) presented numerical experiments in which block-like patterns are obtained as a result of nonlinear interactions (triad resonance) between orographically forced standing waves (with wave numbers different from the linearly resonant values), and free slowly moving waves. Many of Egger's (1978) arguments are highly heuristic since he neglected to account for the nonlinear interaction of members of the triad with other modes, and how the development of one member of the triad will influence the other members.

An extension of the Charney and DeVore (1979) idea to a barotropic model including wave-wave interaction by Benzi et al. (1986), shows that the presence

of the wave-wave interaction causes the orographically forced wave amplitude resonance in Charney and DeVore's (1979) model to become a "folded" resonance in which, for a given value of the zonal wind, more than one stable planetary scale wave amplitude is possible. It appears probable that a block as a nonlinear yet global phenomenon perhaps depends on a wave-wave interaction, rather than interaction between waves and the zonal current.

The nonlinear interactions between Rossby waves, by which the velocity field of one wave advects the vorticity field of another, and leads to a nonlinear coupling and energy transfer between the waves, are of interest for at least two reasons (Longuet-Higgins and Gill, 1967):

1. With Rossby waves in the atmosphere, and possibly the ocean, the ratio of the particle velocity to the phase velocity (which is an index of the nonlinearity) may be appreciable.
2. Resonant interactions between planetary waves take place at the second order and not only at third order, as in surface gravity waves.

Therefore the interactions are of dynamically greater importance.

Longuet-Higgins and Gill (1967) determined the geometrical conditions for two waves to form a resonant triplet with a given third wave. They also showed conservation of energy and enstrophy for a resonant triad in the absence of any forcing. In addition they showed solutions to the amplitude equations in the absence of forcing. It was also noted by Longuet-Higgins and Gill that if the waves are truly discrete, then due to the vanishing of the coupling coefficient, the triad resonance mechanism cannot be responsible for exciting zonal flows, and that the zonal flow merely acts as a catalyst for energy exchange between the other two members of the triad.

Newell (1969) showed that it is possible for waves neighboring the resonant waves to excite zonal flows on a longer time scale. It was also shown that a single Rossby wave packet can exchange energy with the zonal flow in the presence of a weak shear.

Loesch (Part 1: 1974) considered resonant interactions between a marginally unstable wave and a pair of baroclinic waves in a quasi-geostrophic, inviscid, two layer model on the beta plane. It was shown that, when the vertical shear slightly exceeds the minimum critical value required for instability, the finite amplitude state exhibits a long period oscillation of the amplitudes of the three waves which form the resonant triad. Energy is continuously being exchanged between the wave field and the mean field, and among triad members.

In Loesch (Part 2: 1974) an examination of the energy exchange between the triad in Loesch (Part 1), for different values of the internal rotational Froude number was examined. Pedlosky (1970, 1979) and Drazin (1970) investigated the weakly finite amplitude evolution of slowly growing modes in a baroclinic model. They concentrated on the evolution of a particular unstable linear eigenmode, as it is circumscribed by weak non-linear effects.

Meacham (1988) demonstrated another type of a weakly nonlinear model in which there appears a different version of the baroclinic instability mechanism. His model investigated the evolution of a triad of neutral Rossby waves of weak amplitude in a vertically sheared flow. He showed that nonlinear interactions between the waves produced slight phase shifts that enabled the modified waves to generate non-zero heat fluxes, and so exchange energy with the mean flow. He further showed that there exists some triads for which the net effect of the heat fluxes is an extraction of energy from the mean flow by the triad. As a consequence the triad grows. In general this growth is faster than exponential.

Investigations of triad resonance have so far dealt only with the study of wave-wave and wave-mean-flow interaction. The study of triad resonance under the influence of some type of forcing, eg., thermal or topographic, has yet to be investigated. It is clear from previous studies listed above, that there may be some interesting differences between resonant triads under the influence of forcing and their counterparts, which are not under the influence of forcing. A simple environment in which to observe the dynamics of resonant triads is a barotropic model.

The principal objective of this thesis is to examine the effects of topography on resonantly interacting Rossby wave triads in a barotropic model. The topography is assumed to be the same small order of magnitude as the nonlinear Jacobian terms in the quasi-geostrophic potential vorticity equation.

The outline of this thesis is as follows: In Chapter 2, we review the derivation of the quasi-geostrophic potential vorticity equation for a barotropic, homogeneous, incompressible atmosphere on a beta plane, including friction and topography. We then proceed to develop the equations which will describe the evolution of the wave amplitudes, and finally we convert those equations to standard form.

In Chapter 3, we show that in the absence of friction, the equations governing the evolution of the amplitudes conserve both energy and enstrophy. In addition we show that in the absence of friction, the equations conserve three other quantities which are expressed by the Manley-Rowe relations. In Chapter 4, we present solutions to the equations which describe the evolution of the wave triads. We begin by looking at the "pump-wave approximation" which describes the situation in which one of the three wave packets in the triad has an initially large amplitude relative to the other two. We then give a brief discussion and show how the general initial value problem may be treated by the method of inverse scattering. Finally, we show how solutions to the steady state problem may be solved in terms of Jacobi elliptic functions. In Chapter 5 we derive wave numbers which form a resonant triad, and for piecewise linear topographic configurations, we illustrate the full analytical solution. In Chapter 6 the thesis is summarized and conclusions are presented.

CHAPTER 2.

DERIVATION OF THE GOVERNING EQUATIONS

2.1 Derivation of the Quasigeostrophic Potential Vorticity Equation

To focus attention on the resonant interaction problem, we reduce the model of the atmosphere to a simple form. In fact we assume that it can be modelled as a barotropic incompressible fluid on an infinite β -plane, in the presence of Ekman dissipation and bottom topography. Therefore, the governing non-dimensional equations of motion are the shallow water equations given in the form (Pedlosky, 1987)

$$R_0[u_t + uu_x + vv_y + ww_z] - (1 + R_0\beta y)v = -P_x + \frac{E}{2}u_{zz}, \quad (2.1.1a)$$

$$R_0[v_t + uv_x + vv_y + ww_z] + (1 + R_0\beta y)u = -P_y + \frac{E}{2}v_{zz}, \quad (2.1.1b)$$

$$\delta^2 R_0[w_t + uw_x + vw_y + ww_z] = -P_z + \frac{\delta^2 E}{2}w_{zz}, \quad (2.1.1c)$$

$$u_x + v_y + w_z = 0, \quad (2.1.1d)$$

while the boundary conditions on the tropopause are

$$\left. \begin{array}{l} \text{kinematic } w = R_0 F[\eta_t + u\eta_x + v\eta_y] \\ \text{dynamic } P = \eta \end{array} \right\} \text{ at } z = 1 + R_0 F\eta(x, y, t) \quad (2.1.1e)$$

and the boundary conditions on the earths surface are

$$w = R_0[u\eta_{B_x} + v\eta_{B_y}] + R_0 w_E \text{ at } z = R_0 \eta_B(x, y) \quad (2.1.1f)$$

where w_E is the nondimensional vertical velocity associated with an Ekman boundary layer. The topography is assumed to be $O(R_0)$ Pedlosky (1987).

Nondimensional (unprimed) variables are introduced as follows

$$\left. \begin{aligned}
 (x, y) &= (x', y')/L, \\
 z &= z'/D, \\
 (u, v) &= (u', v')/U, \\
 w &= (L/D)w'/U, \\
 t &= (U/L)t', \\
 \eta &= \eta'/N_0 \text{ where } N_0 = \frac{fUL}{g}, \\
 p'(x', y', z', t') &= -\rho g(z' - H) + (fUL\rho)p(x, y, z, t), \\
 \eta_B(x, y) &= R_0 D h'_B(x', y'), \\
 w_E(x, y, t) &= (R_0 L/DU)w'_E(x', y', t').
 \end{aligned} \right\} \quad (2.1.2)$$

We demand that the scales L , U , N_0 characterize the magnitudes of length, velocity and free surface elevation respectively. Several nondimensional parameters are introduced, viz:

$$\left. \begin{aligned}
 R_0 &= U/fL, \text{ the Rossby number,} \\
 E &= 2\nu/fD^2, \text{ the Ekman number,} \\
 \beta &= \beta' L^2/U, \text{ the planetary vorticity factor,} \\
 F &= f^2 L^2/gD, \text{ the external rotational Froude number,} \\
 \delta &= D/L, \text{ the aspect ratio.}
 \end{aligned} \right\} \quad (2.1.3)$$

Equations (2.1.1a), (2.1.1b) and (2.1.1c) are the zonal, meridional and vertical nondimensional momentum equations respectively; (2.1.1d) is the nondimensional continuity equation. Subscripts t, x, y, z denote partial derivatives. The parameters f, ν, g , are respectively the Coriolis parameter, the eddy viscosity and the acceleration due to gravity. η is the departure of the free surface from its level, rest height, and η_B is the measure of bottom variation which produces a scale departure $R_0 D$, the depth of the resting fluid, from the constant value D (see Fig. 1 for geometry of the flow). The parameters R_0, E and δ are assumed to be small with respect to unity while β and F are taken to be $O(1)$. As long as

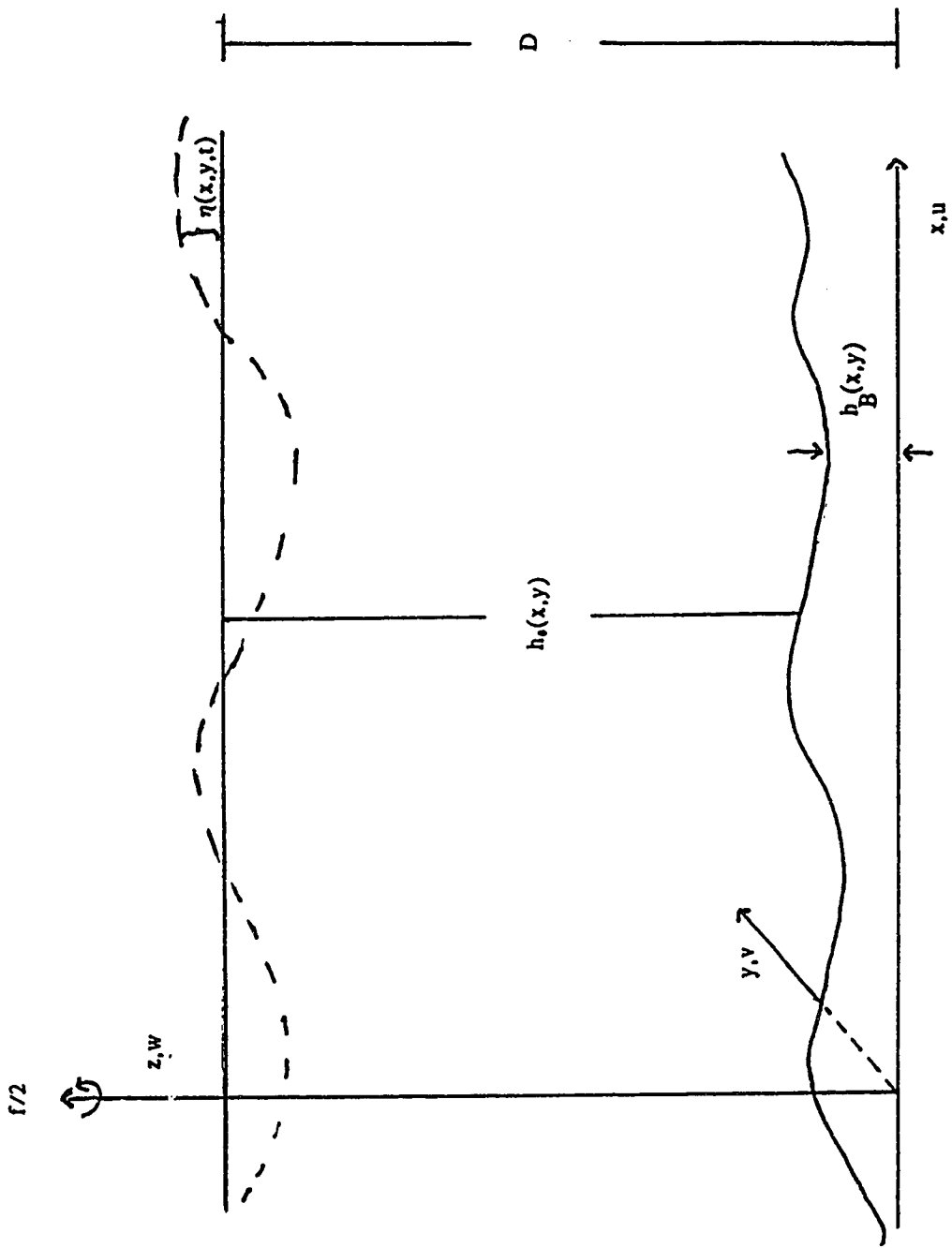


Fig. 1. Geometry of the inviscid shallow-water model.

$R_0 > O(E^{1/2})$, an asymptotic expansion of the dependent variables in powers of R_0 is appropriate (Pedlosky, 1987)

$$\left. \begin{aligned} u &\sim u^{(0)} + R_0 u^{(1)} + \dots, \\ v &\sim v^{(0)} + R_0 v^{(1)} + \dots, \\ w &\sim R_0 w^{(0)} + \dots, \\ \eta &\sim \eta^{(0)} + R_0 \eta^{(1)} + \dots, \\ P &\sim P^{(0)} + R_0 P^{(1)} + \dots, \\ w_E &\sim w_E^{(0)} + \dots \end{aligned} \right\} \quad (2.1.4)$$

From this it follows, after substitution of (2.1.4) into (2.1.1), that to $O(1)$

$$v^{(0)} = P_z^{(0)}, \quad (2.1.5a)$$

$$u^{(0)} = -P_y^{(0)}, \quad (2.1.5b)$$

$$P_z^{(0)} = 0, \quad (2.1.5c)$$

$$u_x^{(0)} + v_y^{(0)} = 0 \quad (2.1.5d)$$

with the $O(1)$ Taylor expanded boundary conditions

$$\left. \begin{aligned} P^{(0)} &= \eta^{(0)} \\ w^{(0)} &= F[\eta_t^{(0)} + u^{(0)}\eta_x^{(0)} + v^{(0)}\eta_y^{(0)}] \end{aligned} \right\} \quad (2.1.6)$$

at $z = 1$, and

$$w^{(0)} = u^{(0)}\eta_{Bx} + v^{(0)}\eta_{By} + w_E^{(0)} \quad (2.1.7)$$

at $z = 0$. It follows from the hydrostatic relation and the dynamic boundary condition on the tropopause that

$$p^{(0)} = \eta^{(0)} \quad (2.1.8)$$

everywhere in the atmosphere. Since $\eta^{(0)}$ is independent of z the geostrophic relations will imply that $u^{(0)}$ and $v^{(0)}$ are independent of height. Any solution which satisfies (2.1.5a) and (2.1.5b) also satisfies the momentum equation (2.1.5d),

therefore the $O(1)$ approximation simply does not contain enough information to complete the dynamical determination of the motion. This situation is referred to as geostrophic degeneracy. It is clear that the resolution of this difficulty will require the consideration of higher-order dynamics. To $O(R_0)$ the momentum and continuity equations are

$$u_t^{(0)} + u^{(0)}u_x^{(0)} + v^{(0)}u_y^{(0)} - v^{(1)} - \beta y v^{(0)} = -P_x^{(1)}, \quad (2.1.9a)$$

$$v_t^{(0)} + u^{(0)}v_x^{(0)} + v^{(0)}v_y^{(0)} + u^{(1)} + \beta y u^{(0)} = -P_y^{(1)}, \quad (2.1.9b)$$

$$u_x^{(1)} + v_y^{(1)} + w_z^{(0)} = 0. \quad (2.1.9c)$$

We do not need to examine the $O(R_0)$ boundary conditions. Differentiating (2.1.9a) and (2.1.9b) with respect to y and x respectively, and subtracting yields the vorticity equation

$$\zeta_t^{(0)} + u^{(0)}\zeta_x^{(0)} + v^{(0)}\zeta_y^{(0)} + \beta v^{(0)} = -(u_x^{(1)} + v_y^{(1)}), \quad (2.1.10)$$

where

$$\zeta^{(0)} = v_x^{(0)} - u_y^{(0)}. \quad (2.1.11)$$

Substitution of the geostrophic relations and the $O(R_0)$ continuity equation gives

$$[\partial_t - \eta_y^{(0)}\partial_x + \eta_x^{(0)}\partial_y][\Delta\eta^{(0)} + \beta y] = w_z^{(0)}, \quad (2.1.12)$$

where Δ is the horizontal Laplace operator defined by $\Delta \equiv \partial^2/\partial x^2 + \partial^2/\partial y^2$. We now integrate (2.1.12) with respect to z from $z = 0$ to $z = 1$ recalling that $\eta^{(0)}$ is independent of z

$$[\partial_t - \eta_y^{(0)}\partial_x + \eta_x^{(0)}\partial_y][\Delta\eta^{(0)} + \beta y] = w^{(0)}(x, y, 1, t) - w^{(0)}(x, y, 0, t). \quad (2.1.13)$$

Substituting the $O(1)$ boundary conditions on $w^{(0)}$ yields

$$[\partial_t - \eta_y^{(0)}\partial_x + \eta_x^{(0)}\partial_y][\Delta\eta^{(0)} - F\eta^{(0)} + \beta y + \eta_B] = -w_E^{(0)}. \quad (2.1.14)$$

Pedlosky (1987) has shown that

$$w_E^{(0)} = \frac{E^{1/2}}{2R_0} \Delta \eta^{(0)}. \quad (2.1.15)$$

Using (2.1.15), the vorticity equation (2.1.14) may be written as

$$[\partial_t + \psi_x \partial_y - \psi_y \partial_x][\Delta \psi - F\psi + \beta y + \eta_B] = -r \Delta \psi, \quad (2.1.16)$$

where we have defined

$$\left. \begin{aligned} \psi &= \eta^{(0)}, \\ r &= \frac{E^{1/2}}{2R_0}. \end{aligned} \right\} \quad (2.1.17)$$

The parameter r measures the strength of the Ekman pumping on the lower boundaries. Viscous effects at the interface have, for the sake of simplicity in presentation only, been ignored and would only affect the quantitative details of the subsequent results (Pedlosky, 1987).

The terms in (2.1.16) are defined as follows (Pedlosky, 1987)

$\Delta \psi$, geostrophic relative vorticity

$F\psi$, gravitationally induced or (free surface) relative vorticity

βy , planetary vorticity

η_B , vortex tube stretching due to topography.

In order to focus attention on weakly nonlinear dynamics we set

$$\left. \begin{aligned} \psi &= \varepsilon \psi, \\ \eta_B &= \varepsilon \eta_B, \\ r &= \varepsilon r, \end{aligned} \right\} \quad (2.1.18)$$

where ε is a nondimensional wave amplitude parameter which will form the correct inverse space time scaling for resonant interactions and ε satisfies $0 < \varepsilon \ll 1$.

We substitute (2.1.18) into (2.1.16) and rewrite (2.1.16) in its final form as

$$(\Delta - 1)\psi_t + \psi_x = -\varepsilon J(\psi, \Delta \psi) - \varepsilon J(\psi, \eta_B) - \varepsilon r \Delta \psi. \quad (2.1.19)$$

In (2.1.19) we choose the scaling length L , otherwise free to be the Rossby deformation radius (R_*) for the layer of depth D , so that $F = 1$. The Rossby radius of deformation is the distance over which the gravitational tendency to render the free surface flat is balanced by the tendency of the Coriolis acceleration to deform the surface. Typical synoptic scales for L might be 1000 km thus giving time scales $t = \frac{1}{R_*}\beta$, of approximately 1 day. With this scaling $U = \beta R_*^2$ thus $\beta = 1$.

2.2 Derivation of the Amplitude Equations

In this section we take (2.1.19) and derive equations which describe the evolution of the amplitudes of a resonant triad. We begin by setting

$$\eta_B = \varepsilon^{-1} \int_0^{\varepsilon x} \gamma(x') dx', \quad (2.2.1)$$

and substituting into (2.1.19).

The governing equation simplifies to

$$(\Delta - 1)\psi_t + \psi_x = -\varepsilon J(\psi, \Delta\psi) + \varepsilon\gamma(\varepsilon x)\psi_y - \varepsilon r\Delta\psi. \quad (2.2.2)$$

We define slow time and space variables as:

$$\left. \begin{aligned} T &= \varepsilon t \\ X &= \varepsilon x. \end{aligned} \right\} \quad (2.2.3)$$

The introduction of (2.2.3) permits us to restrict our discussion to the slow time and length scales over which the amplitude of the wave field gradually changes and the topography is large scale, i.e., the topography changes slowly in spatial variables (Pedlosky, 1987), consistently with the magnitude of the nonlinear terms.

According to multiple-scale theory (Bender and Orszag, 1978), the fast and slow variables can be formally treated as independent variables. Thus the stream function is explicitly written in the form

$$\psi = \psi(x, y, t; X, T). \quad (2.2.4)$$

Derivatives are given by the usual chain rule

$$\left. \begin{aligned} \partial_t &= \partial_t + \varepsilon\partial_T, \\ \partial_x &= \partial_x + \varepsilon\partial_X, \\ \partial_y &= \partial_y. \end{aligned} \right\} \quad (2.2.5)$$

In terms of these variables, the governing equation (2.2.2) can be written in the form

$$Q\psi = -\varepsilon J(\psi, \Delta\psi) - \varepsilon \Delta\psi_T - 2\varepsilon\psi_{txX} + \varepsilon\psi_T - \varepsilon\psi_X + \varepsilon\gamma(X)\psi_y - \varepsilon r\Delta\psi + O(\varepsilon^2). \quad (2.2.6)$$

Where Q is the operator

$$Q = (\Delta - 1)\partial_t + \partial_x. \quad (2.2.7)$$

Since ε is a small parameter we may assume an expansion of the dependent variable ψ of the form

$$\psi = \psi^{(0)} + \varepsilon\psi^{(1)} + \dots \quad (2.2.8)$$

The $O(1)$ problem which results from inserting (2.2.8) into (2.2.6) is the linear equation

$$Q\psi^{(0)} = 0. \quad (2.2.9)$$

Following (Benny and Newell, 1967; Pedlosky, 1987; Bender and Orszay, 1978) we may begin by considering as our basic solution to (2.2.9) a linear superposition of three wave packets of the form

$$\psi^{(0)} = \sum_{j=1}^3 A_j(\bar{X}, T) \exp(i\theta_j) + c.c., \quad (2.2.10)$$

where the amplitudes A_j are slowly varying functions of position and time and $\theta_j = k_j x + \ell_j y - \omega_j t$, and (c.c.) denotes complex conjugate. Substitution of (2.2.10) into (2.2.9) yields the local dispersion relation given by

$$\omega_j(k_j^2 + \ell_j^2 + 1) = -k_j, \quad (2.2.11)$$

where j is cycled over (1, 2, 3). Longuet-Higgins and Gill (1967) investigated the interaction of these discrete waves and noted that because of the existence of resonance conditions, energy can be transferred from one component to another.

In order for resonance to occur the three waves must satisfy (without loss of generality)

$$\theta_1 + \theta_2 + \theta_3 = 0, \quad (2.2.12)$$

so that there must exist classes of triads such that

$$\left. \begin{aligned} k_1 + k_2 + k_3 &= 0, \\ \ell_1 + \ell_2 + \ell_3 &= 0, \\ \omega_1(k_1, \ell_1) + \omega_2(k_2, \ell_2) + \omega_3(k_3, \ell_3) &= 0 \end{aligned} \right\} \quad (2.2.13)$$

are satisfied simultaneously.

The existence of such triads was first pointed out by Kenyon (1964) and later, in greater detail by Longuet-Higgins and Gill (1967). The $O(\varepsilon)$ problem which results from inserting (2.2.8) into (2.2.6) is:

$$\begin{aligned} Q\psi^{(1)} = & -J(\psi^{(0)}, \Delta\psi^{(0)}) - \Delta\psi_T^{(0)} + \psi_T^0 - 2\psi_{tzX}^{(0)} \\ & - \psi_X^{(0)} + \gamma(X)\psi_y^{(0)} - r\Delta\psi^{(0)}, \end{aligned} \quad (2.2.14)$$

which may be solved using the putative solution (2.2.10). The problem for $\psi^{(1)}$ is

$$\begin{aligned} Q\psi^{(1)} = & \sum_{j=1}^3 [(k_j^2 + \ell_j^2 + 1)A_{jT} + (-2k_j\omega_j - 1)A_{jX} + iA_j\ell_j\gamma(X) + A_jr(k_j^2 + \ell_j^2)] \exp(i\theta_j) \\ & + \sum_{n=1}^3 \sum_{m=1}^3 A_n^* A_m^* [z \cdot (\underline{K}_m \times \underline{K}_n) (\underline{K}_m \cdot \underline{K}_m - \underline{K}_n \cdot \underline{K}_n)] \exp(-i\theta_n - i\theta_m) \\ & + \text{nonresonant terms} + c.c. \end{aligned} \quad (2.2.15)$$

where $\underline{K}_n = (k_n, \ell_n)$ and (j, m, n) is cycled over $(1, 2, 3)$. The asterisk (*) has been used to denote the complex conjugate. A complete derivation of (2.2.15) is given in Appendix 1.

We may further simplify (2.2.15) by writing it as

$$\begin{aligned}
Q\psi^{(1)} = & \sum_{j=1}^3 (k_j^2 + \ell_j^2 + 1) \left[(\partial_t + c_j \partial_X) A_j + \frac{i A_j \ell_j \gamma(X)}{(k_j^2 + \ell_j^2 + 1)} \right. \\
& \left. + \frac{A_j r(k_j^2 + \ell_j^2)}{(k_j^2 + \ell_j^2 + 1)} \right] \exp(i\theta_j) \\
& + \sum_{n=1}^3 \sum_{m=1}^3 A_n^* A_m^* [z \cdot (\underline{K}_m \times \underline{K}_n) (\underline{K}_m \cdot \underline{K}_m - \underline{K}_n \cdot \underline{K}_n)] \exp(-i\theta_n - i\theta_m) \\
& + \text{c.c.} + \text{nonresonant terms}, \tag{2.2.16}
\end{aligned}$$

where

$$c_j = \partial\omega_j / \partial k_j = \frac{k_j^2 - \ell_j^2 - 1}{(k_j^2 + \ell_j^2 + 1)^2}, \tag{2.2.17}$$

is the group velocity of the j th wave (Pedlosky, 1987). We note that (2.2.18) tells us that two waves of either the same wave length ($\underline{K}_m^2 = \underline{K}_n^2$) or parallel wave vectors ($\underline{K}_m \times \underline{K}_n = 0$) will not interact, for their interaction coefficient is zero. The first case corresponds to a situation where the vorticity of the sum of the pair is a constant multiple of the sum of their stream functions, so that the Jacobian of the two wave fields identically vanishes, while the second situation corresponds to parallel motion in a single direction, for which the nonlinear advection term in (2.2.14) is also zero (Pedlosky, 1987).

We shall ignore the nonresonant terms because as we shall show in Chapter 3, the energy transfer between the nonresonant terms is so feeble and slow compared to the resonant exchange that, to the lowest order, the resonant interaction is energy preserving.

In order to preclude the appearance of secular terms in the solution for $\psi^{(1)}$ (Bender and Orszag, 1978) we require that

$$(\partial_T + c_1 \partial_X) A_1 = -B_1 A_2^* A_3^* - \frac{il_1 \gamma(X) A_1}{k_1^2 + \ell_1^2 + 1} - \frac{r(k_1^2 + \ell_1^2) A_1}{k_1^2 + \ell_1^2 + 1}, \tag{2.2.18a}$$

$$(\partial_T + c_2 \partial_X) A_2 = -B_2 A_3^* A_1^* - \frac{il_2 \gamma(X) A_2}{k_2^2 + \ell_2^2 + 1} - \frac{r(k_2^2 + \ell_2^2) A_2}{k_2^2 + \ell_2^2 + 1}, \tag{2.2.18b}$$

$$(\partial_T + c_3 \partial_X) A_3 = -B_3 A_1^* A_2^* - \frac{il_3 \gamma(X) A_3}{k_3^2 + \ell_3^2 + 1} - \frac{r(k_3^2 + \ell_3^2) A_3}{k_3^2 + \ell_3^2 + 1}. \tag{2.2.18c}$$

where

$$\begin{aligned}
 B_1 &= \frac{z \cdot (\underline{K}_2 \times \underline{K}_3)(\underline{K}_2 \cdot \underline{K}_2 - \underline{K}_3 \cdot \underline{K}_3)}{(k_1^2 + \ell_1^2 + 1)}, \\
 B_2 &= \frac{z \cdot (\underline{K}_3 \times \underline{K}_1)(\underline{K}_3 \cdot \underline{K}_3 - \underline{K}_1 \cdot \underline{K}_1)}{(k_2^2 + \ell_2^2 + 1)}, \\
 B_3 &= \frac{z \cdot (\underline{K}_1 \times \underline{K}_2)(\underline{K}_1 \cdot \underline{K}_1 - \underline{K}_2 \cdot \underline{K}_2)}{(k_3^2 + \ell_3^2 + 1)},
 \end{aligned}$$

are the interaction coefficients. It is important to realize that because of the resonance conditions (2.2.12) $\theta_j = -\theta_n - \theta_m$ whenever n and m are different from j and each other. It is this property that gives rise to the appearance of the nonlinear wave-wave interaction terms in (2.2.18).

2.3 Conversion of the Amplitude Equations to Standard Form

The equations of the resonant triad (2.2.18) may be rewritten in the form

$$D_1 A_1 = -B_1 A_2^* A_3^* - i\mu_1 \gamma(X) A_1 - \sigma_1 A_1, \quad (2.3.1a)$$

$$D_2 A_2 = -B_2 A_3^* A_1^* - i\mu_2 \gamma(X) A_2 - \sigma_2 A_2, \quad (2.3.1b)$$

$$D_3 A_3 = -B_3 A_1^* A_2^* - i\mu_3 \gamma(X) A_3 - \sigma_3 A_3, \quad (2.3.1c)$$

where

$$\left. \begin{aligned} \mu_j &= \frac{\ell_j}{k_j^2 + \ell_j^2 + 1}, \\ \sigma_j &= \frac{r(k_j^2 + \ell_j^2)}{k_j^2 + \ell_j^2 + 1}, \\ D_j &= \partial_T + c_j \partial_X. \end{aligned} \right\} \quad (2.3.2)$$

If we set

$$\left. \begin{aligned} \alpha_1(X, T) &= A_1(X, T) \exp\left[i \int \frac{\mu_1 \gamma(X)}{c_1} dX\right], \\ \alpha_2(X, T) &= A_2(X, T) \exp\left[i \int \frac{\mu_2 \gamma(X)}{c_2} dX\right], \\ \alpha_3(X, T) &= A_3(X, T) \exp\left[i \int \frac{\mu_3 \gamma(X)}{c_3} dX\right], \end{aligned} \right\} \quad (2.3.3)$$

and substitute into (2.3.1), we get the following equations of the resonant triad in standard form

$$D_1 \alpha_1 = -B_1 \alpha_2^* \alpha_3^* \exp\left[i \int \mu_0 \gamma(X) dX\right] - \sigma_1 \alpha_1, \quad (2.3.4a)$$

$$D_2 \alpha_2 = -B_2 \alpha_3^* \alpha_1^* \exp\left[i \int \mu_0 \gamma(X) dX\right] - \sigma_2 \alpha_2, \quad (2.3.4b)$$

$$D_3 \alpha_3 = -B_3 \alpha_1^* \alpha_2^* \exp\left[i \int \mu_0 \gamma(X) dX\right] - \sigma_3 \alpha_3, \quad (2.3.4c)$$

where

$$\mu_0 = \mu_1/c_1 + \mu_2/c_2 + \mu_3/c_3. \quad (2.3.5)$$

CHAPTER 3

CONSERVATION THEOREMS

3.1 Conservation of Energy

If we ignore friction, we may show that the energy of the resonant triad is conserved even though energy is transferred between the waves. We start with the full dynamical equation (2.2.2), with the friction terms set to zero, which may be written as

$$\Delta\psi_t - \psi_t + \psi_x + \varepsilon\psi_x\Delta\psi_y - \varepsilon\psi_y\Delta\psi_x - \varepsilon\gamma(\varepsilon x)\psi_y = 0. \quad (3.1.1)$$

Multiplying (3.1.1) by ψ , and adding

$$\partial_t(\psi_x\psi_x) + \partial_t(\psi_y\psi_y)$$

to the left and right sides, and rearranging terms gives

$$\begin{aligned} & \partial_t(1/2(\psi_x)^2 + 1/2(\psi_y)^2 + 1/2\psi^2) \\ &= \partial_x(\psi\psi_{xt} + 1/2\psi^2 - \varepsilon\psi\psi_y\Delta\psi) \\ &+ \partial_y(\psi\psi_{yt} + \varepsilon\psi\psi_x\Delta\psi - 1/2\varepsilon\gamma(\varepsilon x)\psi^2). \end{aligned} \quad (3.1.3)$$

If we integrate (3.1.3) over a large area the right hand side becomes an integral along the boundary, which increases like the linear dimension L . The left hand side, however, increases like L^2 (Longuet-Higgins and Gill). If the amplitude of ψ is bounded it follows that

$$\int \int (1/2(\psi_x)^2 + 1/2(\psi_y)^2 + 1/2\psi^2) dx dy = \text{constant}. \quad (3.1.4)$$

The first two terms in (3.1.4) represent the kinetic energy density, and the third term represents the potential energy, both in nondimensional form.

It is evident that for a plane-wave type solution, (2.2.10) the average densities of kinetic and potential energy are equal to

$$\left. \begin{aligned} & \frac{(k^2 + \ell^2)A^2}{4}, \\ & \frac{A^2}{4} \end{aligned} \right\} \quad (3.1.5)$$

respectively.

For short planetary waves, $((k^2 + \ell^2)^{1/2} > 1)$ (3.1.5) tells us that kinetic energy exceeds potential energy whereas for long planetary waves the potential energy exceeds kinetic energy.

Using (3.1.5), the wave energy for each member of the resonant triad is

$$E_j = (k_j^2 + \ell_j^2 + 1) \frac{A_j^2}{4}, \quad (3.1.6)$$

where j is cycled over $(1, 2, 3)$.

The equations of the resonant triad (2.2.18), with the friction terms set to zero, may be written as

$$D_1(k_1^2 + \ell_1^2 + 1)A_1 = -B(\underline{K}_2, \underline{K}_3)(\underline{K}_2^2 - \underline{K}_3^2)A_2^*A_3^* - i\ell_1\gamma(X)A_1, \quad (3.1.7a)$$

$$D_2(k_2^2 + \ell_2^2 + 1)A_2 = -B(\underline{K}_3, \underline{K}_1)(\underline{K}_3^2 - \underline{K}_1^2)A_3^*A_1^* - i\ell_2\gamma(X)A_2, \quad (3.1.7b)$$

$$D_3(k_3^2 + \ell_3^2 + 1)A_3 = -B(\underline{K}_1, \underline{K}_2)(\underline{K}_1^2 - \underline{K}_2^2)A_1^*A_2^* - i\ell_3\gamma(X)A_3, \quad (3.1.7c)$$

where

$$\left. \begin{aligned} D_j &= (\partial_T + c_j \partial_X), \\ B(\underline{K}_m, \underline{K}_n) &= z \cdot (\underline{K}_m \times \underline{K}_n), \\ \text{and } \underline{K}_n &= (k_n, \ell_n). \end{aligned} \right\} \quad (3.1.8)$$

Multiplying (3.1.7) with A_1^*, A_2^*, A_3^* respectively gives

$$\begin{aligned} D_1(k_1^2 + \ell_1^2 + 1)|A_1|^2 &= -B(\underline{K}_2, \underline{K}_3)(\underline{K}_2^2 - \underline{K}_3^2)A_1^*A_2^*A_3^* \\ &\quad - B(\underline{K}_2, \underline{K}_3)(\underline{K}_2^2 - \underline{K}_3^2)A_1A_2A_3 \\ &\quad - \gamma(X)_i\ell_1A_1A_1^* + \gamma(X)_i\ell_1A_1A_1^*, \end{aligned} \quad (3.1.9a)$$

$$\begin{aligned} D_2(k_2^2 + \ell_2^2 + 1)|A_2|^2 &= -B(\underline{K}_3, \underline{K}_1)(\underline{K}_3^2 - \underline{K}_1^2)A_1^*A_2^*A_3^* \\ &\quad - B(\underline{K}_3, \underline{K}_1)(\underline{K}_3^2 - \underline{K}_1^2)A_1A_2A_3 \\ &\quad - \gamma(X)_i\ell_2A_2A_2^* + \gamma(X)_i\ell_2A_2A_2^*, \end{aligned} \quad (3.1.9b)$$

$$\begin{aligned} D_3(k_3^2 + \ell_3^2 + 1)|A_3|^2 &= -B(\underline{K}_1, \underline{K}_2)(\underline{K}_1^2 - \underline{K}_2^2)A_1^*A_2^*A_3^* \\ &\quad - B(\underline{K}_1, \underline{K}_2)(\underline{K}_1^2 - \underline{K}_2^2)A_1A_2A_3 \\ &\quad - \gamma(X)_i\ell_3A_3A_3^* + \gamma(X)_i\ell_3A_3A_3^*, \end{aligned} \quad (3.1.9c)$$

If the conditions for resonance (2.2.12) are met, it follows that

$$z \cdot \underline{K}_2 \times \underline{K}_3 = z \cdot \underline{K}_3 \times \underline{K}_1 = z \cdot \underline{K}_1 \times \underline{K}_2 = d, \quad (3.1.10a)$$

where d is a constant. A proof of (3.1.10a) is given in Appendix 2. Using (3.1.6) and (3.1.10a) and adding the three equations (3.1.9) together yields

$$\left. \begin{aligned} DE_1 + DE_2 + DE_3 = & -dA_1^*A_2^*A_3^*(\underline{K}_2^2 - \underline{K}_3^2 + \underline{K}_3^2 - \underline{K}_1^2 + \underline{K}_1^2 - \underline{K}_2^2) \\ & -dA_1A_2A_3(\underline{K}_2^2 - \underline{K}_3^2 + \underline{K}_3^2 - \underline{K}_1^2 + \underline{K}_1^2 - \underline{K}_2^2). \end{aligned} \right\} \quad (3.1.10b)$$

Simplifying (3.1.10b) we get

$$D_1E_1 + D_2E_2 + D_3E_3 = 0, \quad (3.1.11)$$

so that the energy of the triad is preserved. The waves in this approximation only exchange energy among themselves, a remarkable result, for as we suggested in (2.2), some energy must be passed on to the non-resonant terms, but (3.1.11) shows that the transfer of energy to the non-resonant terms is so slow compared to the resonant exchange that to the lowest order the triad is energy preserving.

If we write (3.1.9) as

$$D_1E_1 = -B_1A_1^*A_2^*A_3^* - B_1A_1A_2A_3, \quad (3.1.12a)$$

$$D_2E_2 = -B_2A_1^*A_2^*A_3^* - B_2A_1A_2A_3, \quad (3.1.12b)$$

$$D_3E_3 = -B_3A_1^*A_2^*A_3^* - B_3A_1A_2A_3. \quad (3.1.12c)$$

We add equations (3.1.12) to give

$$\begin{aligned} D_1E_1 + D_2E_2 + D_3E_3 = & -[B_1 + B_2 + B_3]A_1^*A_2^*A_3^* \\ & -[B_1 + B_2 + B_3]A_1A_2A_3 \end{aligned} \quad (3.1.13).$$

It is easily seen from (3.1.13) that energy conservation implies that two of the B_j 's are of one sign and the other is of a different sign. Craik (1985) has shown that if two of the B_j 's are of one sign and the other is of a different sign, the solution to the general initial value problem exists and is unique and bounded.

3.2. Conservation of Enstrophy

The average of half the square of the potential vorticity is called the potential enstrophy (Pedlosky, 1987). To show that the total enstrophy of the resonant triad is preserved, we start with (3.1.1) which we write as

$$\partial_t(\Delta\psi - \psi) = -\partial_x(\varepsilon\psi\Delta\psi_y + \psi) + \partial_y(\varepsilon\psi\Delta\psi_x + \varepsilon\gamma(\varepsilon x)\psi), \quad (3.2.1)$$

from which it follows from arguments given in (3.1) that

$$\int \int (\Delta\psi - \psi)^2 dx dy = \text{constant}, \quad (3.2.2)$$

which expresses the conservation of the total potential enstrophy. It is easily seen that for a plane-wave type solution, (2.2.10) the potential enstrophy for each member of the triad is

$$\left. \begin{aligned} (k_j^2 + \ell_j^2 + 1)^2 \frac{A^2}{2} &= V_j, \\ (k_j^2 + \ell_j^2 + 1)E_j & \end{aligned} \right\} \quad (3.2.3)$$

which equals

If we multiply (3.1.11) by $(k_j^2 + \ell_j^2 + 1)$ respectively and add the three equations we get

$$D_1 V_1 + D_2 V_2 + D_3 V_3 = 0. \quad (3.2.4)$$

Thus the total wave enstrophy of the triad is also preserved.

3.3 The Manley-Rowe Relations

In addition to conservation of energy and enstrophy, three other conserved quantities are expressed by the Manley-Rowe relations (Craig, 1985). We begin with equations (2.3.4), and set the friction terms to zero. We multiply each equation by $\alpha_1^*, \alpha_2^*, \alpha_3^*$ respectively. This yields

$$D_1|\alpha_1|^2 = -B_1[\alpha_1^*\alpha_2^*\alpha_3^* + \alpha_1\alpha_2\alpha_3], \quad (3.3.1a)$$

$$D_2|\alpha_2|^2 = -B_2[\alpha_1^*\alpha_2^*\alpha_3^* + \alpha_1\alpha_2\alpha_3], \quad (3.3.1b)$$

$$D_3|\alpha_3|^2 = -B_3[\alpha_1^*\alpha_2^*\alpha_3^* + \alpha_1\alpha_2\alpha_3]. \quad (3.3.1c)$$

Multiplying (3.3.1a) by $(-B_2)$, and (3.3.1b) by (B_1) and adding the two equations yields

$$D_2B_1|\alpha_2|^2 - D_1B_2|\alpha_1|^2 = 0. \quad (3.3.2a)$$

Following the same type of procedure employed in the derivation of (3.3.2a) readily reveals the relations

$$D_3B_1|\alpha_3|^2 - D_1B_3|\alpha_1|^2 = 0, \quad (3.3.2b)$$

$$D_3B_2|\alpha_3|^2 - D_2B_3|\alpha_2|^2 = 0. \quad (3.3.2c)$$

We now integrate (3.3.2), and assume each $\alpha_j \rightarrow 0$ as X goes to $\pm\infty$ which gives us

$$\partial_T \int_{-\infty}^{\infty} (B_1|\alpha_2|^2 - B_2|\alpha_1|^2)dX = 0, \quad (3.3.3a)$$

$$\partial_T \int_{-\infty}^{\infty} (B_1|\alpha_3|^2 - B_3|\alpha_1|^2)dX = 0, \quad (3.3.3b)$$

$$\partial_T \int_{-\infty}^{\infty} (B_2|\alpha_3|^2 - B_3|\alpha_2|^2)dX = 0. \quad (3.3.3c)$$

When the α_j 's depend on the two variables X, T , (3.3.3) readily reveals that the Manley-Rowe relations may be written in the following form

$$\int_{-\infty}^{\infty} (B_1|\alpha_2|^2 - B_2|\alpha_1|^2)dX = \text{constant}, \quad (3.3.4a)$$

$$\int_{-\infty}^{\infty} (B_1|\alpha_3|^2 - B_3|\alpha_1|^2)dX = \text{constant}, \quad (3.3.4b)$$

$$\int_{-\infty}^{\infty} (B_2|\alpha_3|^2 - B_3|\alpha_2|^2)dX = \text{constant}. \quad (3.3.4c)$$

CHAPTER 4

SOLUTIONS TO THE AMPLITUDE EQUATIONS

4.1 The Pump-Wave Approximation

There is no known solution to the general initial value problem (2.3.4) for general $\gamma(X)$. We may however, make some simplifying assumptions which allow us to demonstrate the behavior of the resonant triad when it is forced by topography.

The first such assumption we will look at is the “pump-wave approximation”. This describes the situation in which one of the three wave packets in the triad has an initially large amplitude relative to the other two. For this configuration, it can be assumed that the large amplitude wave packet α_3 , remains relatively constant in comparison to $\alpha_1(X, T)$ and $\alpha_2(X, T)$. Consequently, the dynamics of $\alpha_1(X, T)$ and $\alpha_2(X, T)$ is linear (Swaters 1988). This approximation inevitably breaks down if the amplitudes of the three waves become comparable, unless the “pump-wave”, α_3 , is artificially maintained at constant amplitude.

If we take equation (2.3.4) and consider the wave α_3 to be of much greater amplitude than waves α_1 and α_2 , and if α_3 is regarded as constant in the region of space and interval of time of interest, we may write the dynamics of (2.34) as

$$(\partial_T + c_2 \partial_X + \sigma_2) \hat{b}_1 = B_1 B_2 |\alpha_{30}|^2 \alpha_1 + (i c_2 \mu_0 \gamma(X) - \sigma_2) \hat{b}_1, \quad (4.1.1)$$

$$(\partial_T + c_1 \partial_X + \sigma_1) \hat{b}_2 = B_1 B_2 |\alpha_{30}|^2 \alpha_2 + (i c_1 \mu_0 \gamma(X) - \sigma_1) \hat{b}_2. \quad (4.1.2)$$

Where

$$\left. \begin{aligned} \alpha_{30} &= \text{constant pump wave amplitude} \\ (\partial_T + c_1 \partial_X + \sigma_1) \alpha_1 &= \hat{b}_1, \\ (\partial_T + c_2 \partial_X + \sigma_2) \alpha_2 &= \hat{b}_2. \end{aligned} \right\} \quad (4.1.3)$$

We may write (4.1.1) and (4.1.3a) in the following form

$$\underline{u}_T + A \underline{u}_X = B(X) \underline{u}, \quad (4.1.4)$$

where

$$\left. \begin{aligned} \underline{u} &= \begin{bmatrix} \alpha_1 \\ b_1 \end{bmatrix}, \\ A &= \begin{bmatrix} c_1 & 0 \\ 0 & c_2 \end{bmatrix}, \\ B &= \begin{bmatrix} -\sigma_2 & 1 \\ B_1 B_2 |\alpha_3|^2 & ic_2 \mu_0 \gamma(X) - 2\sigma_2 \end{bmatrix}. \end{aligned} \right\} \quad (4.1.5)$$

We can develop asymptotic solutions to equations of the form (4.1.4) using linear geometrical acoustics (Seymour and Mortell, 1974). We note that a similar expression can be derived for α_2 and b_2 .

Another ‘‘pump-wave’’ solution can be developed if we consider the topography to be a linear function of X and set the friction terms to zero. We once again take equations (2.3.4) and consider the wave α_3 to be constant in the region of space and interval of time of interest. The dynamics may be written as

$$(\partial_T + c_1 \partial_X) \alpha_1 = -B_1 \alpha_2^* \alpha_{30}^* \exp[i\hat{\gamma}X], \quad (4.1.6a)$$

$$(\partial_T + c_2 \partial_X) \alpha_2 = -B_2 \alpha_{30}^* \alpha_1^* \exp[i\hat{\gamma}X], \quad (4.1.6b)$$

where

$$\left. \begin{aligned} \alpha_{30}^* &= \text{constant pump wave amplitude,} \\ \hat{\gamma} &= \text{slope of topography times } \mu_0. \end{aligned} \right\} \quad (4.1.7)$$

Following Riemann, Bers, and Kaup (1977) we may transform away the exponential dephasing terms by absorbing the appropriate phase factors into the amplitudes.

By setting

$$\alpha_1(X, T) = \hat{\alpha}_1(X, T) \exp[i\hat{\theta}_1 \hat{\gamma}(X - c_1 T)], \quad (4.1.8a)$$

$$\alpha_2(X, T) = \hat{\alpha}_2(X, T) \exp[i\hat{\theta}_2 \hat{\gamma}(X - c_2 T)], \quad (4.1.8b)$$

where

$$\left. \begin{aligned} \hat{\theta}_1 &= -\frac{c_2}{c_2 - c_1}, \\ \hat{\theta}_2 &= -\frac{c_1}{c_1 - c_2}, \end{aligned} \right\} \quad (4.1.9)$$

we may transform (4.1.6) to

$$(\partial_T + c_1 \partial_X) \hat{\alpha}_1 = -B_1 \hat{\alpha}_2^* \alpha_{30}^*, \quad (4.1.10a)$$

$$(\partial_T + c_2 \partial_X) \hat{\alpha}_2 = -B_2 \hat{\alpha}_1^* \alpha_{30}^*. \quad (4.1.10b)$$

Following Craik and Adam (1978) and Swaters (1988), we may combine (4.1.10) into an equation of the form

$$[\partial_\tau^2 - \partial_\chi^2 + \text{sgn}(B_1 B_2)] \hat{\alpha}_j = 0, \quad (4.1.11)$$

where $i = 1, 2$, and where the real variables τ and χ are given respectively by

$$\tau = |\alpha_{30}| |B_1 B_2|^{1/2} T, \quad (4.1.12a)$$

$$\chi = 2|\alpha_{30}| |B_1 B_2|^{1/2} [X - (c_2 + c_3)T/2]/(c_2 - c_3). \quad (4.1.12b)$$

When $\text{sgn}(B_1 B_2) = 1$, (4.1.11) is a Klein-Gordon equation and the initial value problem can be solved by Fourier integrals (Whitham, 1974). If $\text{sgn}(B_1 B_2) = -1$, (4.1.11) is the telegraph equation and the initial value problem may be solved by Riemann's method (Craik and Adam, 1978).

4.2 Solutions Using the Method of Inverse Scattering

In this section we investigate solutions to the initial value problem (2.3.4) using the method of inverse scattering. We begin by taking the equations of the resonant triad (2.3.4) and setting the friction and topography terms to zero. This yields the following system of equations

$$D_1\alpha_1 = -B_1\alpha_2^*\alpha_3^*, \quad (4.2.1a)$$

$$D_2\alpha_2 = -B_2\alpha_3^*\alpha_1^*, \quad (4.2.1b)$$

$$D_3\alpha_3 = -B_3\alpha_1^*\alpha_2^*. \quad (4.2.1c)$$

Solutions to (4.2.1) may be obtained by the method of inverse scattering. The equations (4.2.1) are usually converted to standard form by scaling the three α_j 's so that the interaction coefficients have values of ± 1 . A complete review and further details of the inverse scattering problem may be found, for example, in Kaup, Riemann and Bers (1978), Ablowitz and Segur (1981) or Craik (1985).

If we consider the topography to be a quadratic function of X , we may write equations (2.3.4) in the following way

$$D_1\alpha_1 = -B_1\alpha_2^*\alpha_3^*\exp[i\hat{\gamma}X^2], \quad (4.2.2a)$$

$$D_2\alpha_2 = -B_2\alpha_3^*\alpha_1^*\exp[i\hat{\gamma}X^2], \quad (4.2.2b)$$

$$D_3\alpha_3 = -B_3\alpha_1^*\alpha_2^*\exp[i\hat{\gamma}X^2], \quad (4.2.2c)$$

where $\hat{\gamma}$ is now

$$\hat{\gamma} = \text{constant times } \mu_0.$$

Once again we follow Riemann, Bers and Kaup (1977), and transform away the exponential dephasing terms by absorbing the appropriate phase factors into the amplitudes.

By setting

$$\alpha_1(X, T) = \hat{\alpha}_1(X, T)\exp[i\theta_1'\hat{\gamma}(X - c_1T)^2], \quad (4.2.3a)$$

$$\alpha_2(X, T) = \hat{\alpha}_2(X, T)\exp[i\theta_2'\hat{\gamma}(X - c_2T)^2], \quad (4.2.3b)$$

$$\alpha_3(X, T) = \hat{\alpha}_3(X, T)\exp[i\theta_3'\hat{\gamma}(X - c_2T)^2], \quad (4.2.3c)$$

where

$$\left. \begin{aligned} \theta'_1 &= -\theta'(1, 2, 3), \\ \theta'_2 &= -\theta'(2, 3, 1), \\ \theta'_3 &= -\theta'(3, 1, 2), \\ \theta'(i, j, k) &= \frac{c_j c_k}{(c_j - c_i)(c_i - c_k)}, \end{aligned} \right\} \quad (4.2.4)$$

we may transform (4.2.2) to the following system

$$D_1 \hat{\alpha}_1 = -B_1 \hat{\alpha}_2^* \hat{\alpha}_3^*, \quad (4.2.5a)$$

$$D_2 \hat{\alpha}_2 = -B_2 \hat{\alpha}_3^* \hat{\alpha}_1^*, \quad (4.2.5b)$$

$$D_3 \hat{\alpha}_3 = -B_3 \hat{\alpha}_1^* \hat{\alpha}_2^*. \quad (4.2.5c)$$

Solutions to (4.2.5) are obtained by the method of inverse scattering (Riemann, Bers and Kaup, 1977).

4.3. The Steady State Solution in the Absence of Topography and Friction

In many practical situations, equations (2.3.4) can be approximated by retaining either the space or time dependence (Hsieh and Mysak, 1980). If we retain only the spatial dependence, and set the topography and friction terms to zero, equations (2.3.4) may be written as

$$\alpha_{1X} = -B'_{10}\alpha_2^*\alpha_3^*, \quad (4.3.1a)$$

$$\alpha_{2X} = -B'_{20}\alpha_3^*\alpha_1^*, \quad (4.3.1b)$$

$$\alpha_{3X} = -B'_{30}\alpha_1^*\alpha_1^*, \quad (4.3.1c)$$

where $B'_{j0} = B_j/c_j$; $j = 1, 2, 3$. There are well known solutions to (4.3.1) and they may be written in terms of Jacobi elliptic functions (Bretherton, 1964).

Recall from Chapter 3 that we showed energy conservation implies that two of the B_j 's in (4.3.1) are of one sign and the other is of a different sign. Without loss of generality we may assume B'_{10}, B'_{20} are of one sign and B'_{30} of a different sign, and that at $X = 0$, $\alpha_1(0) = \alpha_{10} > 0$; $\alpha_2(0) = \alpha_{20} > 0$; and $\alpha_3(0) = 0$. The solutions to (4.3.1) can be written

$$\alpha_1(X) = \alpha_{10}dn(\hat{\sigma}X|\hat{m}), \quad (4.3.2a)$$

$$\alpha_2(X) = \alpha_{20}cn(\hat{\sigma}X|\hat{m}), \quad (4.3.2c)$$

$$\alpha_3(X) = \alpha_{20}(-B'_{30}/B'_{20})^{1/2}sn(\hat{\sigma}X|\hat{m}), \quad (4.3.2c)$$

where

$$\hat{\sigma} = \alpha_{10}(-B'_{20}B'_{30}),$$

$$\hat{m} = (B'_{10}/B'_{20})(\alpha_{20}/\alpha_{10})^2 \quad 0 \leq \hat{m} \leq 1,$$

and dn , cn , and sn are the Jacobi elliptic functions in the notation of Abramowitz and Stegun (1965).

If $\hat{m} = 1$ the Jacobi elliptic functions reduce to hyperbolic functions, and for $\hat{m} > 1$ Abramowitz and Stegun (1965) give the following transformation

$$\left. \begin{aligned} dn(\hat{\sigma}X|\hat{m}) &= cn(\hat{m}^{1/2}\hat{\sigma}X|\hat{m}^{-1}), \\ cn(\hat{\sigma}X|\hat{m}) &= dn(\hat{m}^{1/2}\hat{\sigma}X|\hat{m}^{-1}), \\ sn(\hat{\sigma}X|\hat{m}) &= sn(\hat{m}^{1/2}\hat{\sigma}X|\hat{m}^{-1})\hat{m}^{-1/2}. \end{aligned} \right\} \quad (4.3.3)$$

Assuming $0 \leq \hat{m} \leq 1$, the spatial scale, i.e. wave length of the energy transfer is given by Abramowitz and Stegun (1965) to be

$$X_d = 2K(\hat{m})/\hat{\sigma}, \quad (4.3.4)$$

where $K(\hat{m})$ is the complete elliptic integral of the first kind.

The solutions (4.3.2) describe the following situation. During the interval $0 < X < 1/2X_d$, the third wave extracts energy from the first two waves, and during the last half of the cycle, the third wave transfers energy back to the first two waves until the conditions at $X = 0$ are once again reached (Swaters, 1988).

4.4 The Steady State Solution in the Presence of Linear Topography

As we have shown in section 4.3, analytic solutions to the steady state problem in the absence of topography and friction, can be obtained in terms of Jacobian elliptic functions. In this section we retain the topography, and assume that it is a linear function of X . Analytic solutions to this problem can be given in terms of an elliptic function. We may model many different topographic configurations as piecewise linear functions. For example we may model ridges, plateaus and mountains.

It is convenient to express the dynamics by means of an equation which formally corresponds to the motion of a particle in a non-linear potential. In this description, the coordinate giving the position of the particle is proportional to the deviation of the squared values of the wave amplitudes from their initial values.

The influence of topography and of arbitrary initial values for the interacting waves, is included in the expression for the potential, which is in general a third order polynomial in the squared amplitudes. The initial values of the amplitudes will determine the roots of the potential, which determines the strength of the interaction of the three waves.

We start with (2.3.4) and set the friction and the temporal derivative to zero. We may now write the system of equations (2.3.4) in the form

$$\alpha_{1X} = B_{10}\alpha_2^*\alpha_3^*\exp[-ih(X)], \quad (4.4.1a)$$

$$\alpha_{2X} = B_{20}\alpha_3^*\alpha_1^*\exp[-ih(X)], \quad (4.4.1b)$$

$$\alpha_{3X} = B_{30}\alpha_1^*\alpha_2^*\exp[-ih(X)], \quad (4.4.1c)$$

where $B_{j0} = -B_j/c_j$ and $h(X)$ is a continuous linear function of X , and the slope of $h(X)$ is given by $-\mu_0\hat{c}$, where \hat{c} is the slope of the topography. To obtain solutions to (4.4.1) we follow Craik (1985) and Weiland and Wilhelmsson (1977).

To this end we write

$$b_j = |\alpha_j|, \quad \Phi_j = \text{phase } \alpha_j,$$

so that

$$\alpha_j = b_j e^{i\Phi_j} \quad j = 1, 2, 3. \quad (4.4.2)$$

If we substitute (4.4.2) into the system (4.4.1) we obtain

$$b_{1X} + ib_1 \Phi_{1X} = B_{10} b_2 b_3 \exp[-i(h(X) + \Phi_1 + \Phi_2 + \Phi_3)], \quad (4.4.3a)$$

$$b_{2X} + ib_2 \Phi_{2X} = B_{20} b_3 b_1 \exp[-i(h(X) + \Phi_1 + \Phi_2 + \Phi_3)], \quad (4.4.3b)$$

$$b_{3X} + ib_3 \Phi_{3X} = B_{30} b_1 b_2 \exp[-i(h(X) + \Phi_1 + \Phi_2 + \Phi_3)]. \quad (4.4.3c)$$

Taking the real and imaginary parts of (4.4.3) yields

$$b_{1X} = B_{10} b_2 b_3 \cos \Phi, \quad (4.4.4a)$$

$$b_1 \Phi_{1X} = -B_{10} b_2 b_3 \sin \Phi, \quad (4.4.4b)$$

$$b_{2X} = B_{20} b_3 b_1 \cos \Phi, \quad (4.4.4c)$$

$$b_2 \Phi_{2X} = -B_{20} b_3 b_1 \sin \Phi, \quad (4.4.4d)$$

$$b_{3X} = B_{30} b_1 b_2 \cos \Phi. \quad (4.4.4e)$$

$$b_3 \Phi_{3X} = -B_{30} b_1 b_2 \sin \Phi, \quad (4.4.4f)$$

where $\Phi = h(X) + \Phi_1 + \Phi_2 + \Phi_3$. We now multiply equations (4.4.4b), (4.4.4d) and (4.4.4f) by b_1, b_2 and b_3 respectively to obtain

$$\Phi_{1X} = -B_{10}/b_1^2 b_1 b_2 b_3 \sin \Phi, \quad (4.4.5a)$$

$$\Phi_{2X} = -B_{20}/b_2^2 b_1 b_2 b_3 \sin \Phi, \quad (4.4.5b)$$

$$\Phi_{3X} = -B_{30}/b_3^2 b_1 b_2 b_3 \sin \Phi. \quad (4.4.5c)$$

From (4.4.4) and (4.4.5) we now obtain the following real system

$$b_{1X} = B_{10} b_2 b_3 \cos \Phi, \quad (4.4.6a)$$

$$b_{2X} = B_{20} b_3 b_1 \cos \Phi, \quad (4.4.6b)$$

$$b_{3X} = B_{30} b_1 b_2 \cos \Phi, \quad (4.4.6c)$$

$$\Phi_X = -\mu_0 \hat{c} - b_1 b_2 b_3 \left(\frac{B_{10}}{b_1^2} + \frac{B_{20}}{b_2^2} + \frac{B_{30}}{b_3^2} \right) \sin \Phi. \quad (4.4.6d)$$

Applying the following renormalizations (Weiland and Wilhelmsson, 1977)

$$\left. \begin{aligned} b_1 &\rightarrow (|B_{20}B_{30}|^{-1/2}b_1, \\ b_2 &\rightarrow (|B_{30}B_{10}|^{-1/2}b_2, \\ b_3 &\rightarrow (|B_{10}B_{20}|^{-1/2}b_3, \end{aligned} \right\} \quad (4.4.7)$$

to (4.4.6) yields the following system

$$b_{1X} = s_1 b_2 b_3 \cos \Phi, \quad (4.4.8a)$$

$$b_{2X} = s_2 b_3 b_1 \cos \Phi, \quad (4.4.8b)$$

$$b_{3X} = s_3 b_1 b_2 \cos \Phi, \quad (4.4.8c)$$

$$\Phi_X = -\mu_0 \hat{c} - b_1 b_2 b_3 \left(\frac{s_1}{b_1^2} + \frac{s_2}{b_2^2} + \frac{s_3}{b_3^2} \right) \sin \Phi, \quad (4.4.8d)$$

where $s_j = \text{sgn}(B_{j0})$, $j = 1, 2, 3$.

The Manley-Rowe relations (3.3.4) are satisfied by (4.4.8). They may be integrated with respect to X and written as

$$\begin{aligned} s_1 [b_1^2(X) - b_1^2(0)] &= s_2 [b_2^2(X) - b_2^2(0)] \\ &= s_3 [b_3^2(X) - b_3^2(0)] = \hat{y}(X). \end{aligned} \quad (4.4.9)$$

A further constant of motion for equations (4.4.8) is

$$\Gamma = b_1 b_2 b_3 \sin \Phi - 1/2(-\mu_0 \hat{c}) s_j b_j^2, \quad j = 1, 2, 3. \quad (4.4.10)$$

A proof of (4.4.10) is given in Appendix 3. Without loss of generality, we may choose $s_2 = s_3 = 1$ and introduce $s = s_1$.

With the use of (4.4.9) we define

$$\hat{y}(X) = s [b_1^2(X) - b_1^2(0)] = [b_j^2(X) - b_j^2(0)] \quad j = 2, 3. \quad (4.4.11)$$

Considering equation (4.4.b) we may write

$$b_{2X}^2 = 2b_1 b_2 b_3 \cos \Phi = \pm 2 \sqrt{b_1^2 b_2^2 b_3^2 (1 - \sin^2 \Phi)} \quad (4.4.12)$$

where \pm indicates the sign of $\cos \Phi$.

We proceed further by introducing (4.4.11) and (4.4.10) into (4.4.12) obtaining

$$\partial_X \hat{y}(X) = \pm 2 \sqrt{[s\hat{y} + b_1^2(0)][\hat{y} + b_2^2(0)][\hat{y} + b_3^2(0)] - \{\Gamma + (-\mu_0 \hat{c}/2)[\hat{y} + b_2^2(0)]\}^2}. \quad (4.4.13)$$

Equation (4.4.13) is a separable differential equation in the variable $\hat{y}(X)$. By taking the square of (4.4.13), we may write

$$1/2(\partial_X \hat{y}(X))^2 + \pi(X) = 0, \quad (4.4.14)$$

where

$$\begin{aligned} \pi(X) = & 2\{-s\hat{y}^3 - [b_1^2(0) + sb_3^2(0) + sb_2^2(0) - \frac{(-\mu_0 \hat{c})^2}{4}]\hat{y}^2 \\ & - [b_1^2(0)b_3^2(0) + b_1^2(0)b_2^2(0) + sb_2^2(0)b_3^2(0) - \Gamma(-\mu_0 \hat{c}) - \frac{(-\mu_0 \hat{c})^2}{2}b_2^2(0)]\hat{y} \\ & - b_1^2(0)b_2^2(0)b_3^2(0) + \Gamma^2 + \Gamma(-\mu_0 \hat{c})^2 b_2^2(0) + \frac{(-\mu_0 \hat{c})^2}{4}b_2^4(0)\}. \end{aligned} \quad (4.4.15)$$

Equation (4.4.14) is analogous to equations which describe the motion in a potential $\pi(X)$. Only the range of X for which $\pi(X) \leq 0$ has a physical significance, and $\partial_X \hat{y}(X) = 0$ when $\pi(X) = 0$. If we consider the case where $\Gamma = (-\mu_0 \hat{c}) = 0$, the roots of $\pi(X) = 0$, are $X = -sb_1^2(0)$, $X = -b_2^2(0)$ and $X = -b_3^2(0)$. Therefore the character of $\pi(X)$ is strongly dependent on the sign s .

For the case $s = -1$ all three roots will remain real and we will, in general, have an oscillating solution with X varying between the two largest roots of $\pi(X) = 0$. If $s = 1$, Weiland and Wilhelmsson (1977) have shown that an explosively unstable solution is possible. The influence of $(-\mu_0 \hat{c})$ is similar for both cases. From the form of $\pi(X)$, we find that for large values of $|(-\mu_0 \hat{c})|$ and $s = -1$, the two largest roots will approach each other and the interaction effectively disappears. For the case $s = 1$ and large $|(-\mu_0 \hat{c})|$, it is possible to delay or eliminate the instability.

A comprehensive review of equations of the form (4.4.14), is given by Craik (1985) and Weiland and Wilhelmsson (1977). To obtain analytical solutions for the b_j 's, we write (4.4.14) as

$$X - c = \pm 1/\sqrt{2} \int_0^{\hat{y}(X)} \frac{d\hat{y}}{\sqrt{-\pi(X)}}, \quad (4.4.16)$$

which is an elliptic integral and c is a constant of integration. From Chapter 3 we know that the equations of the resonant triad are energy conserving. Therefore $s = -1$, otherwise an instability could develop.

Since $s = -1$, $\pi(X)$ has three roots \hat{y}_1, \hat{y}_2 , and \hat{y}_3 which are all real. We assume that \hat{y}_1, \hat{y}_2 and \hat{y}_3 satisfy $\hat{y}_1 > \hat{y}_2 > \hat{y}_3$ and write (4.4.16) in the form

$$X - c = \pm \frac{1}{\sqrt{2}} \int_0^{\hat{y}(X)} \frac{d\hat{y}}{\sqrt{s(\hat{y} - \hat{y}_1)(\hat{y} - \hat{y}_2)(\hat{y} - \hat{y}_3)}}. \quad (4.4.17)$$

Since the roots are always real the solution for $\hat{y}(X)$ may be written

$$\hat{y}(X) = (\hat{y}_2 - \hat{y}_1)sn^2[(\hat{y}_1 - \hat{y}_3)^{1/2}(X - c) + \hat{\theta}|\hat{K}] + \hat{y}_1, \quad (4.4.18)$$

where $\hat{K} = \sqrt{\hat{y}_1 - \hat{y}_2/\hat{y}_1 - \hat{y}_3}$ is the modulus of the elliptic function, and $\hat{\theta} = sn^{-1}\left[\left(\frac{\hat{y}_1}{\hat{y}_1 - \hat{y}_2}\right)\middle|\hat{K}\right]$. From the relations (4.4.11) the final solution for the b_j 's may be written as

$$b_1(X) = \sqrt{b_1^2(0) - \hat{y}(X)} \quad (4.4.19a)$$

$$b_2(X) = \sqrt{b_2^2(0) + \hat{y}(X)}, \quad (4.4.19b)$$

$$b_3(X) = \sqrt{b_3^2(0) + \hat{y}(X)}. \quad (4.4.19c)$$

The spatial scale of the interaction is given by

$$X_d = \int_0^{2\pi} (1 - \hat{K} \sin^2 u')^{-\frac{1}{2}} du'. \quad (4.4.20)$$

Cases where two or more roots of $\pi(X)$ are equal, are simple but require separate treatment.

When $\Gamma = -\mu\hat{c} = 0$, and two or more wave amplitudes are initially equal, a review of solutions to this problem is given by Craik (1985).

CHAPTER 5

RESULTS OF THE THEORY

5.1. Calculation of Wave Numbers.

Chapter 4 provides us with several methods by which to examine the equations of the resonant triad. The “pump-wave” solutions are too cumbersome and cannot be easily interpreted. Solutions by the method of inverse scattering are very complex to obtain. The solution presented in section 4.4 is both direct and tractable, and in addition it clearly illustrates the behavior of the triad in response to topographic forcing. It is for these reasons that we will investigate the solution to the resonant triad presented in section 4.4. In order to apply this solution, we must first calculate wave numbers which will form a resonant triad, specifically equations (2.2.13) must be satisfied. Such wave numbers if found, form a very restricted set of all possible interactions, distinguished by the efficiency of their mutual interaction. The analytical search for such triads is a very complicated algebraic problem. Longuet-Higgins and Gill (1967) have investigated this problem in great detail and have presented equations, from which it is possible to calculate wave numbers, which form a resonant triad.

There are special cases that have been noted by Longuet-Higgins and Gill (1967) and Kenyon (1964), in which the resonance mechanism of two discrete waves producing a third, could not be responsible for producing time or space independent zonal flows. One component of the zonal flow could be thought of as the wave $(k_3, \ell_3) = (0, -2\ell_1)$. The natural frequency response of this is zero from (2.2.11). Waves that resonantly interact with this are $(k_1, \ell_1) = (k_1, \ell_1)$ and $(k_2, \ell_2) = (-k_1, \ell_1)$. Since the moduli of these two waves are equal, by (2.2.18), $B_3 = 0$, the wave (k_3, ℓ_3) acts as a catalyst for interaction between (k_1, ℓ_1) and (k_2, ℓ_2) , but does not gain or lose energy itself at our time or length scales. Newell (1969) has shown that at later time scales, through the action of resonating sidebands, it is possible for zonal flows to be excited.

We will consider only those triads in which each wave participates in the energy exchange process, i.e., $B_{j0} \neq 0$, $B_j \neq 0$, $j = 1, 2, 3$. By doing this we are assured that we are looking at wave-wave interactions. In order to calculate wave numbers which form a resonant triad, a Fortran program has been developed, which uses equations presented by Longuet-Higgins and Gill (1967) to calculate the wave numbers. The program is listed in Appendix 4. In Tables 1 and 2, we show examples of wave numbers which combine to form resonant triads. Also shown in these figures, are the frequencies (ω_j), group velocities (c_j), interaction coefficients (B_{j0}), and topography terms (μ_0), of the resonant triads.

	k_i Wave Number	ℓ_i Wave Number	ω_j Frequency	c_j Group Velocity	B_{j0} Interaction Coefficient	μ_0 Topography Term
1	-0.26854	-0.48782	0.20498	-0.67928	0.01431	-0.01607
2	0.32139	0.38302	-0.25712	-0.66778	-0.01914	-0.01607
3	-0.5285	0.10479	0.5213	-0.98098	0.00326	-0.01607
-	- - - -	- - - -	- - - -	- - - -	- - - -	- - - -
1	-1.15315	-2.16826	0.16401	-0.08843	5.87361	-1.68543
2	1.28558	1.53209	-0.25712	-0.06778	-16.89236	-1.68543
3	-0.13242	0.63617	0.09311	-0.68577	2.12563	-1.68543
-	- - - -	- - - -	- - - -	- - - -	- - - -	- - - -
1	-1.76358	-3.34540	0.11525	-0.03879	31.82619	-4.40504
2	1.92836	2.29813	-0.19284	-0.02563	-123.31445	-4.40504
3	-0.16478	1.04727	0.07758	-0.45879	13.04867	-4.40504
-	- - - -	- - - -	- - - -	- - - -	- - - -	- - - -
1	-2.37148	-4.51559	0.08779	-0.02160	103.10274	-7.53879
2	2.57115	3.06418	-0.15124	-0.01307	-466.45774	-7.53879
3	-0.19967	1.45141	0.06346	-0.30976	44.63003	-7.53879
-	- - - -	- - - -	- - - -	- - - -	- - - -	- - - -
1	-2.97705	-5.67938	0.07068	-0.01375	254.60241	-10.73504
2	3.21394	3.83022	-0.12361	-0.00790	-1255.25322	-10.73504
3	-0.23689	1.84916	0.05293	-0.21784	113.25631	-10.73504
-	- - - -	- - - -	- - - -	- - - -	- - - -	- - - -
1	-3.58111	-6.83903	0.05910	-0.00952	531.20343	-13.89420
2	3.85673	4.59627	-0.10424	-0.00530	-2757.18031	-13.89420
3	-0.27561	2.24276	0.4514	-0.15970	239.96739	-13.89420

Table 1. Table of wave numbers, frequencies, group velocities, interaction coefficients, and topography terms which form a resonant triad.

	k_j Wave Number	l_j Wave Number	ω_j Frequency	c_j Group Velocity	B_{j0} Interaction Coefficient	μ_0 Topography Term
1	0.34639	1.82546	-0.07780	-0.21250	0.56476	-5.70041
2	1.04199	-1.07901	-0.32061	-0.10211	6.63514	-5.70041
3	-1.38838	-0.74645	0.39841	0.03050	25.74176	-5.70041
-	- - - - -	- - - - -	- - - - -	- - - - -	- - - - -	- - - - -
1	0.57185	3.03432	-0.05429	-0.08904	4.07423	4.00201
2	1.73665	-1.79835	-0.23954	-0.02317	100.35639	4.00201
3	-2.30849	-1.23597	0.29382	0.04538	58.00397	4.00201
-	- - - - -	- - - - -	- - - - -	- - - - -	- - - - -	- - - - -
1	0.79806	4.24429	-0.04061	-0.04759	15.29165	14.97147
2	2.43130	-2.51769	-0.18349	-0.00813	599.72834	14.97147
3	-3.22936	-1.72661	0.22411	0.03105	176.36581	14.97147
-	- - - - -	- - - - -	- - - - -	- - - - -	- - - - -	- - - - -
1	1.02466	5.45485	-0.03222	-0.02937	41.35611	29.92395
2	3.12596	-3.23703	-0.14710	-0.00378	2195.93733	29.92395
3	-4.15062	-2.21782	0.17932	0.02111	440.03626	29.92395
-	- - - - -	- - - - -	- - - - -	- - - - -	- - - - -	- - - - -
1	1.25146	6.66569	-0.02663	-0.01986	91.78771	47.69247
2	3.82062	-3.95637	-0.12226	-0.00211	5979.47382	47.69247
3	-5.07208	-2.70933	0.14889	0.01498	938.61857	47.69247
-	- - - - -	- - - - -	- - - - -	- - - - -	- - - - -	- - - - -
1	1.36490	7.27119	-0.02449	-0.01674	129.76708	57.27179
2	4.16795	-4.31604	-0.11265	-0.00165	9133.49351	57.27179
3	-5.53285	-2.95515	0.13714	0.01283	1310.25321	57.27179

Table 2. Table of wave numbers, frequencies, group velocities, interaction coefficients, and topography terms which form a resonant triad.

We have shown in (3.3.13) that for the initial value problem, at least one of the interaction coefficients (B_j) is of a sign different than the other two. Table 2 shows that when we divide the B_j 's by the group velocity (c_j) of the wave, it is possible to have all the interaction coefficients for the steady state solution (B_{j0}) of the same sign.

Chapter 4.4 tells us that having all the B_{j0} 's of one sign may lead to explosively unstable solutions for the amplitudes. In fact this would seem to suggest that the waves are always stable in time and may become unstable in space, depending on whether the group velocities of the waves are all of one sign, or one is of a sign which is different from the other two. Therefore, in order for the possibility of unstable solutions for the amplitudes to exist, at least one of the c_j 's must be of the sign which is different than the other two.

From Chapter 3, we know that since the initial value problem always conserves energy in time and space, explosive instability in space cannot occur. The reason we do not get explosive instability in space is that the steady state solution is no longer valid. The solution is fully time dependent, since the group velocities are not of the same sign. Only for a brief time do the waves interact. As time increases the wave envelopes rapidly separate. The short period of time the waves interact is unlikely to give rise to an explosive instability. If we were to allow explosive instability, we would break our initial scaling demands, hence the theory would break down. In our investigation the resonant triad we shall use is given by

$$\begin{aligned}
(k_1, \ell_1) &= (-1.0808487, -1.3533314), \\
(k_2, \ell_2) &= (1.00, 1.7320508), \\
(k_3, \ell_3) &= (0.0807487, -0.3787194), \\
\omega_1 &= 0.2702194, \\
\omega_2 &= -0.200, \\
\omega_3 &= -0.702194, \\
c_1 &= -0.1039928, \\
c_2 &= -0.1200, \\
c_3 &= -0.8597425, \\
B_{10} &= -4.800329, \\
B_{20} &= 2.46288, \\
B_{30} &= 0.524778, \\
\mu_0 &= 0.750126, \\
\mu_1/c_1 &= 3.253817, \\
\mu_2/c_2 &= 2.8867513, \\
\mu_3/c_3 &= 0.3830634.
\end{aligned} \tag{5.1.1}$$

The triad given in (5.1.1) has wave numbers (k_j, ℓ_j) which are small, therefore we are looking at the wave-wave interaction between long planetary waves. The group velocities (c_1, c_2, c_3) are all negative, therefore the energy of the waves propagates to the west. Waves for which $k^2 < \ell^2 + 1$ will propagate to the west. We also note that the group velocities are all of the same magnitude, therefore the wave packets do not separate quickly in space, and the waves will interact for a long distance. If the relation between energy and enstrophy (3.2.3) is exploited, not only must

$$\sum_{j=1}^3 E_j = \text{constant} = E_0, \tag{5.1.2}$$

but also

$$\sum_{j=1}^3 (k_j^2 + \ell_j^2) E_j = \text{constant} = K_0^2 E_0, \quad (5.1.3)$$

hence, as Pedlosky (1987) has shown as the amplitudes change they must do so in a way that preserves the ratio of the three waves, i.e.,

$$K_0^2 = \frac{\sum (k_j^2 + \ell_j^2) E_j(X)}{\sum E_j(X)}, \quad (5.1.4)$$

is a constant of the motion. Thus it is impossible, for one wave to lose energy to two other waves, both of which have larger wave numbers. If energy is transmitted to larger wave numbers by nonlinear effects, energy must also be transmitted to a lower wave number in order to preserve both energy and enstrophy. For our triad, for example, $k_1^2 + \ell_1^2 \approx 3.0$, $k_2^2 + \ell_2^2 \approx 4.0$, and $k_3^2 + \ell_3^2 \approx 0.15$. The conservation statements (5.1.4) may be written (Pedlosky, 1987)

$$\frac{E_{1X}}{(k_2^2 + \ell_2^2) - (k_3^2 + \ell_3^2)} = \frac{E_{2X}}{(k_3^2 + \ell_3^2) - (k_1^2 + \ell_1^2)} = \frac{E_{3X}}{(k_1^2 + \ell_1^2) - (k_2^2 + \ell_2^2)}. \quad (5.1.5)$$

Since $(k_3^2 + \ell_3^2) < (k_1^2 + \ell_1^2) < (k_2^2 + \ell_2^2)$. Then if $E_{1X} < 0$, both E_{2X} and E_{3X} must be positive.

5.2 Rossby Wave Triad over Piecewise Linear Topographic Configurations

In this section we use the solution derived in 4.4 to illustrate the effects of topographic forcing on Rossby wave triads.

Figure 2 shows the profile of the topographic configurations we will consider. The topographic configuration is the type we call piecewise linear, i.e. it is continuous, but not continuously differentiable and the equations which describe the topography in Fig. 2 are

$$\left. \begin{aligned} h'(X) &= 0, X > X_0, X < X_2 \\ h'(X) &= \frac{H_0(X - X_0)}{(X_1 - X_0)}, X_1 < X < X_0 \\ h'(X) &= \frac{H_0(X - X_2)}{(X_1 - X_2)}, X_2 < X < X_1 \end{aligned} \right\} \quad (5.2.1)$$

where $H_0/(X_1 - X_0)$, $H_0/(X_1 - X_2)$ are the slopes of the topography (\hat{c}_1) and $h(X) = \frac{-h'(X)}{\mu_0}$. In Fig. 2 we have divided the topography into four regions, to obtain a continuous solution. The conditions at the end points of $b_j(X)$ and $\Phi_j(X)$ of one region must be the initial conditions of the next region. We specify the conditions at $X = 0$.

We now take the solution (4.4.16) and write it as

$$X' - c = \pm \frac{1}{\sqrt{2}} \int_0^{\hat{y}(X')} \frac{d\hat{y}}{\sqrt{-\pi(X')}}. \quad (5.2.2)$$

We now set

$$\left. \begin{aligned} X' &= X, X > X_0, X < X_2 \\ X' &= X - X_0, X_1 < X < X_0 \\ X' &= X - X_2, X_2 < X < X_1. \end{aligned} \right\} \quad (5.2.3)$$

In order for the solutions to be continuous, we get the following constants of integration

$$\begin{aligned} \text{Region I, } c &= 0 \\ \text{Region II, } c &= 0 \\ \text{Region III, } c &= X_1 - X_2 \\ \text{Region IV, } c &= X_2. \end{aligned} \quad (5.2.4)$$

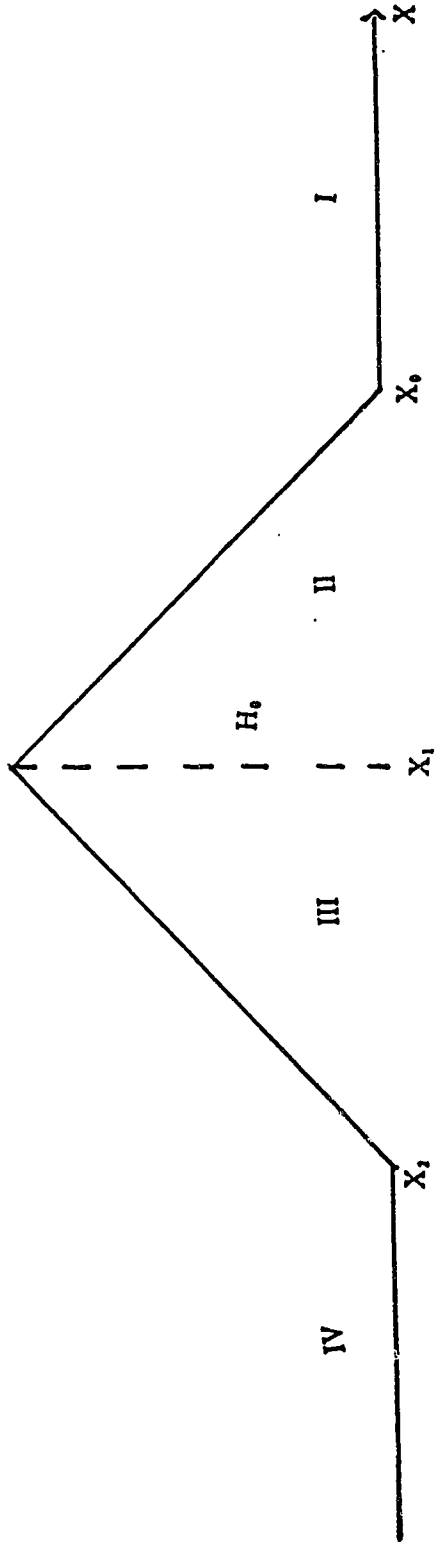


Fig. 2. Cross section of the piecewise linear topographic configuration used in this thesis.

The final solution for each region proceeds as presented in section 4.4. The spatial dependence of the phase Φ is given from the relation (4.4.10) once we know the variation in space of the amplitudes. The derivatives of the Φ_j 's ($j = 1, 2, 3$) are given by equations (4.4.5) once the variations in space of the amplitudes are known. Unfortunately we do not have an analytical solution to the Φ_j 's ($j = 1, 2, 3$). Therefore we employ a numerical integrating routine to solve for the Φ_j 's.

A Fortran program has been developed which calculates the complete solution, and the program is listed in Appendix 4.

It is possible to choose an infinite number of combinations for the initial amplitudes. Equation 4.4.15 tells us that our choice of the initial amplitudes determines the roots of $\pi(X)$, hence the modulus of the elliptic function is dependent upon our choice of the initial amplitudes. The spatial scale of the interaction is given by (4.4.20). It follows from (4.4.20) that if we choose initial amplitudes such that $\hat{K} = 1$ the spatial scale of interaction will be infinite, and if we choose $\hat{K} = 0$ the elliptic function degenerates into a circular function with the spatial scale of interaction, being 2π . Our choice of the initial amplitudes determines the spatial scale of interaction which must be between 2π and infinity.

With the use of (4.4.2), (4.4.7) and (2.3.3) we write the following equation for $A_j(X)$

$$A_j(X) = b_j(X) \exp[i(\Phi_j(X) - \mu_j/c_j h'(X))]. \quad (5.2.5)$$

We now substitute (5.2.5) into (2.2.10) to give

$$\psi^{(0)}(x, y, z) = \sum_{j=1}^3 b_j(\epsilon X) \exp[i(kx + ly - \omega t + \Phi_j(\epsilon X) - \mu_j/c_j h'(\epsilon X))] + c.c. \quad (5.2.6)$$

where the amplitudes $b_j(\epsilon X)$ are slowly varying functions of X and the phase is given by the terms in the exponential.

We begin all of the solutions by assuming that the waves are fully resonant and exchanging energy with maximum efficiency. This requires all of the initial

phases Φ_j ($j = 1, 2, 3$) to be 0. Equations (4.4.6) show that when $\Phi = 0$, the energy exchange between the members of the triad is maximized.

We also start our solutions in a region where there is initially no topographic forcing present. This requires that initially $\Gamma = -\mu_0 \hat{c} = 0$. When we have both $-\mu_0 \hat{c} = 0$ and $\Gamma = 0$, the minimum value of two of the squared amplitudes will be zero as can be seen from (4.3.13). Then the phase derivative (4.4.8d) will be undetermined. For this situation Craik (1985) and Weiland and Wilhelmsson (1977) state that in the limit, we may consider Φ to remain zero for all X .

5.3. Solutions to the Rossby Wave Triad over Piecewise Symmetric Linear Topographic Configurations

In this section we examine the effects of piecewise symmetric linear topographic configurations on the Rossby wave triad. The geometry of the piecewise linear topographic configuration is given in Figure 2. We set

$$\left. \begin{aligned} X_0 &= 10, \\ X_1 &= 20, \\ X_2 &= 30. \end{aligned} \right\} \quad (5.3.1)$$

We choose our amplitudes in such a way that we can examine waves with a long interaction length, medium interaction length, and a short interaction length, i.e. we choose initial amplitudes in such a way that $\hat{K} \approx 1$, $\hat{K} \approx 0.5$ and $\hat{K} \approx 0$. Figures 3-6 show waves with a long interaction length ($\hat{K} \approx 1$) and the initial amplitudes are

$$\left. \begin{aligned} b_1(0) &= 1.0, \\ b_2(0) &= 0.0433, \\ b_3(0) &= 0.02. \end{aligned} \right\} \quad (5.3.2)$$

Figures 7-9 show waves with a medium interaction length ($\hat{K} \approx 0.5$) and the initial amplitudes are

$$\left. \begin{aligned} b_1(0) &= 1.0, \\ b_2(0) &= 0.05, \\ b_3(0) &= 0.01. \end{aligned} \right\} \quad (5.3.3)$$

Finally figures 10-12 show waves with a short interaction length ($\hat{K} \approx 0$) and the initial amplitudes are

$$\left. \begin{aligned} b_1(0) &= 1.0, \\ b_2(0) &= 3.024, \\ b_3(0) &= 4.0. \end{aligned} \right\} \quad (5.3.4)$$

We begin by looking at the case in which H_0 is 0. This corresponds to the situation where $\Gamma = -\mu_0 \hat{c} = 0$ and the Φ_j 's ($j = 1, 2, 3$) are zero. The waves

are exchanging energy with maximum efficiency as they propagate through space. This particular case is illustrated for the initial amplitudes (5.3.2), (5.3.3) and (5.3.4) by Fig. 3, Fig. 7 and Fig. 10, respectively, by plots of the amplitudes (b_j 's). Wave 1, wave 2 and wave 3 are denoted by a thick curve, dashed curve and a dotted curve respectively. We note in these figures that the energy flow among members of the triad, in the absence of topography, pulsates with X , and that the direction of the energy flow is reversible. The wave with the interaction coefficient which has a sign opposite to the other two, in our case wave 1, will always vary in the opposite direction to the other two, and in this way the wave energy will oscillate between the members of the triad.

The energy flows first, say, to waves 2 and 3 and then reverses direction when the initial instability of wave 1 is halted by nonlinear effects (Pedlosky, 1987). The pulsation is perpetual with each member of the triad receiving and then returning energy to the others.

We now turn our attention to the case where $H_0 \neq 0$. By choosing $H_0 = 10$ we introduce a slope of 1. The waves start out exchanging energy with maximum efficiency as in the previous example, but when the triad reaches X_0 , it encounters the topography. At X_0 , Γ and $-\mu_0\hat{c}$ are no longer zero and we know from (4.4.13) that the roots of $\pi(X)$ will begin to approach each other so that the interaction effectively begins to disappear.

The case where $H_0 = 10$ is illustrated by plots of the initial amplitudes given by (5.3.2), (5.3.3) and (5.3.4) in Figures 4A, 8A and 11A respectively. We note in the plots that between X_0 and X_2 , the area where the topography is present, the interaction and exchange of energy between the waves is much less than when the waves were initially resonant. Once the waves propagate past X_2 , i.e. they are in a region of no topography, $-\mu_0\hat{c} = 0$ but, $\Gamma \neq 0$. The influence of Γ is similar to that of the topography ($-\mu_0\hat{c}$). A non-zero Γ causes the roots to approach each other, but the interaction is not as small as when the topography is present. We can see this in the above Figures, if we look at the triad in the area which is less than X_2 . The exchange of energy is greater than when the

waves were propagating over topography, but not as great as when the waves were initially exchanging energy with maximum efficiency i.e. $X > X_0$.

Figure 5A illustrates the effect of $H_0 = 30$, on the initial amplitudes given by (5.3.2). Figures 6A, 9A and 12A illustrate the effect of $H_0 = 50$ on the amplitudes given by (5.3.2), (5.3.3) and (5.3.4) respectively. Thus, it is shown by these Figures that as the slope of the topography increases, the roots of $\pi(X)$ approach each other and once H_0 is large enough, the interaction will effectively disappear no matter what the initial amplitudes may be.

If we examine plots of Φ versus X , the reason topography impedes the flow of energy may be seen. For the initial amplitudes given by (5.3.2), (5.3.3) and (5.3.4), the plots for $H_0 = 10$ of Φ versus X are given by Figures 4B, 8B, and 11B respectively. Initially the phase (Φ) is zero and the waves are exchanging energy with maximum efficiency. As the triad encounters topography at X_0 , the topography begins to dephase the waves, and the waves are no longer fully resonant. The phase oscillates as the triad propagates over the topography. Once we leave the region of topography at X_2 , $-\mu_0 \hat{c}$ is zero, however $\Gamma \neq 0$.

In this region, we know by equation (4.4.10) that $\sin \Phi$ does not change sign, thus Φ must oscillate in such a way that $\sin \Phi$ is always of the same sign. We see this type of oscillation in the above Figures. As we increase H_0 to 30, for initial amplitudes given by (5.3.2), Fig. 5B shows that Φ behaves in the same way. If we further increase H_0 to 50 for initial amplitudes given by (5.3.2), (5.3.3) and (5.3.4), the behavior of Φ versus X is shown by the Figures 6B, 9B and 12B respectively. The behaviour of Φ is analogous to that when $H_0 = 10$.

To examine the cause of the de-phasing of the triad, we begin by looking at the equations of the individual waves given by (5.2.6). Neglecting the complex conjugates, we write the equations as

$$\psi_1^{(0)} = b_1(\epsilon x) \exp[i(k_1 x + l_1 y - \omega_1 t + \Phi_1(\epsilon x) - \mu_1/c_1 h'(\epsilon x))], \quad (5.3.5a)$$

$$\psi_2^{(0)} = b_2(\epsilon x) \exp[i(k_2 x + l_2 y - \omega_2 t + \Phi_2(\epsilon x) - \mu_2/c_2 h'(\epsilon x))], \quad (5.3.5b)$$

$$\psi_3^{(0)} = b_3(\epsilon x) \exp[i(k_3 x + l_3 y - \omega_3 t + \Phi_3(\epsilon x) - \mu_3/c_3 h'(\epsilon x))]. \quad (5.3.5c)$$

We rewrite equations (5.3.5) in the following way

$$\psi_1 = b_1(\varepsilon x) \exp[i\widehat{\Phi}_1(x, y, t)], \quad (5.3.6a)$$

$$\psi_2 = b_2(\varepsilon x) \exp[i\widehat{\Phi}_2(x, y, t)], \quad (5.3.6b)$$

$$\psi_3 = b_3(\varepsilon x) \exp[i\widehat{\Phi}_3(x, y, t)]. \quad (5.3.6c)$$

From (5.3.6) we may write

$$\left. \begin{aligned} \widehat{k}_j &= \widehat{\Phi}_{jx}, \\ \ell_j &= \widehat{\Phi}_{jy}, \omega_j = \widehat{\Phi}_{jt}. \end{aligned} \right\} \quad (5.3.7)$$

For the sake of simplicity we denote the term $\widehat{\Phi}_j(X) - \mu_j/c_j h'(X)$ to be phase2.

We now look at the zonal wave number \widehat{k}_j , in the following way

$$\widehat{k}_1 = \widehat{\Phi}_{1x} = k_1 + \varepsilon \partial_X [\widehat{\Phi}_1(X) - \mu_1/c_1 h'(X)], \quad (5.3.8a)$$

$$\widehat{k}_2 = \widehat{\Phi}_{2x} = k_2 + \varepsilon \partial_X [\widehat{\Phi}_2(X) - \mu_2/c_2 h'(X)], \quad (5.3.8b)$$

$$\widehat{k}_3 = \widehat{\Phi}_{3x} = k_3 + \varepsilon \partial_X [\widehat{\Phi}_3(X) - \mu_3/c_3 h'(X)]. \quad (5.3.8c)$$

Equations (5.3.8) present us with an interesting result. The sign of the derivative of phase2 tells us whether the zonal wave number \widehat{k}_j is getting smaller or larger, and hence tells us whether the zonal wave length

$$\lambda_j = 2\pi/|\widehat{k}_j| \quad (5.3.9)$$

is getting longer or shorter. In the absence of topography $k_j = \widehat{k}_j$.

The conditions for resonance (2.2.13) state that the sum of the zonal wave numbers k_j must be zero. The effect of the topography in equations (5.3.8) is to cause the sum of the zonal wave numbers to be

$$k_1 + k_2 + k_3 = k_0 \quad (5.3.10)$$

where $k_0 \neq 0$. Thus, the topography causes a zonal wave number mismatch. The conditions for resonance are no longer met and the waves are slightly dephased. This is what causes the exchange of energy, when the waves propagate over topography, to become smaller.

From equations (5.3.8), we know the magnitude of ε and the slope of the topography, play a large part in determining the magnitude of the wave number mismatch. The greater the slope of the topography, the larger the wave number mismatch. Hence, the less the interaction between the waves. This result was illustrated previously when we showed the effects of increasing the slope of the topography on the amplitudes.

When $H_0 = 10$, for initial amplitudes (5.3.2), (5.3.3), and (5.3.4), Figures 4C, 8C, and 11C show plots of the phase2 derivative versus X respectively. Once again wave 1, wave 2 and wave 3 are denoted by a thick curve, dashed curve and a dotted curve respectively. The effect of the topography on the zonal wave number k_j , for $X_1 < X < X_0$ is

$$\left. \begin{aligned} \hat{k}_1 &= -1.0807487 + \varepsilon |\partial_X [\Phi_1(X) - \mu_1/c_1 h'(X)]|, \\ \hat{k}_2 &= 1.00 - \varepsilon |\partial_X [\Phi_2(X) - \mu_2/c_2 h'(X)]|, \\ \hat{k}_3 &= 0.0807487 + \varepsilon |\partial_X [\Phi_3(X) - \mu_3/c_3 h'(X)]|, \end{aligned} \right\} \quad (5.3.11)$$

and for $X_2 < X < X_1$

$$\left. \begin{aligned} \hat{k}_1 &= -1.0807487 - \varepsilon |\partial_X [\Phi_1(X) - \mu_1/c_1 h'(X)]|, \\ \hat{k}_2 &= 1.00 + \varepsilon |\partial_X [\Phi_2(X) - \mu_2/c_2 h'(X)]|, \\ \hat{k}_3 &= 0.0807487 - \varepsilon |\partial_X [\Phi_3(X) - \mu_3/c_3 h'(X)]|. \end{aligned} \right\} \quad (5.3.12)$$

Thus, as the triad begins to propagate over the topography between $X_1 < X < X_0$, (5.3.11) indicates that zonal wave numbers \hat{k}_1 and \hat{k}_2 are decreasing, hence by (5.3.9), the zonal wave lengths are increasing. However the zonal wave number \hat{k}_3 is increasing, hence by (5.3.9) the zonal wave length is decreasing and once $X_2 < X < X_1$ (5.3.12) shows the opposite is true for all three waves.

Once the waves are in the region where $X < X_2$, there is a very small zonal wave number mismatch, and the triad is very close to being fully resonant. This is indicated by the large spikes in the phase2 derivatives. Once we are in this region

$$phase2 = \Phi_j(X). \quad (5.3.13)$$

When the triad is very near resonance the minimum value of two of the squared amplitudes will be near zero, hence equations (4.4.5) show the spikes in the phase2 derivative occur when one of the squared amplitudes is nearly equal to zero.

When $H_0 = 30$ and the initial amplitudes are given by (5.3.1), Figure 5C shows the triad behaves as above. Similarly for $H_0 = 50$ and initial amplitudes (5.3.2), (5.3.3) and (5.3.4), Figures 6C, 9C and 12C respectively show the triad behaves as above also.

We now proceed to examine the effects of the topography on the individual waves. To do this we take the real part of equations (5.3.5) and ignore the fast phase variation which gives

$$\psi_1 = b_1(X) \cos(\Phi_1(X) - \mu_1/c_1 h'(X)), \quad (5.3.14a)$$

$$\psi_2 = b_2(X) \cos(\Phi_2(X) - \mu_2/c_2 h'(X)), \quad (5.3.14b)$$

$$\psi_3 = b_3(X) \cos(\Phi_2(X) - \mu_3/c_3 h'(X)). \quad (5.3.14c)$$

We show plots of $\Phi_j(X) - \mu_j/c_j h'(X)$ in Figures 4D, 5D, 6D, 8D, 9D, 11D and 12D to check the performance of the numerical routine used to integrate the derivatives of the Φ_j 's for the initial amplitudes given by (5.3.2), (5.3.3) and (5.3.4) and different values of H_0 .

For initial amplitudes (5.3.2), (5.3.3) and (5.3.4), Figures 4E, 5E, 6E, 8E, 9E, 11E and 12E show plots of equations (5.3.14) for different values of H_0 . Once again wave 1, wave 2 and wave 3 are denoted by a thick curve, dashed curve and dotted curve respectively. The effects of the topography on waves 1 and 2 is dramatic, however, the effect of the topography on wave 3 is not as noticeable. The reason we see rapid oscillations from waves 1 and 2 and not wave 3 is that the magnitude of μ_j/c_j ($j = 1, 2$), is much greater than μ_3/c_3 . Once the waves propagate over the topography into the region where $X < X_2$, the rapid oscillations of waves 1 and 2 ceases. The waves still remain de-phased downstream of the topography as the Figures indicate, although the de-phasing is not as severe as when the waves were propagating over the topography.

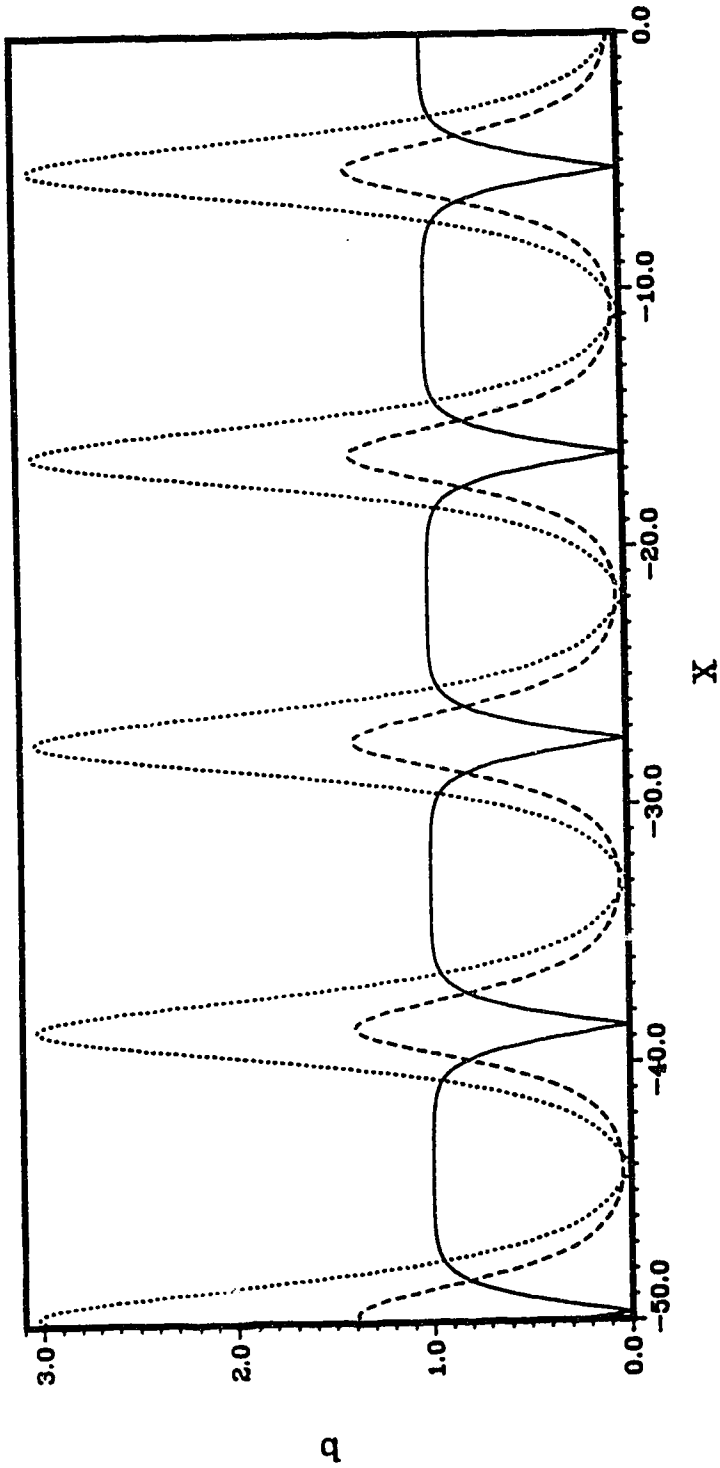


Fig. 3. Plot of b_i versus X for initial amplitudes (5.3.2) and topography given by (5.2.1) and (5.3.1) with $H_0=0.0$. Wave 1, wave 2 and wave 3 are denoted by a thick curve, dashed curve and a dotted curve respectively.

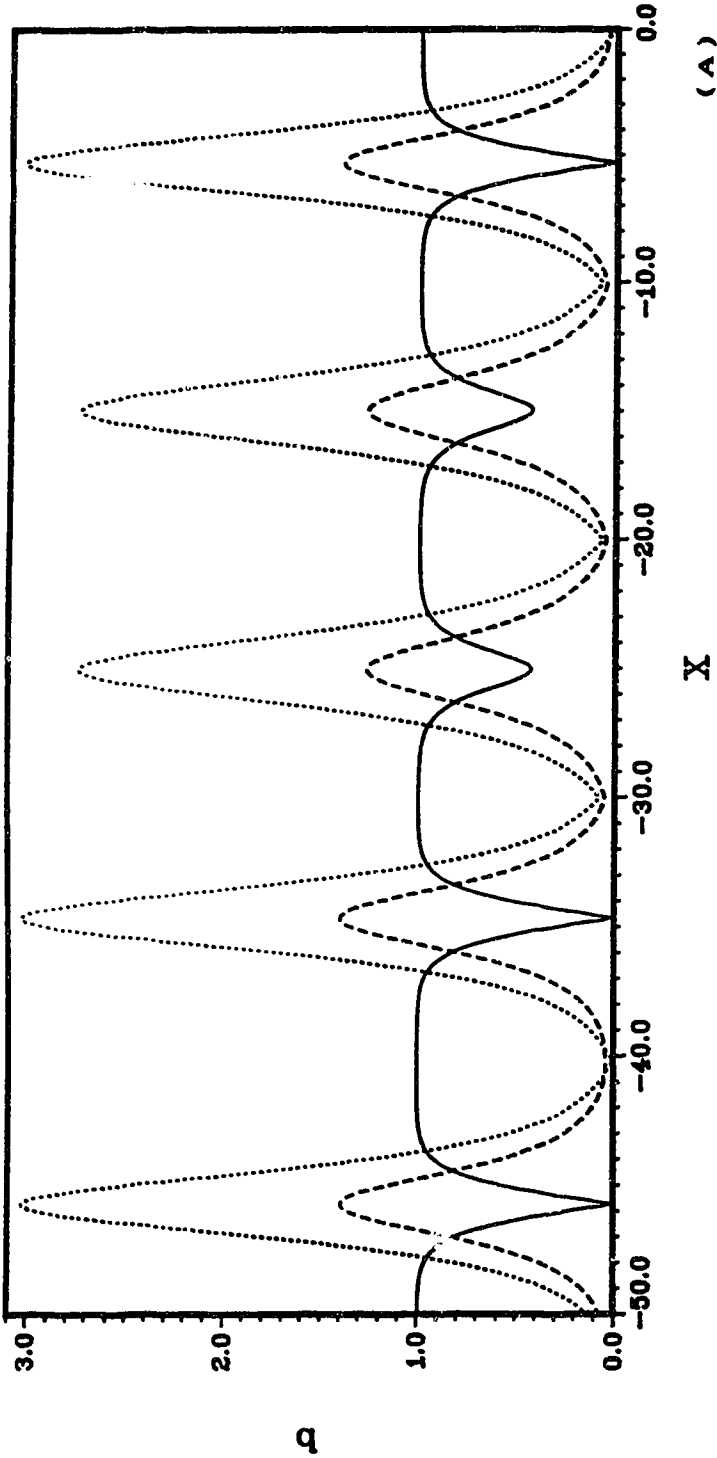
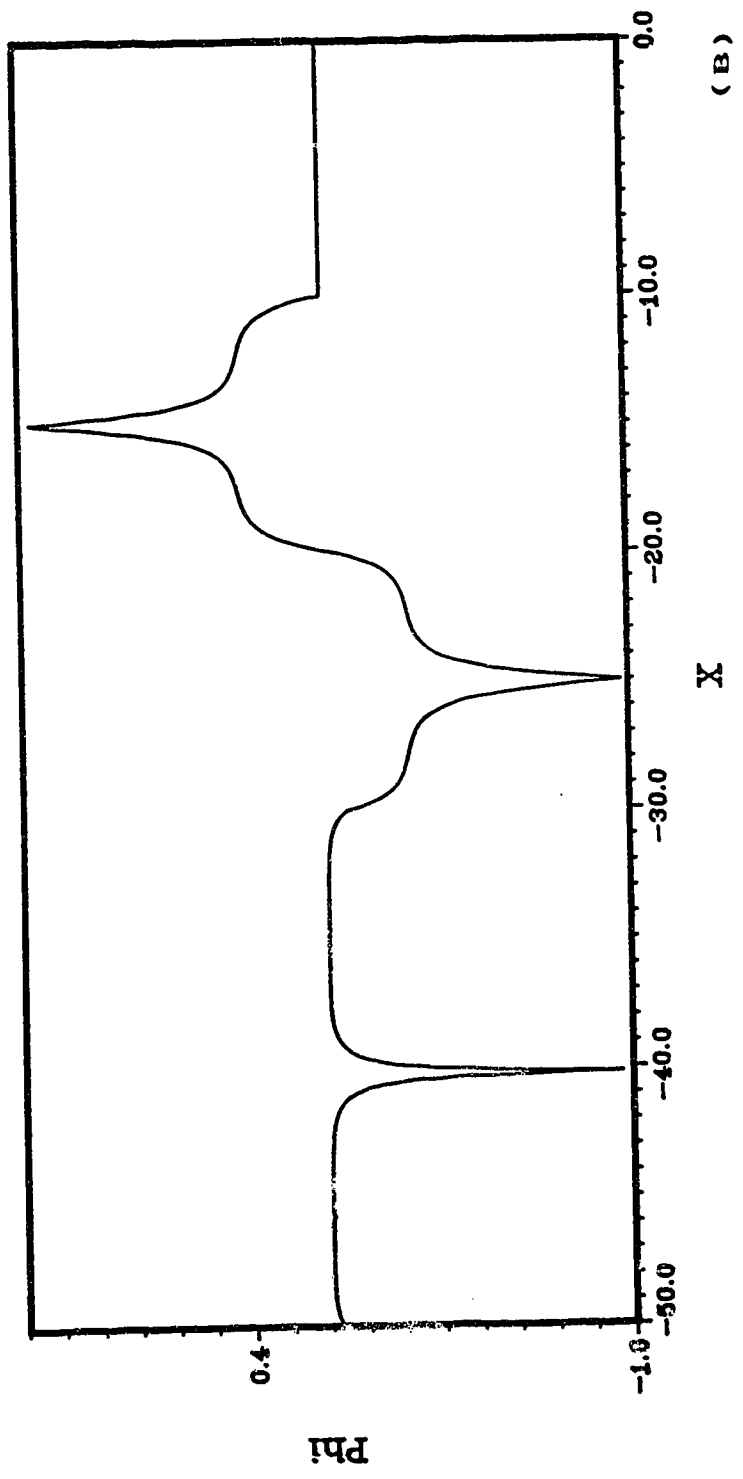
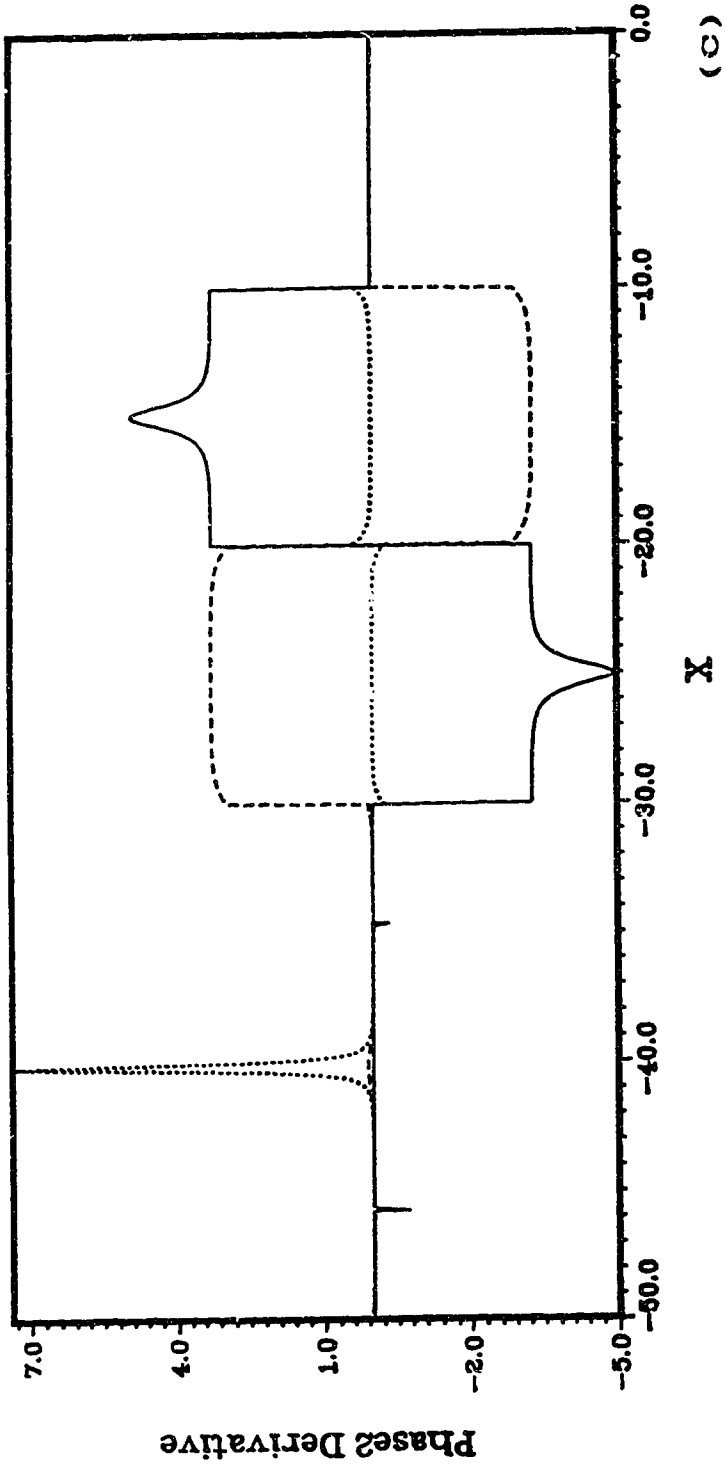


Fig. 4. Plots for initial amplitudes (5.3.2) and topography given by (5.2.1) and (5.3.1) with $H_0=10.0$.

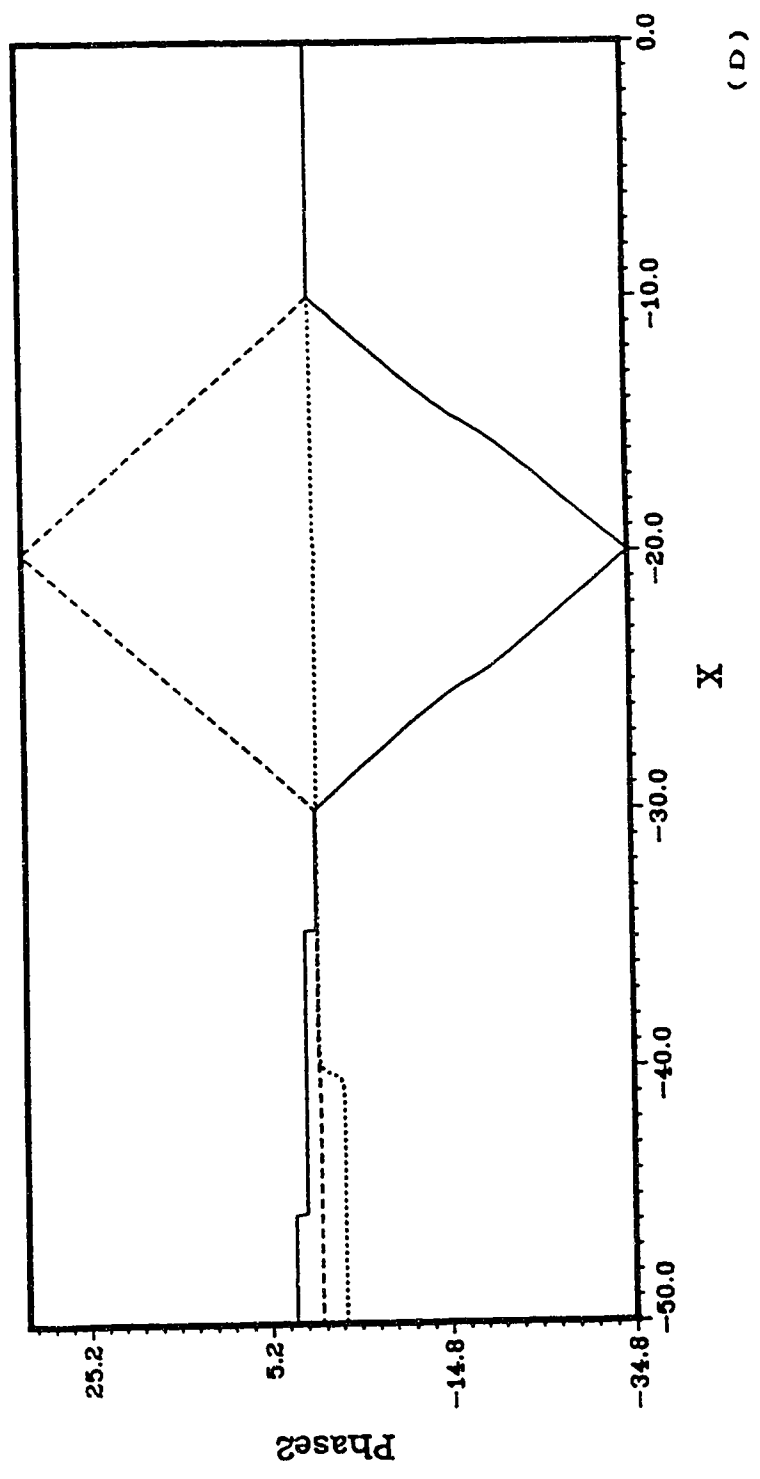
- (A) b_1 versus X
- (B) ϕ versus X
- (C) Phase2 Derivative versus X
- (D) Phase2 versus X
- (E) $b_1 \cos(\text{phase2})$ versus X

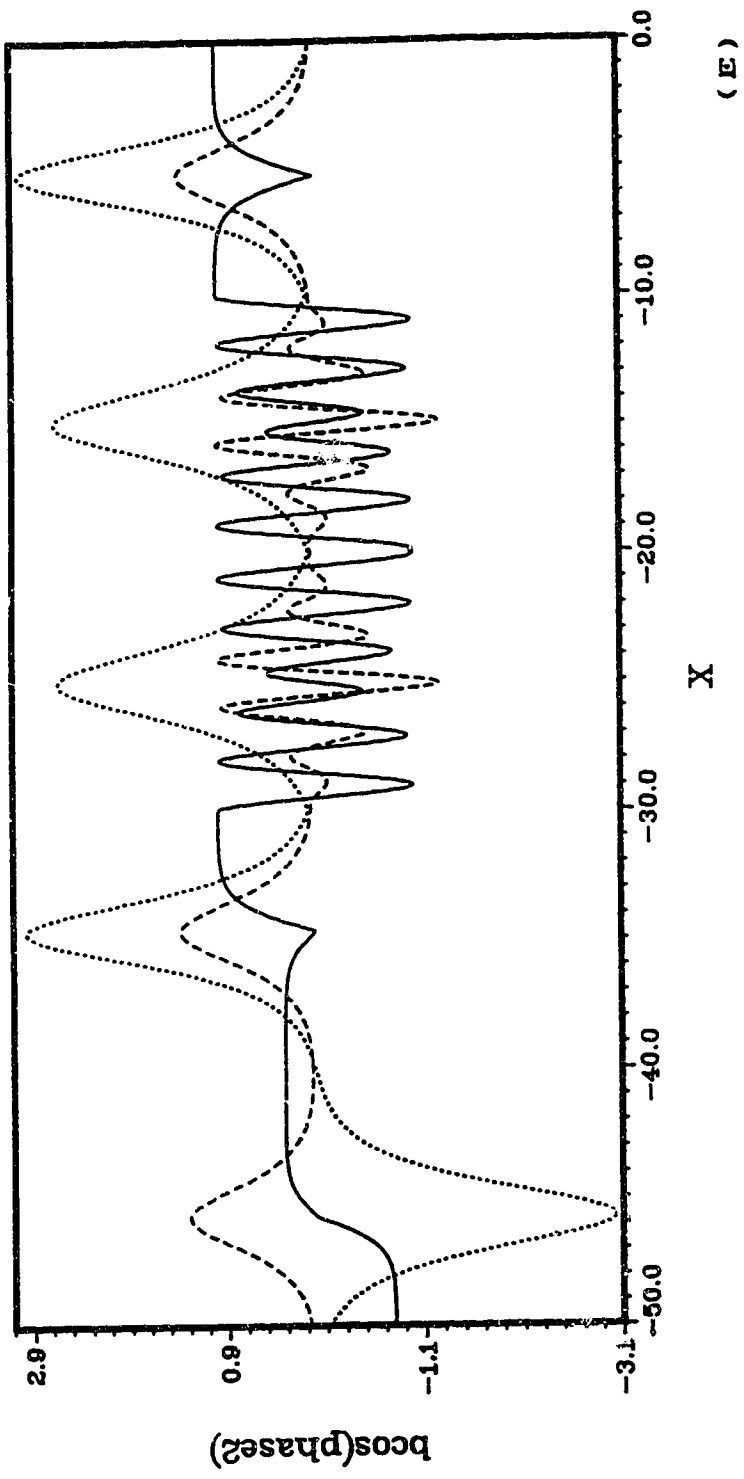
Wave 1, wave 2 and wave 3 are denoted by a thick curve, dashed curve and a dotted curve respectively.





(c)





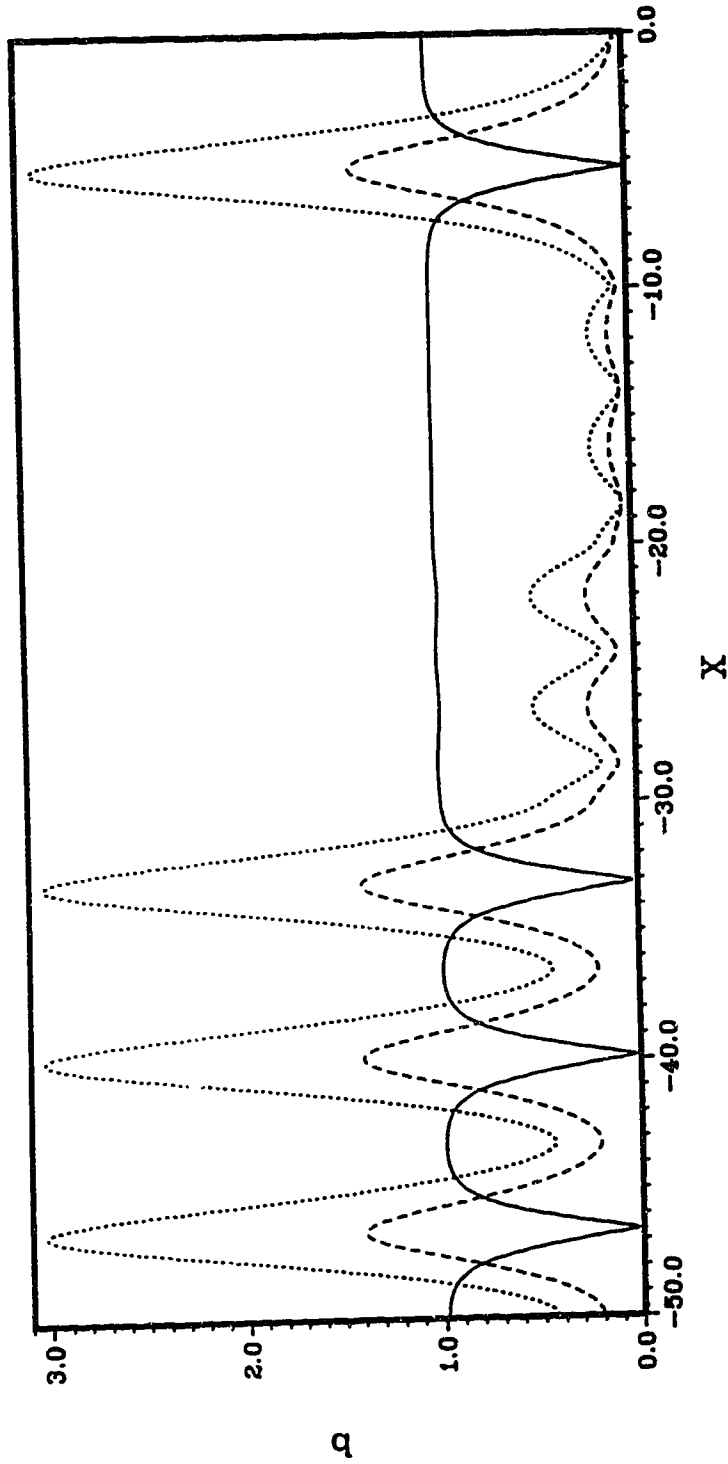
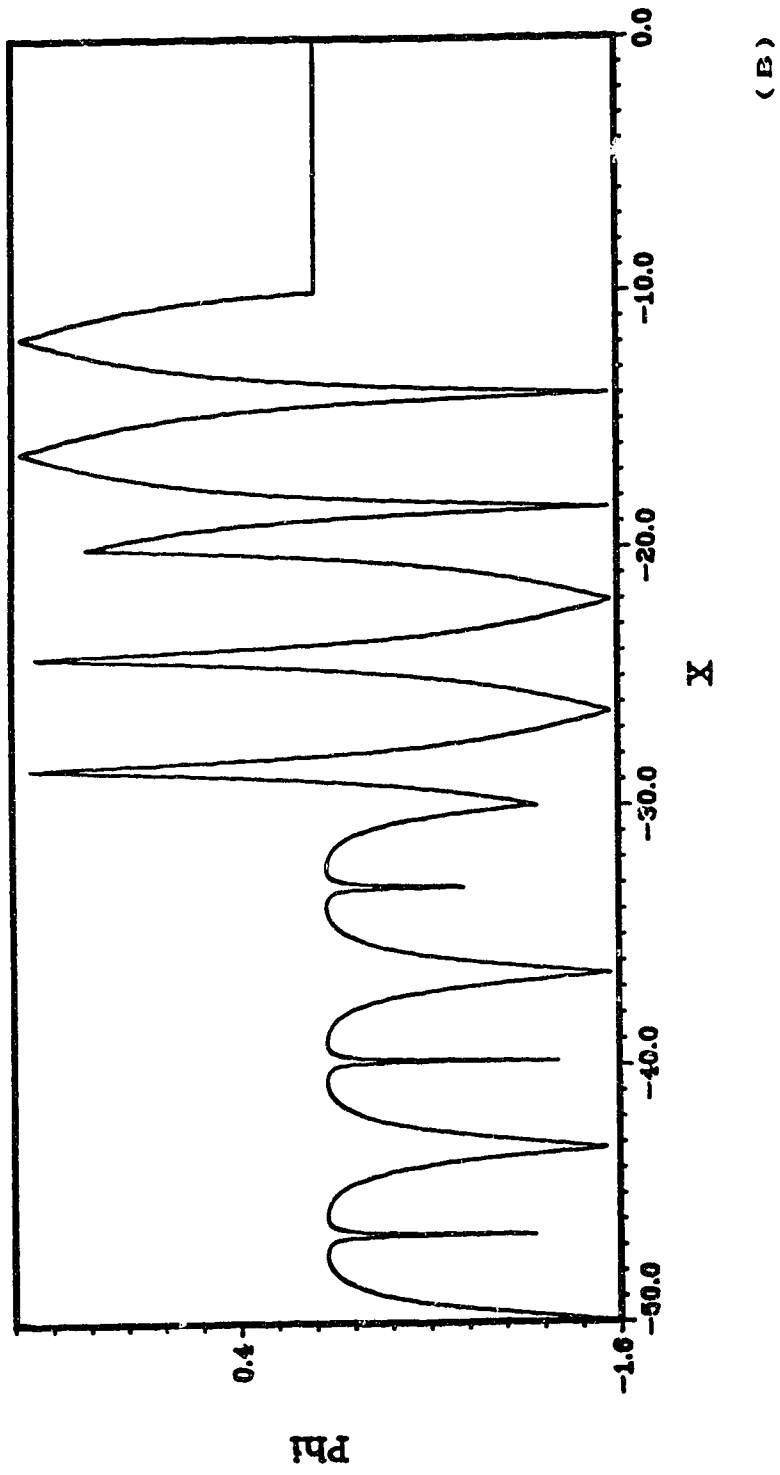


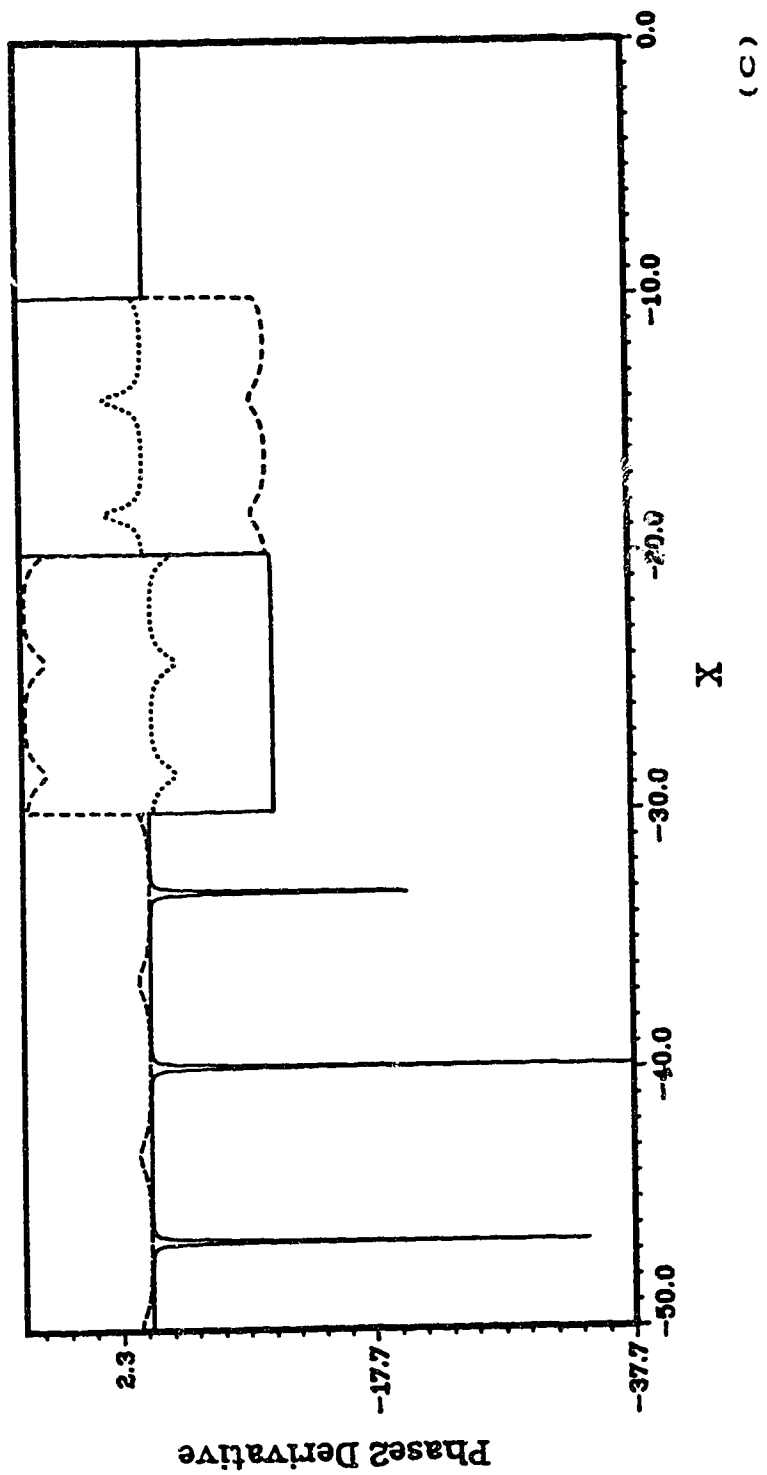
Fig. 5. Plots for initial amplitudes (5.3.2) and topography given by (5.2.1) and (5.3.1) with $H_0=30.0$. (A)

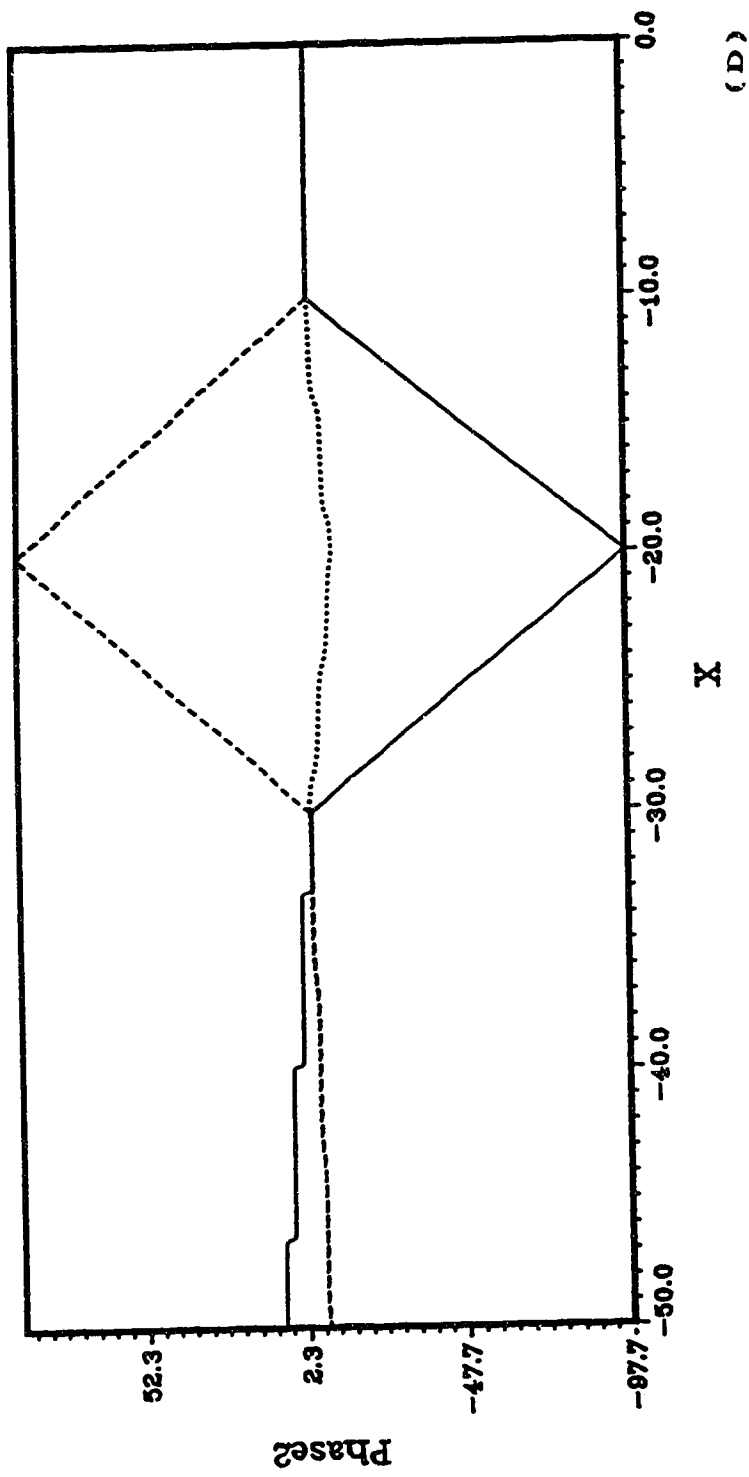
- (A) b_1 versus X
- (B) ϕ_1 versus X
- (C) Phase2 Derivative versus X
- (D) Phase2 versus X
- (E) $b_1 \cos(\text{phase2})$ versus X

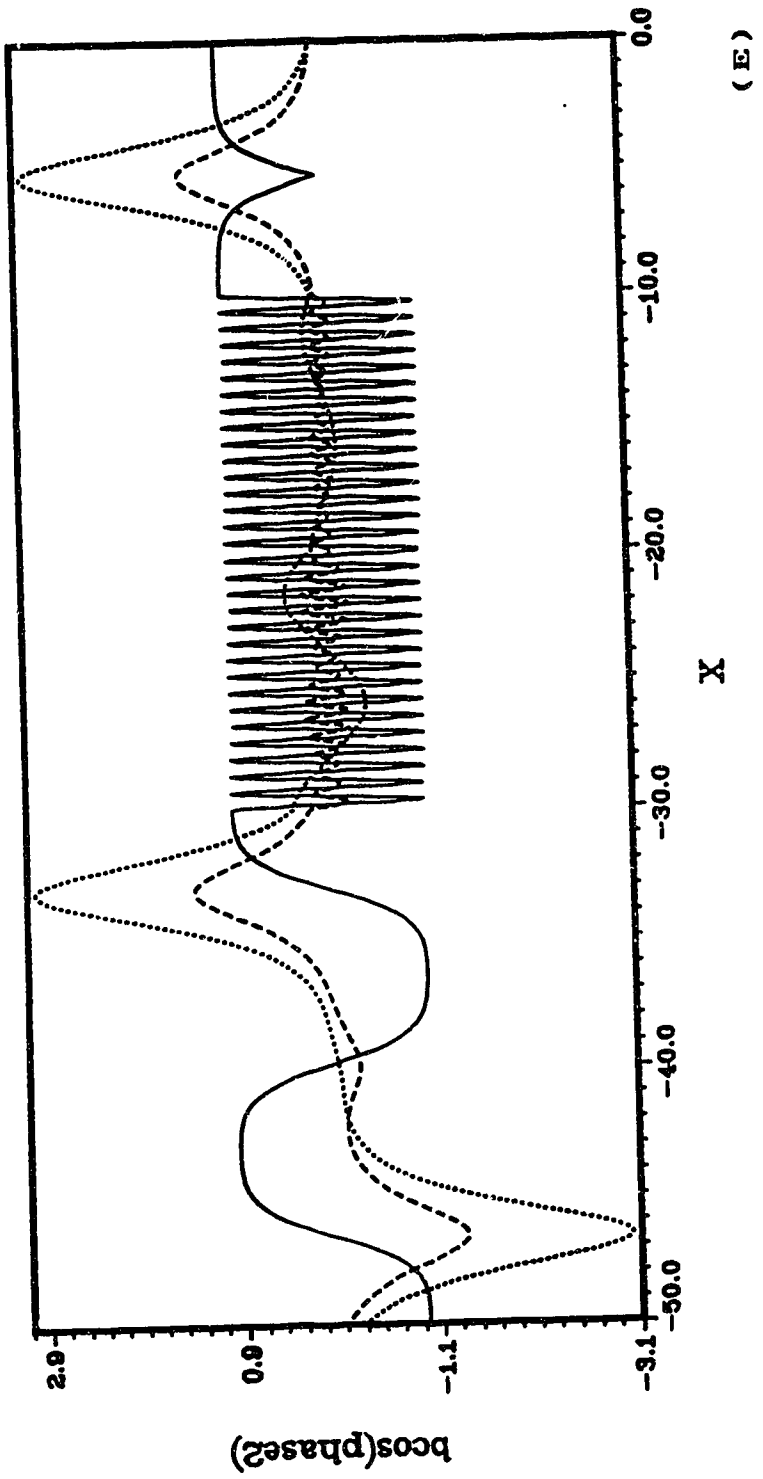
Wave 1, wave 2 and wave 3 are denoted by a thick curve, dashed curve and a dotted curve respectively.



(B)







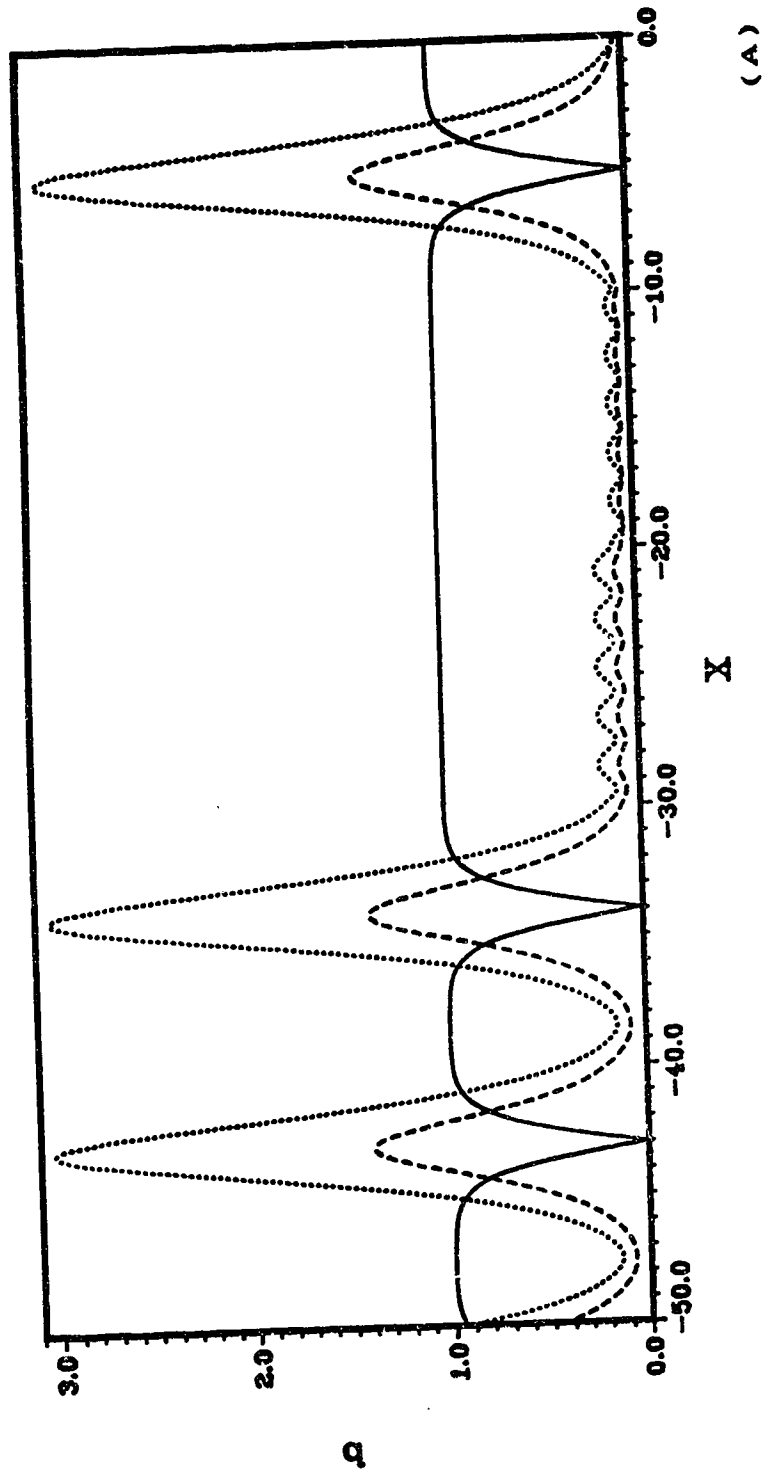
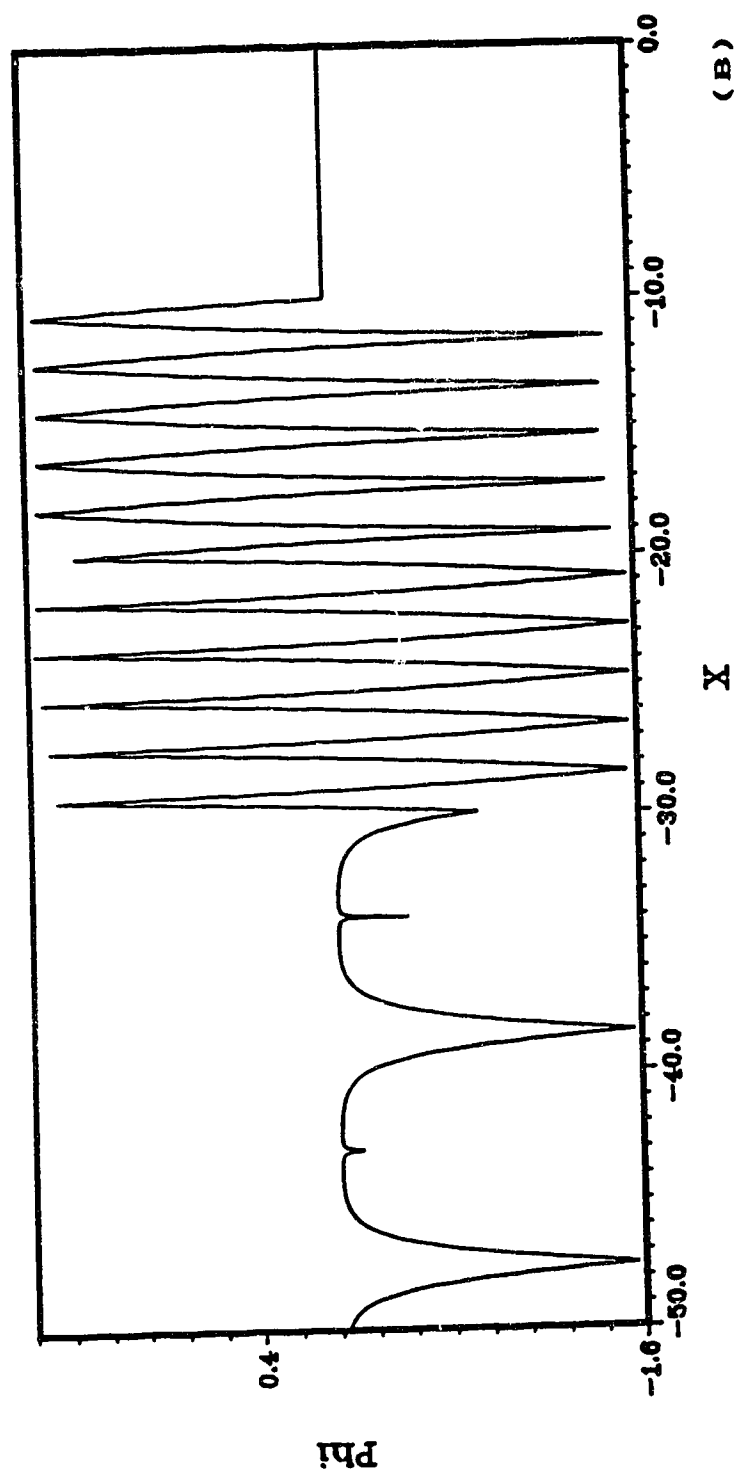
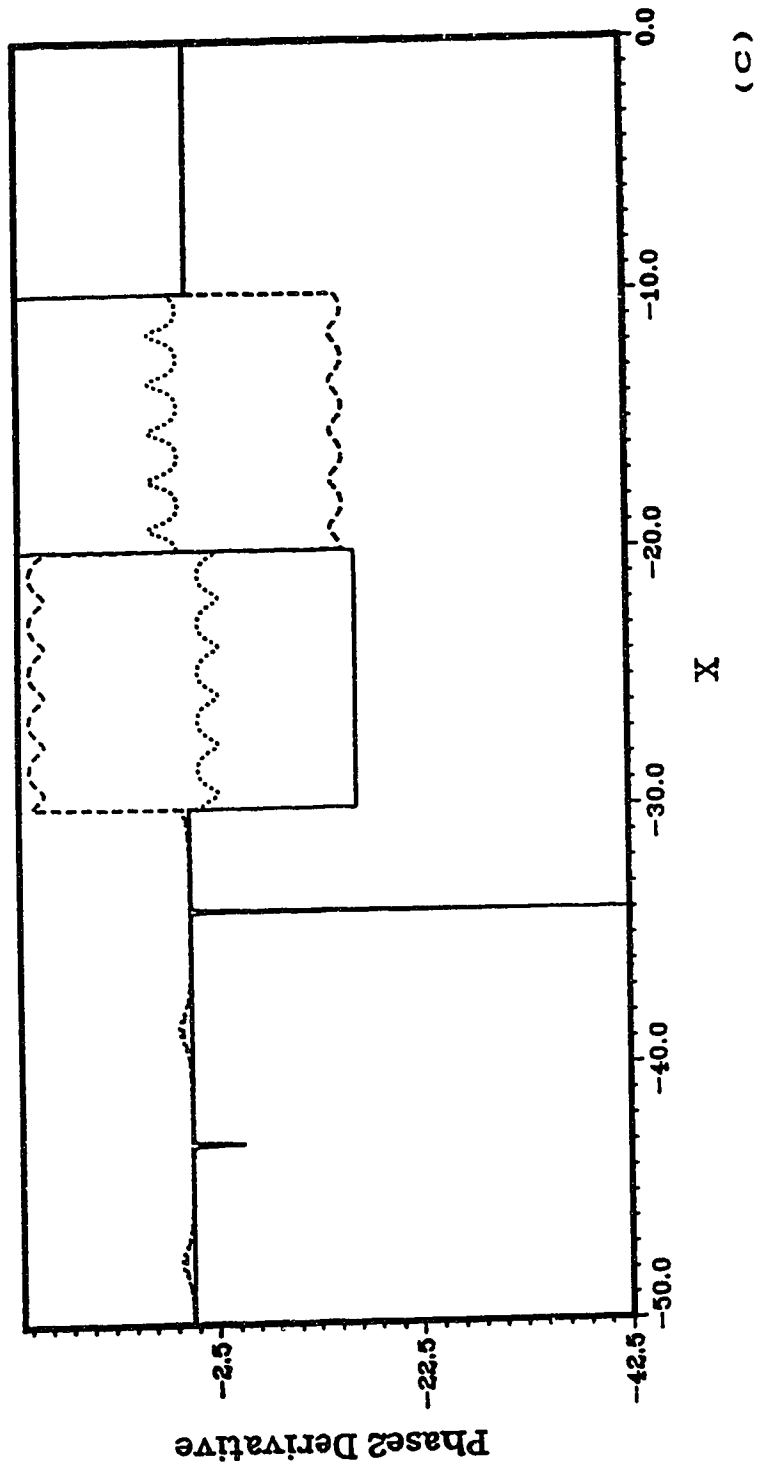


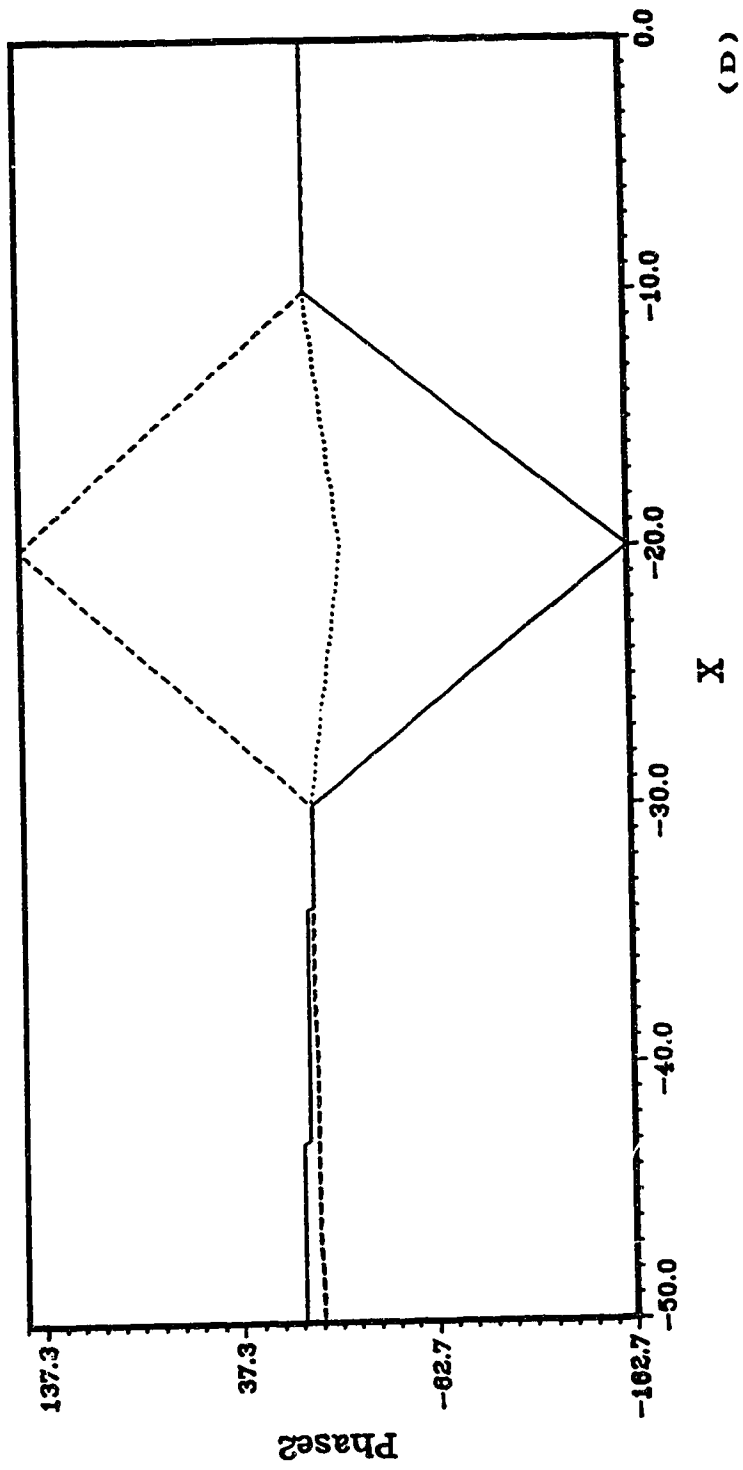
Fig. 6. Plots for initial amplitudes (5.3.2) and topography given by (5.2.1) and (5.3.1) with $H_0=50.0$.

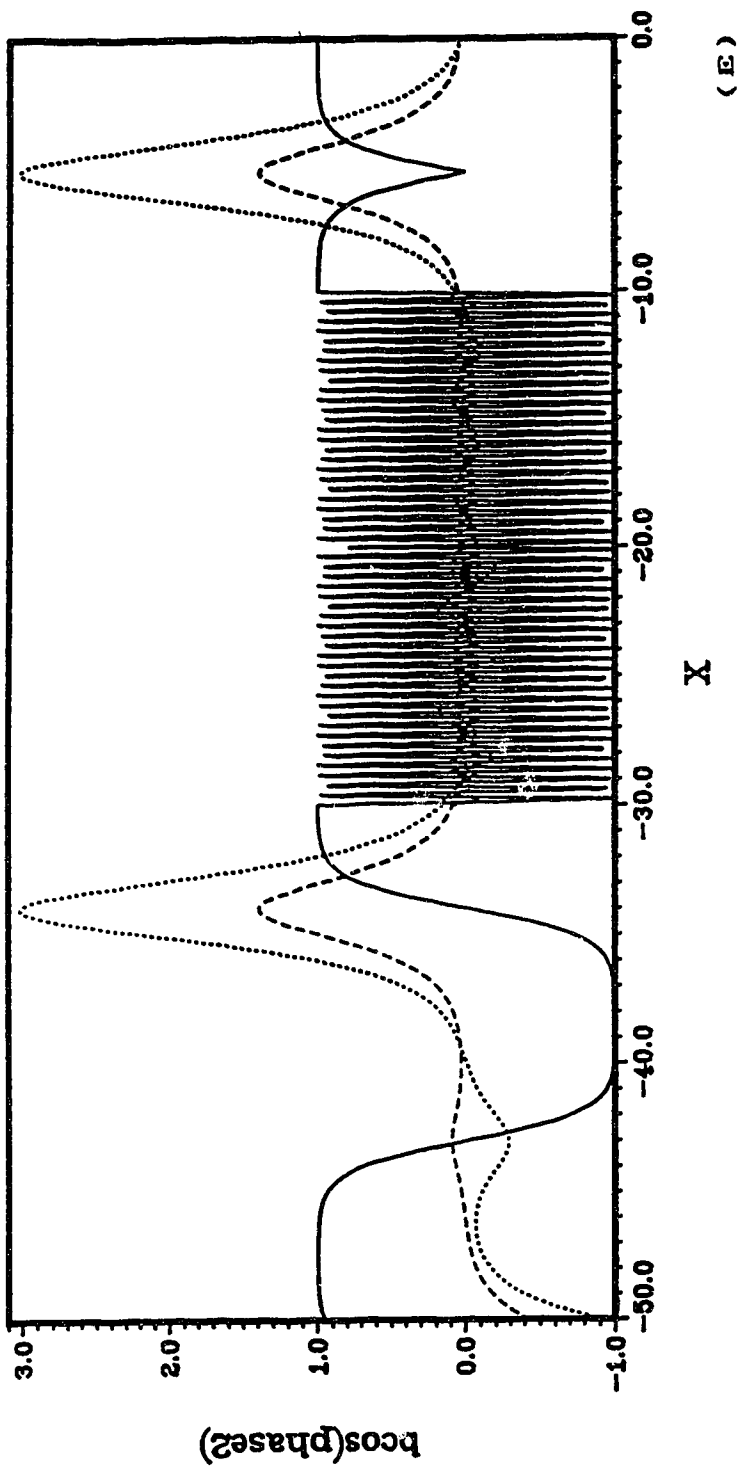
- (A) b_1 versus X
- (B) Φ versus X
- (C) Phase2 Derivative versus X
- (D) Phase2 versus X
- (E) $b_1 \cos(\text{phase2})$ versus X

Wave 1, wave 2 and wave 3 are denoted by a thick curve, dashed curve and a dotted curve respectively.









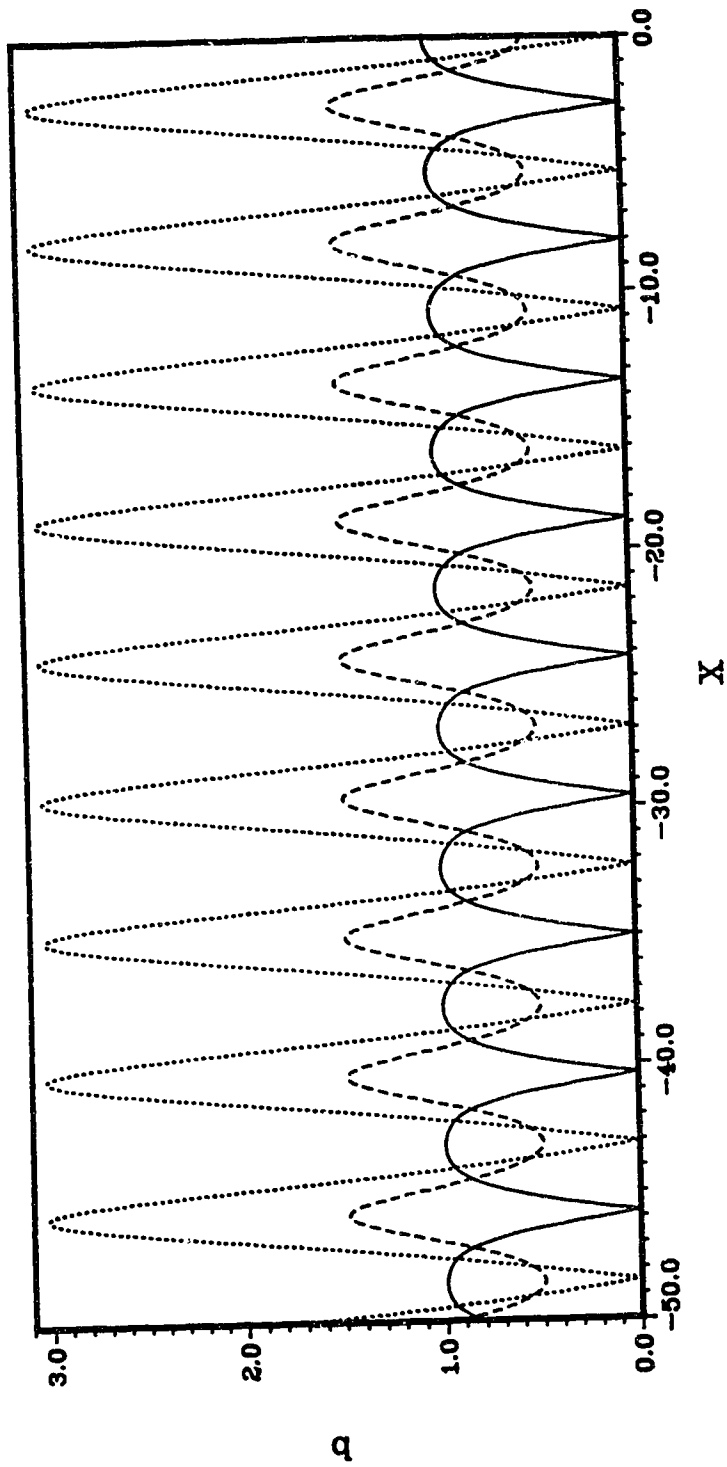


Fig. 7. Plot of b_j versus X for initial amplitudes (5.3.3) and topography given by (5.2.1) and (5.3.1) with $H_0=0.0$. Wave 1, wave 2 and wave 3 are denoted by a thick curve, dashed curve and a dotted curve respectively.

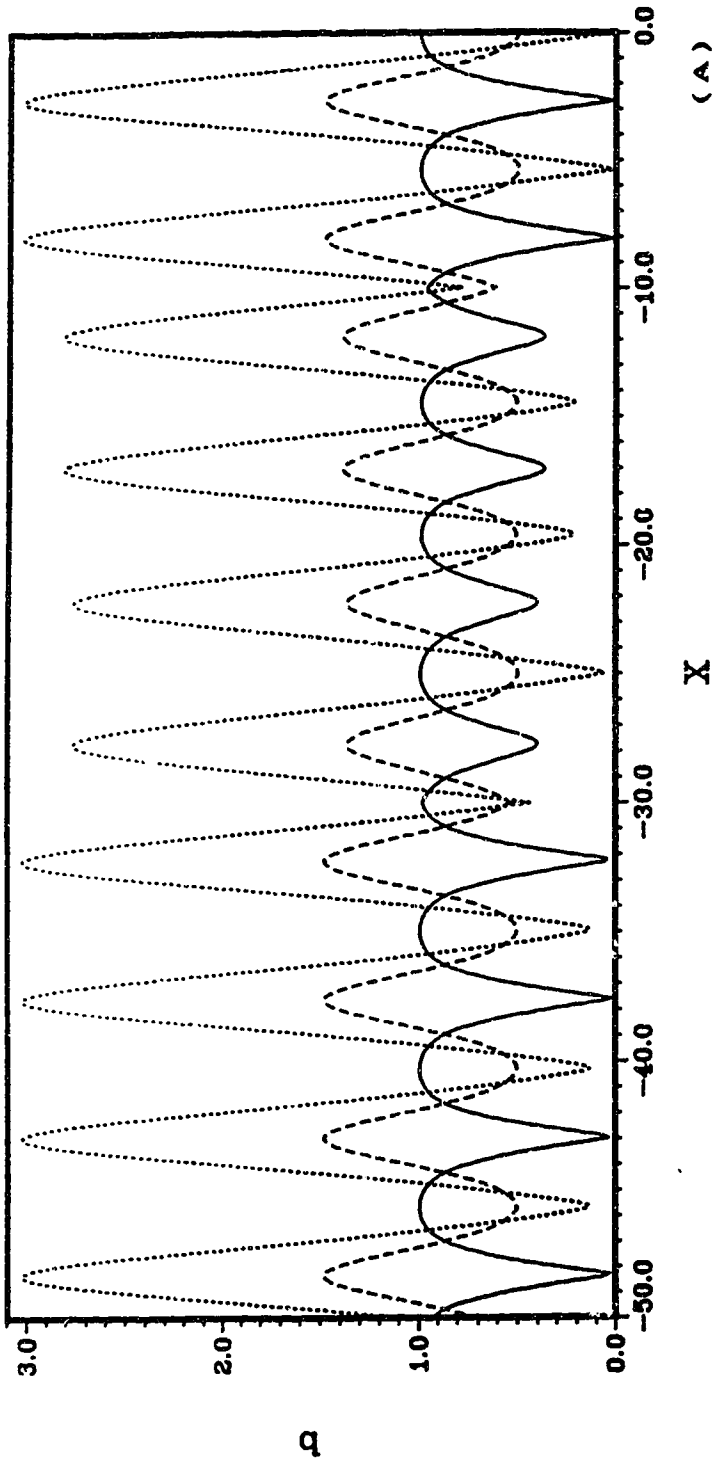
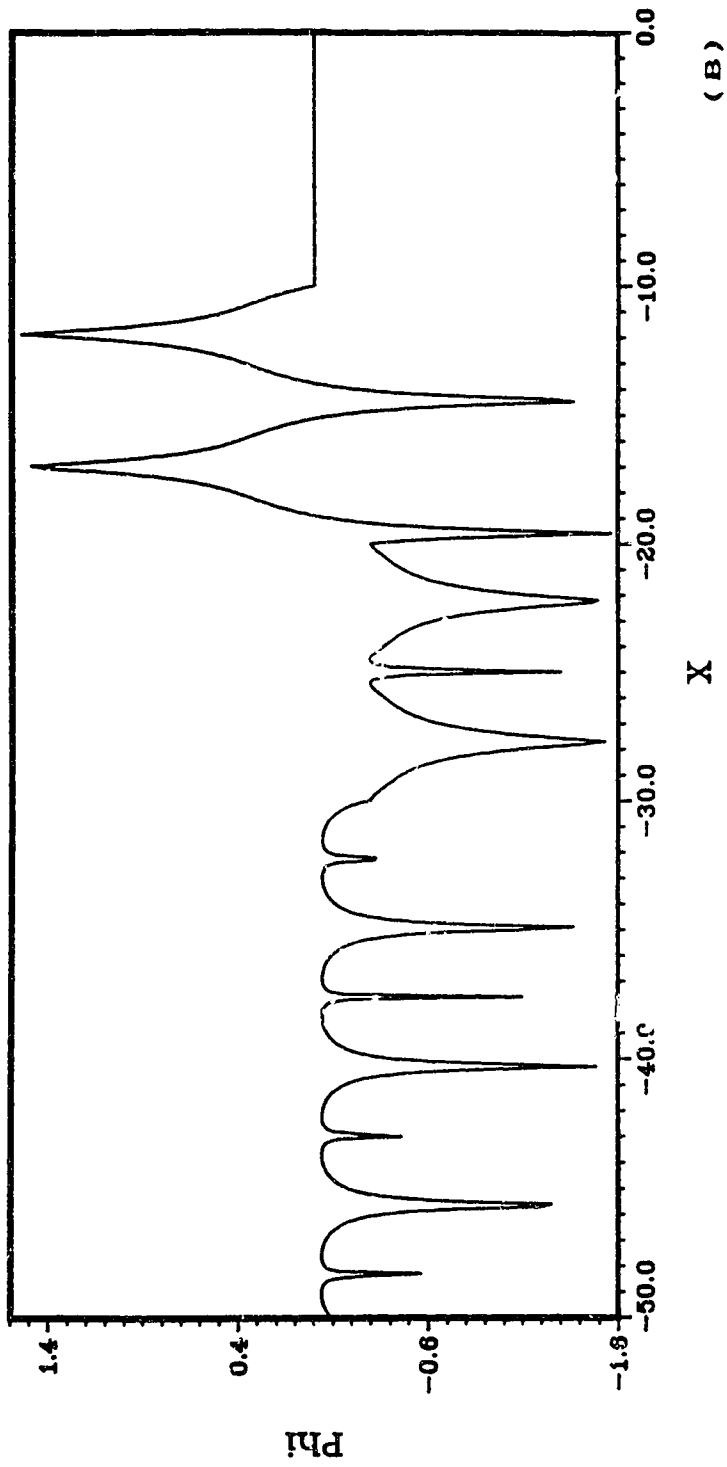
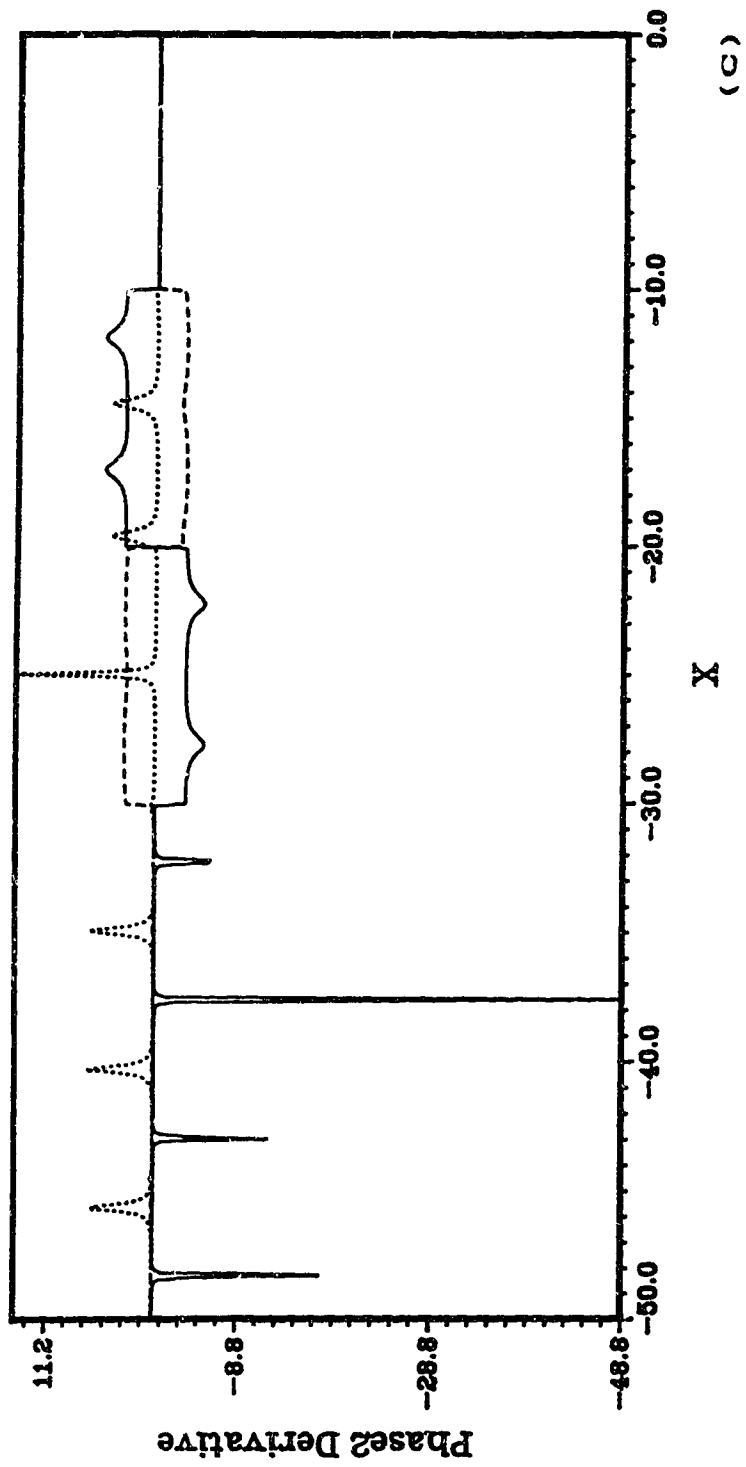


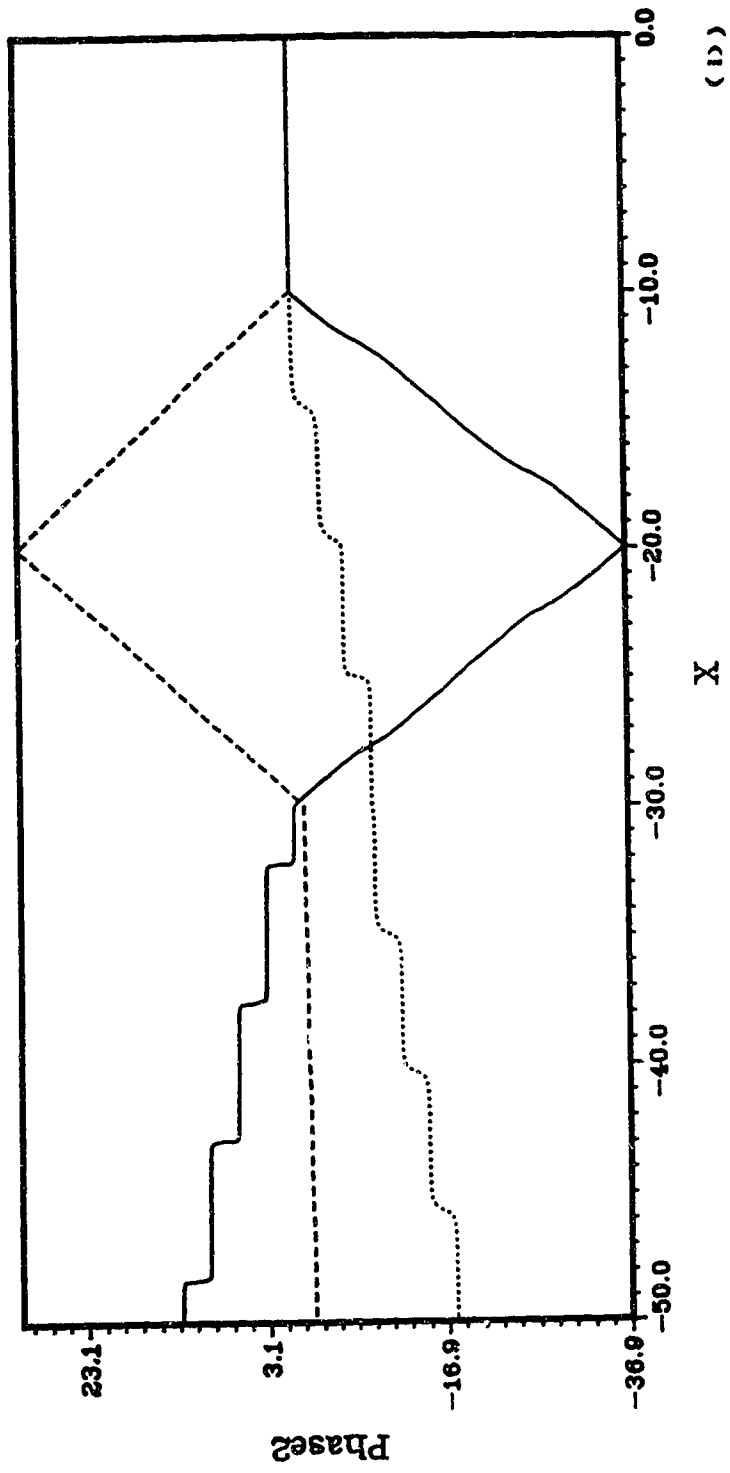
Fig. 8. Plots for initial amplitudes (5.3.3) and topography given by (5.2.1) and (5.3.1) with $H_0=10.0$.

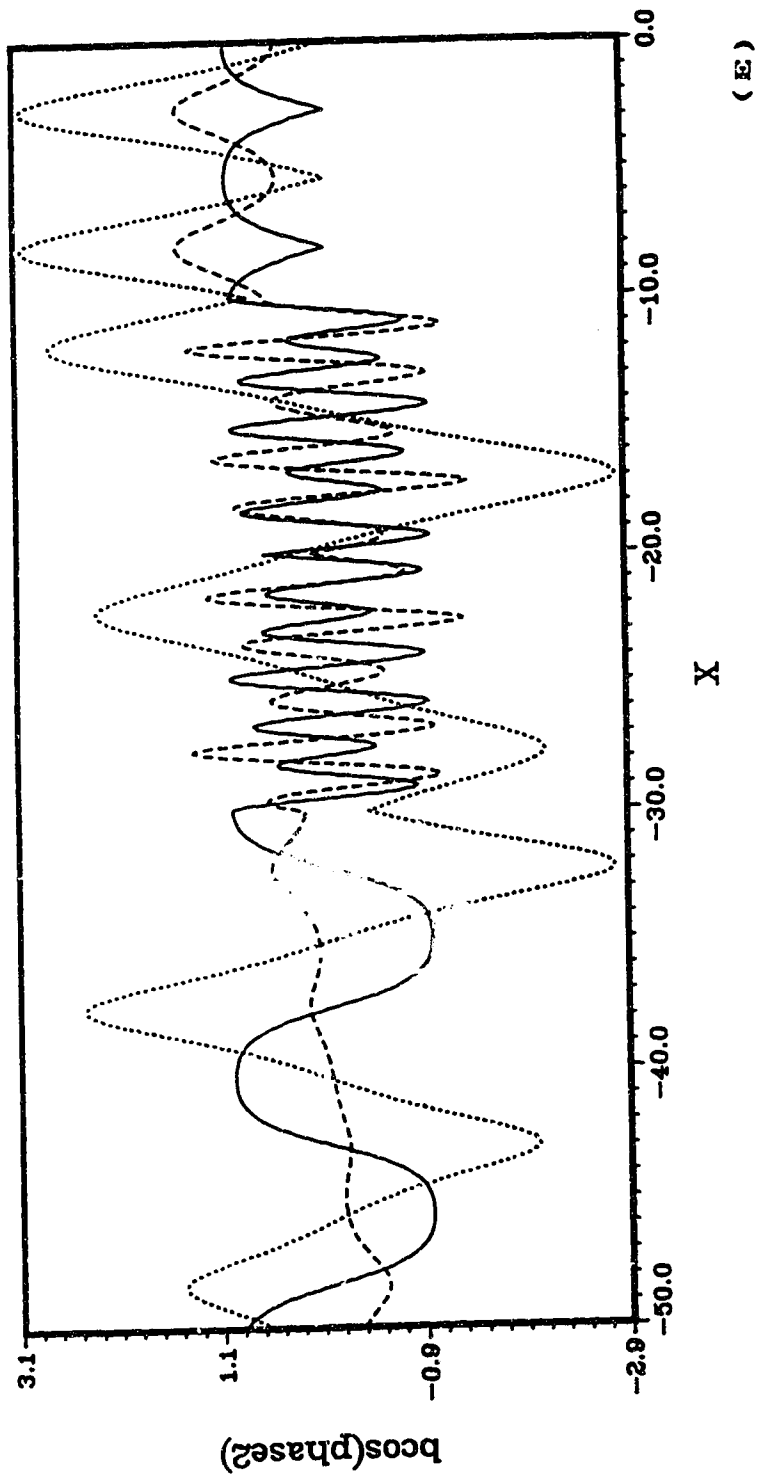
- (A) b_1 versus X
- (B) ϕ_1 versus X
- (C) Phase2 Derivative versus X
- (D) Phase2 versus X
- (E) $b_1 \cos(\text{phase2})$ versus X

Wave 1, wave 2 and wave 3 are denoted by a thick curve, dashed curve and a dotted curve respectively.









(E)

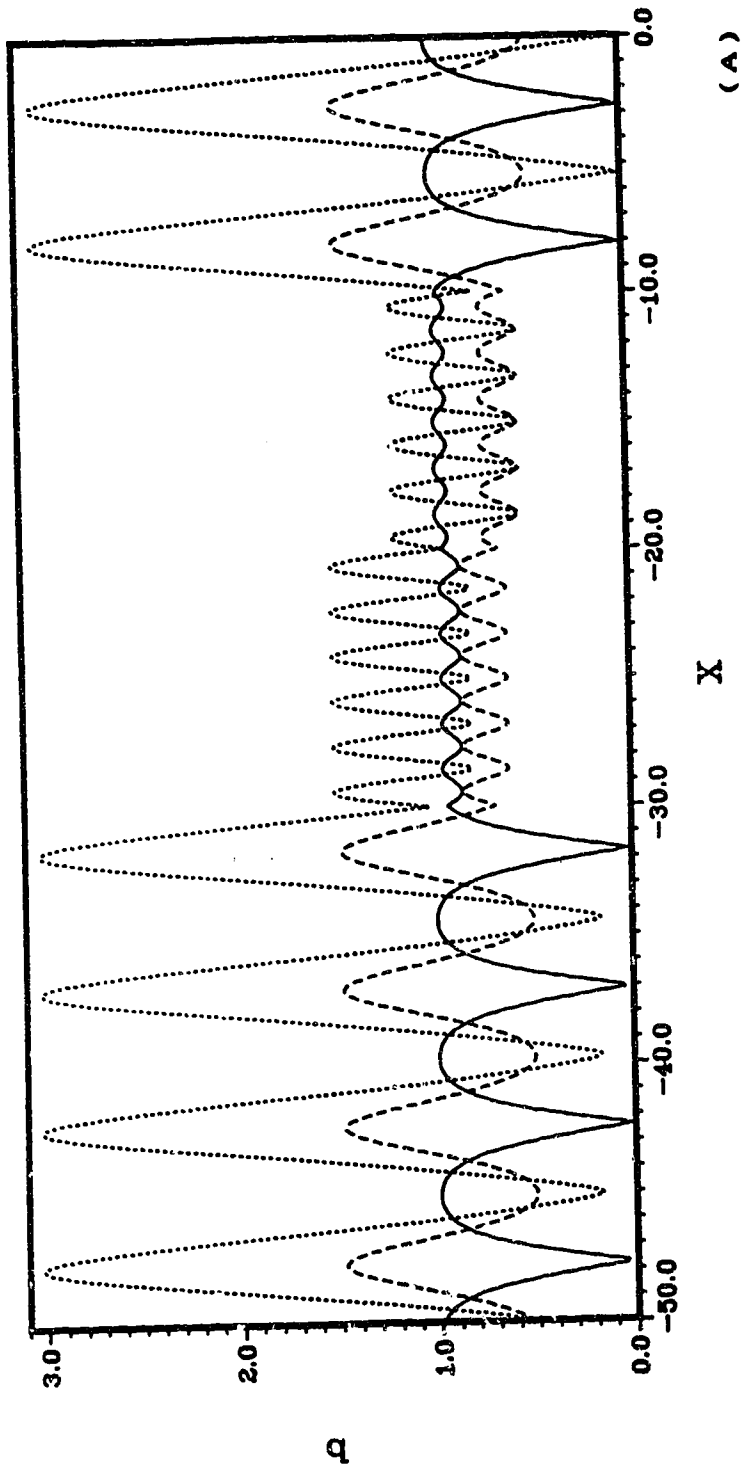
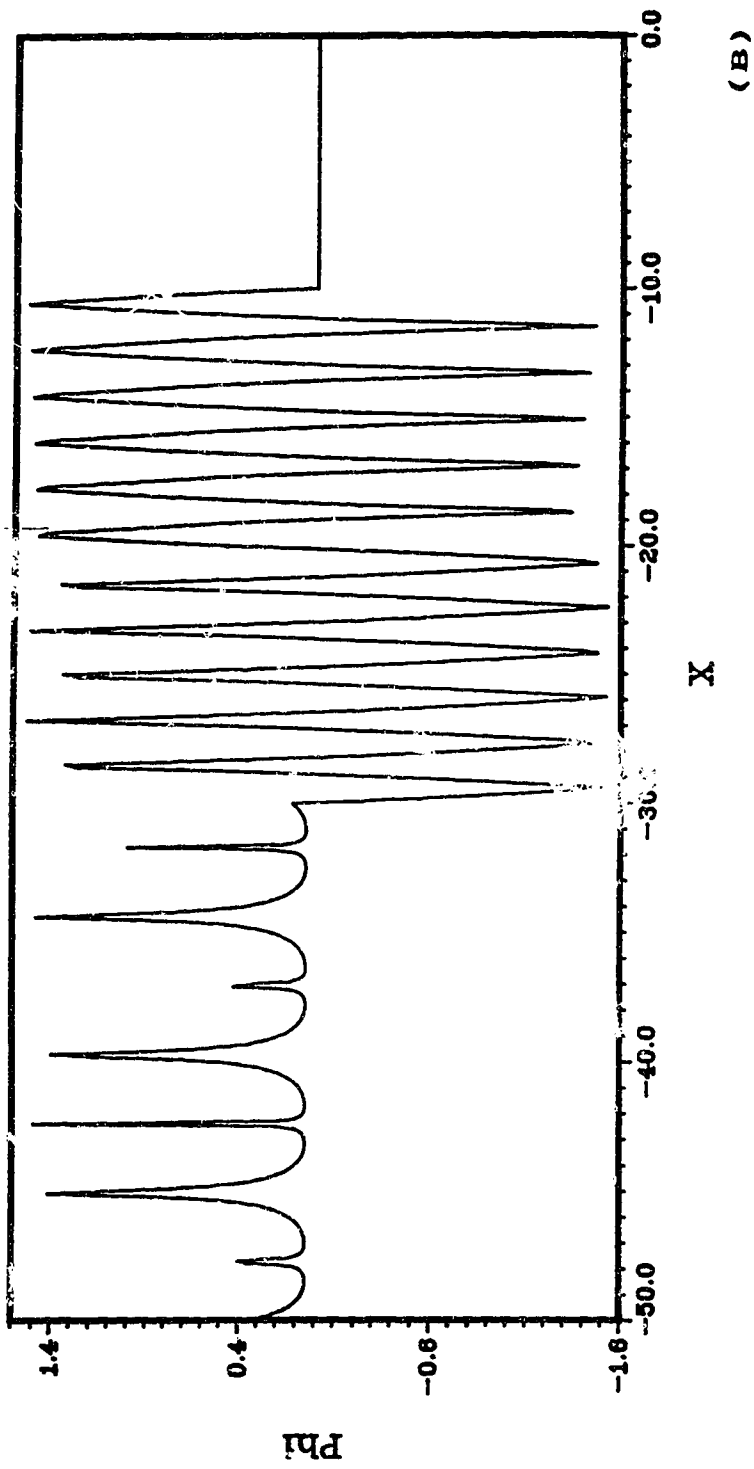
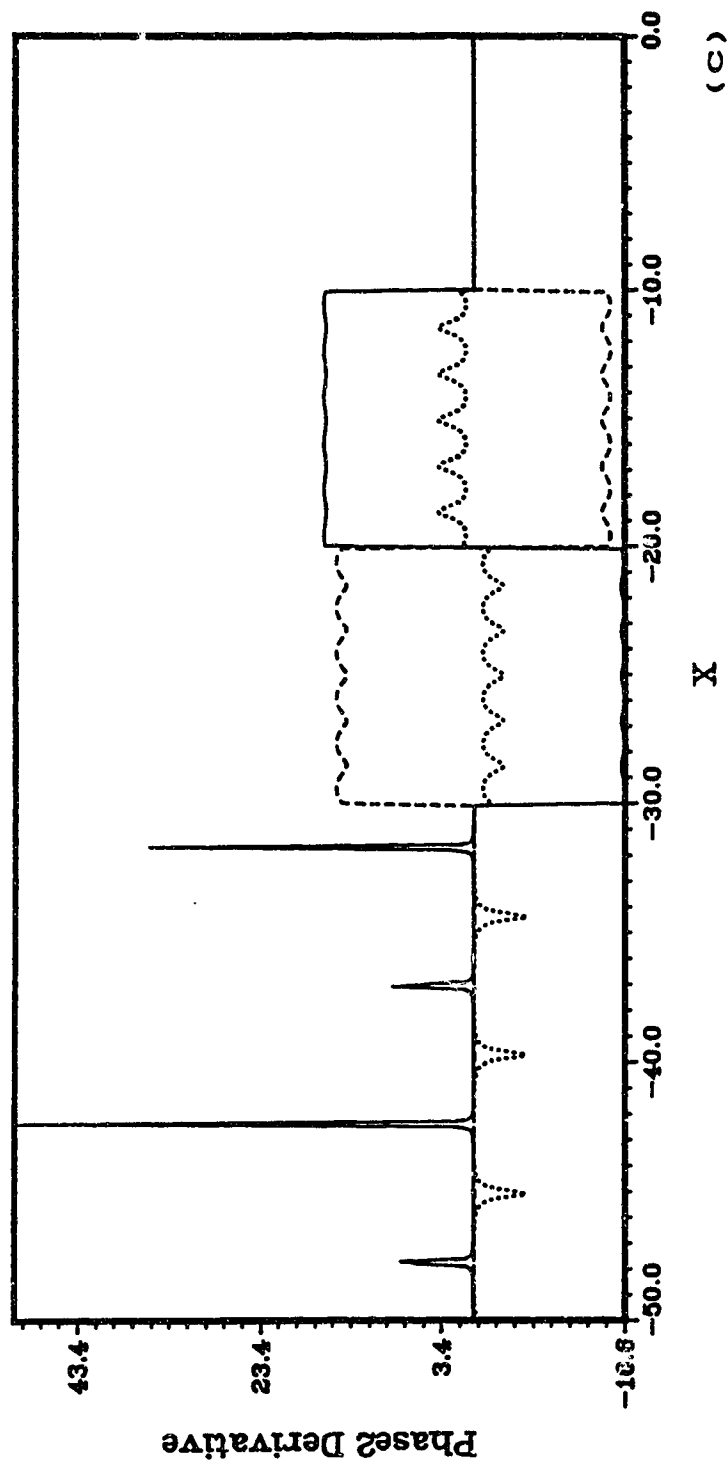


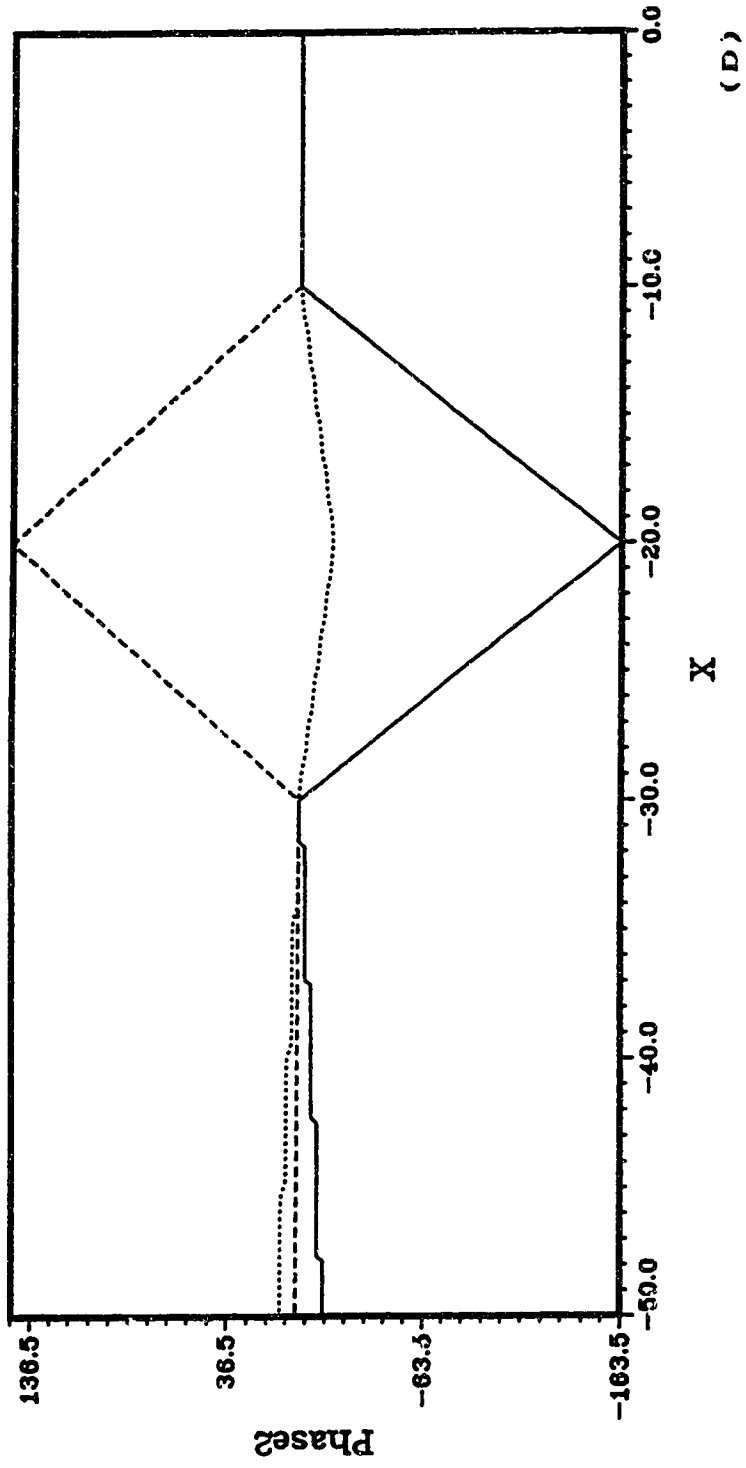
Fig. 9. Plots for initial amplitudes (5.3.3) and topography given by (5.2.1) and (5.3.1) with $H_0=50.0$.

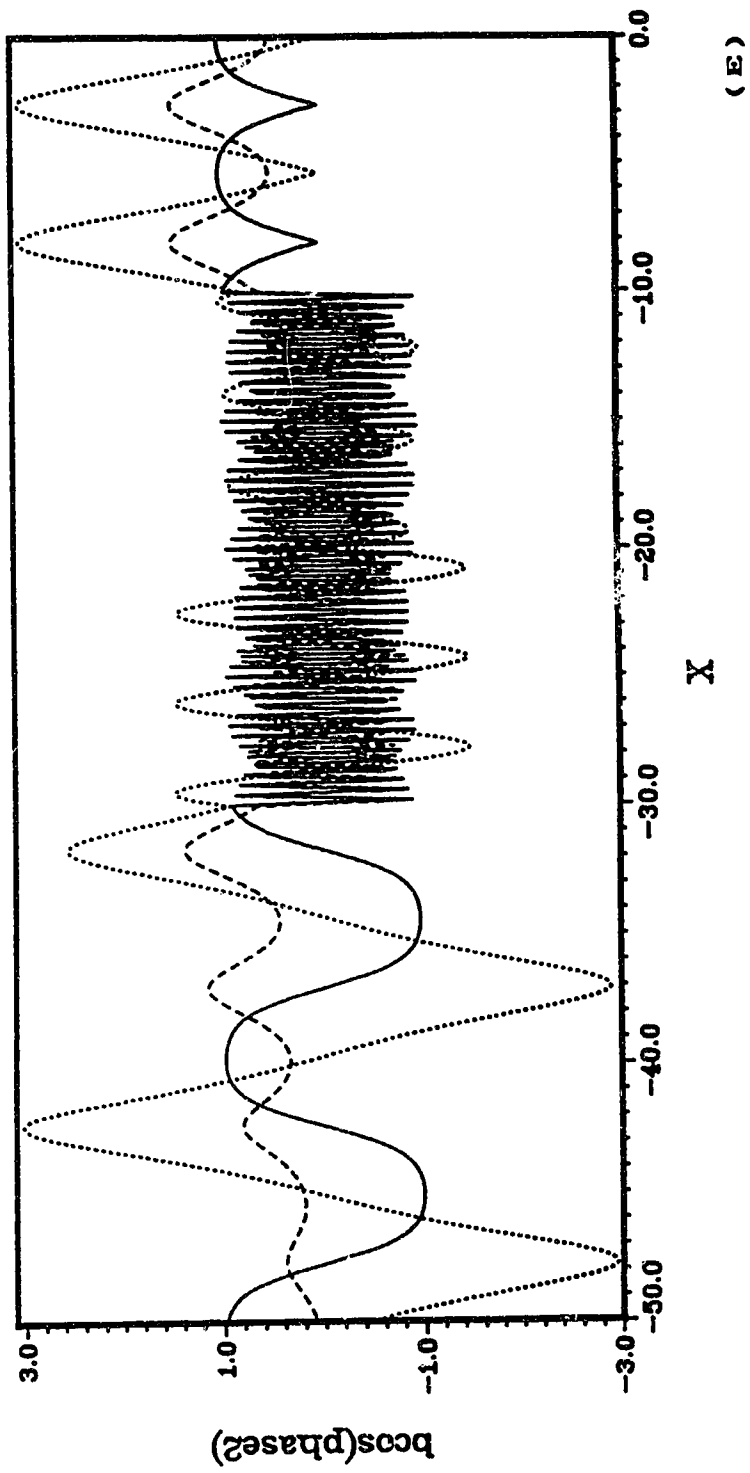
- (A) b_i versus X
- (B) ϕ_{i1} versus X
- (C) Phase2 Derivative versus X
- (D) Phase2 versus X
- (E) $b_i \cos(\text{phase2})$ versus X

Wave 1, wave 2 and wave 3 are denoted by a thick curve, dashed curve and a dotted curve respectively.









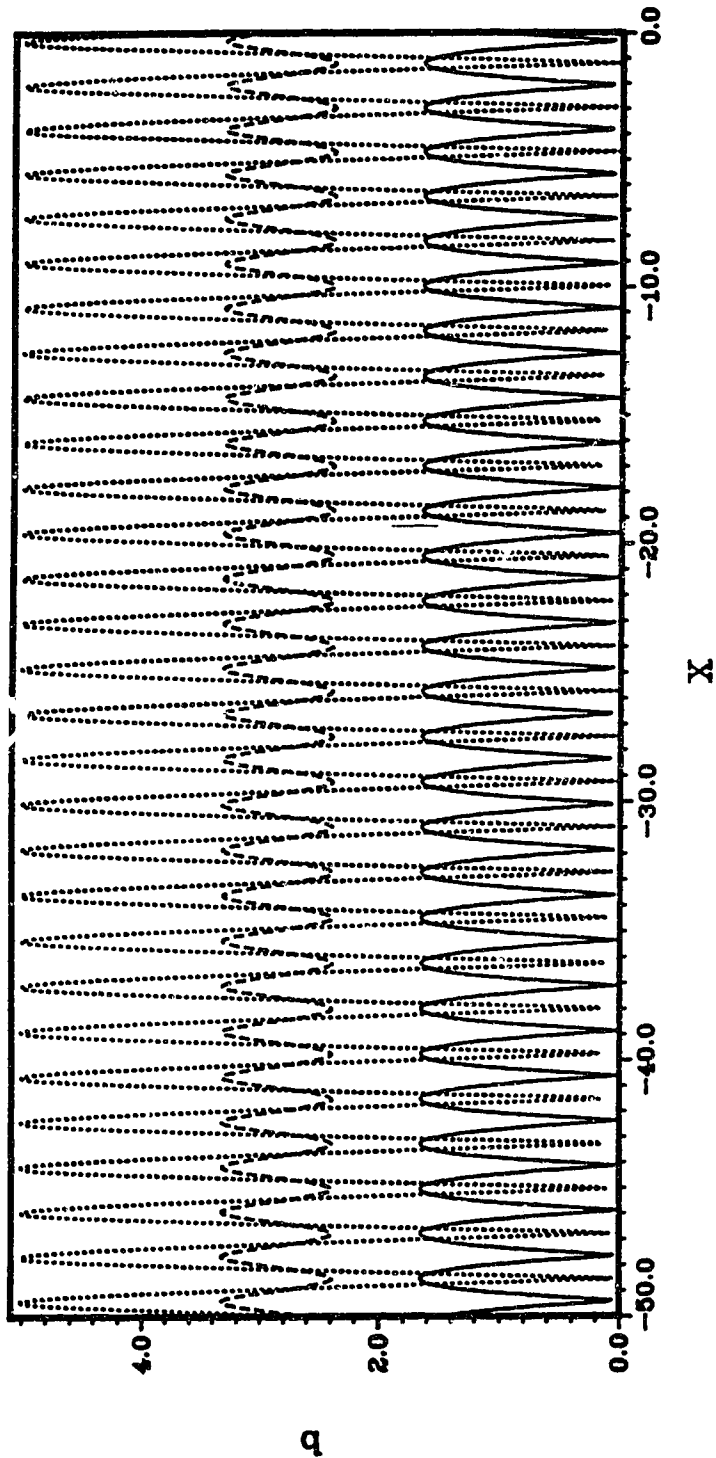


Fig. 10. Plot of b_j versus X for initial amplitudes (5.3.4) and topography given by (5.2.1) and (5.3.1) with $H_0=0.0$. Wave 1, wave 2 and wave 3 are denoted by a thick curve, dashed curve and a dotted curve respectively.

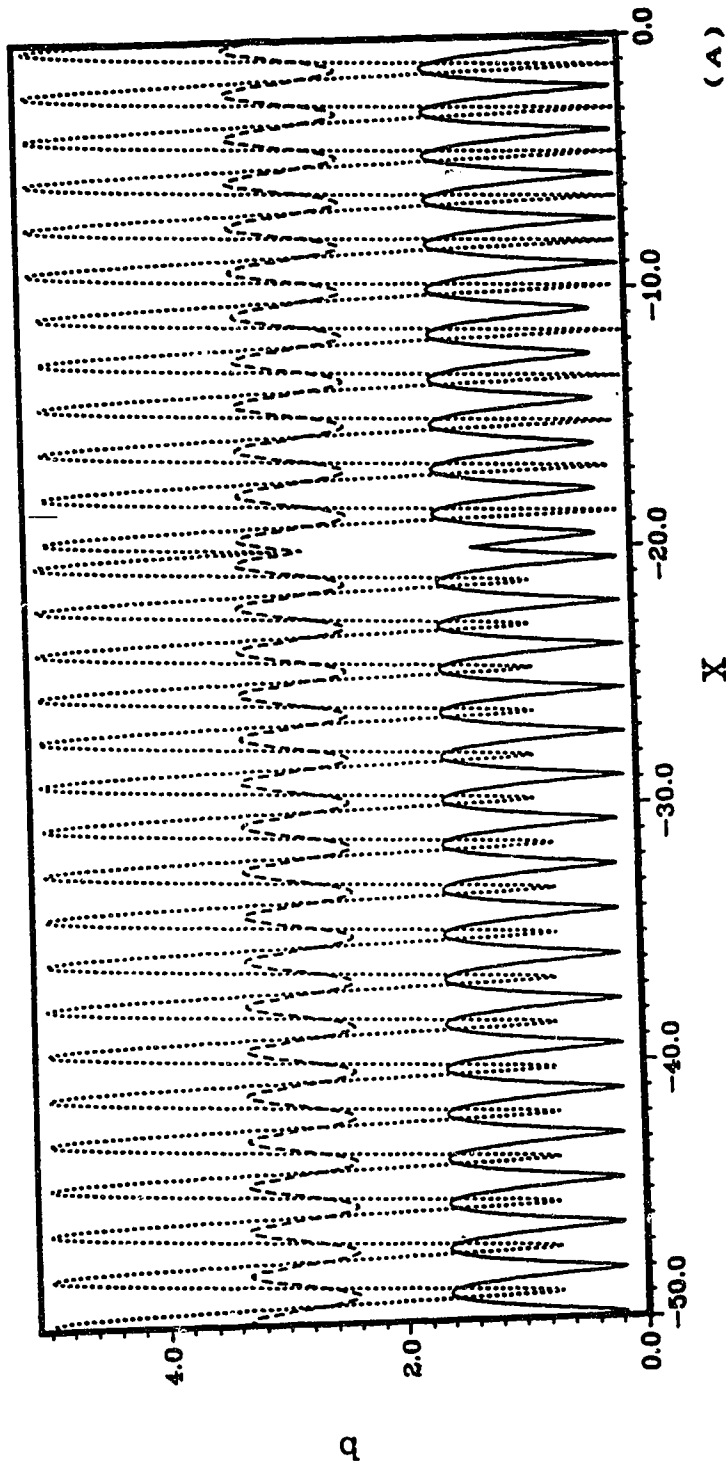
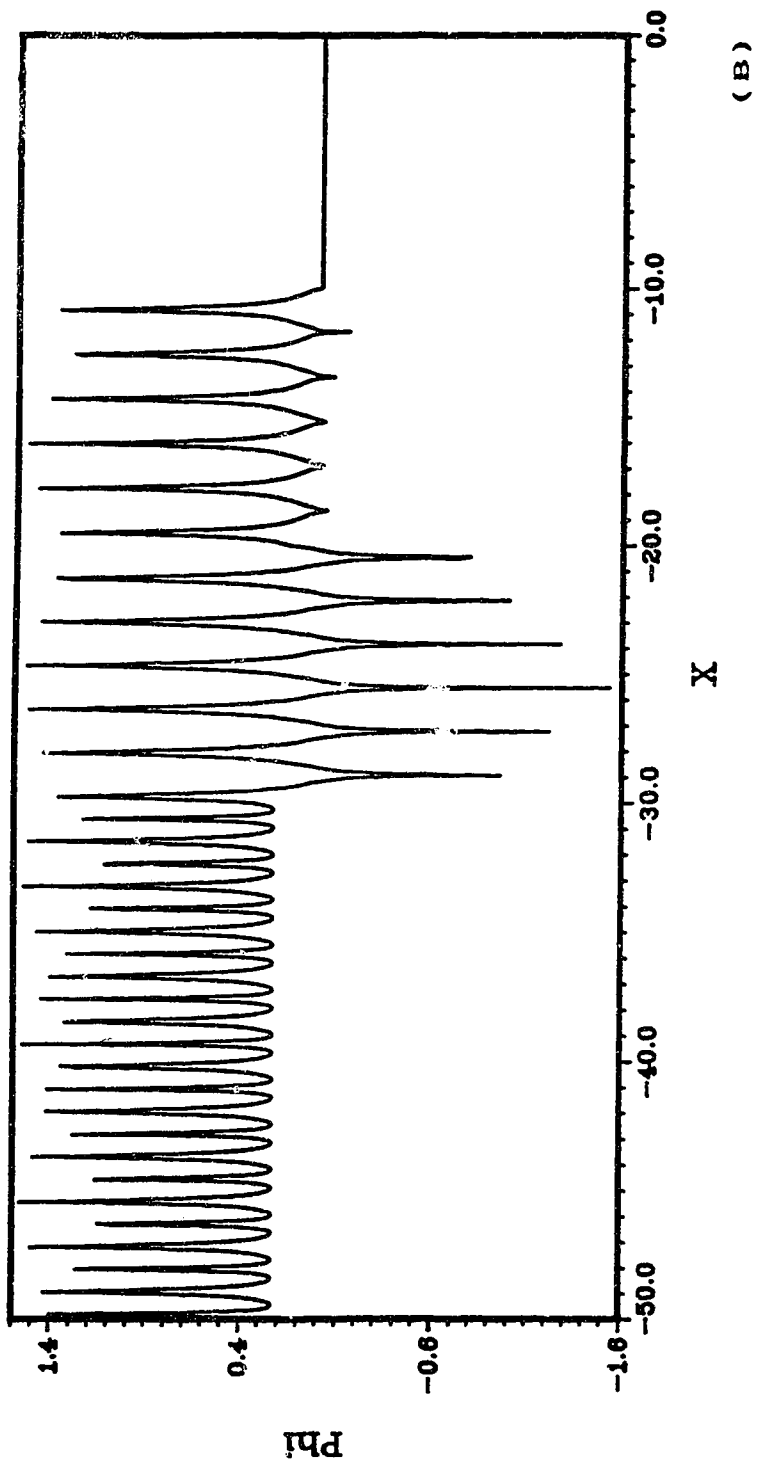


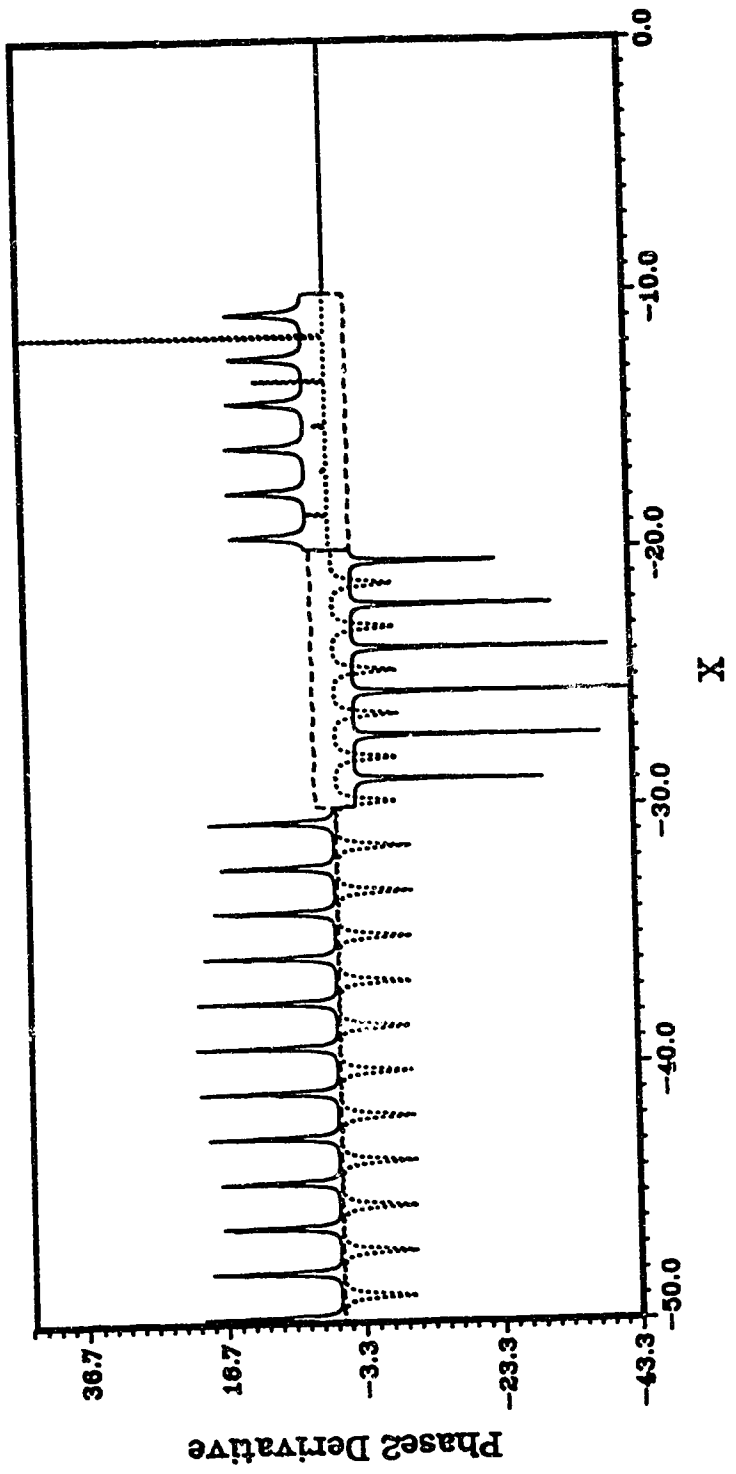
Fig. 11. Plots for initial amplitudes (5.3.4) and topography given by (5.2.1) and (5.3.1) with $H_0=10.0$.

- (A) b_i versus X
- (B) ϕ_i versus X
- (C) Phase2 Derivative versus X
- (D) Phase2 versus X
- (E) $b \cdot \cos(\text{phase2})$ versus X

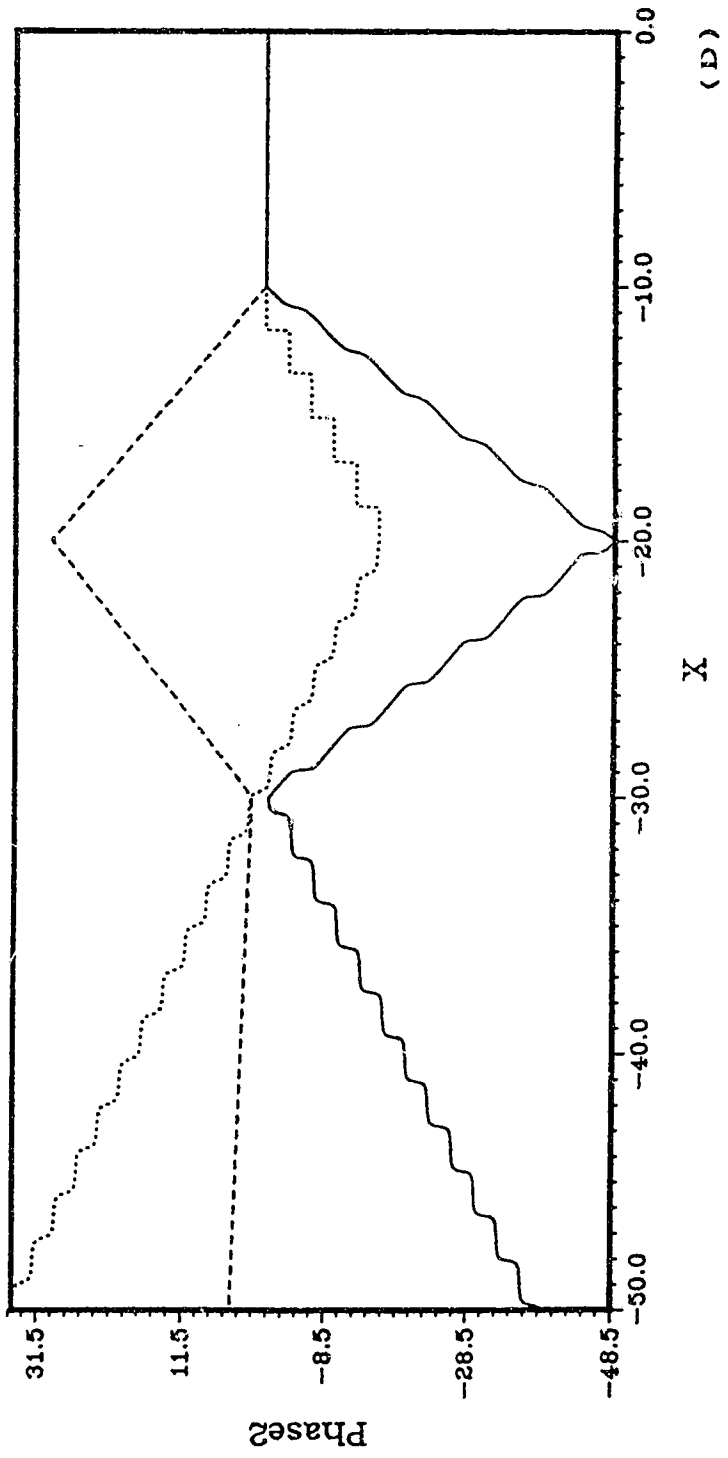
Wave 1, wave 2 and wave 3 are denoted by a thick curve, dashed curve and a dotted curve respectively.

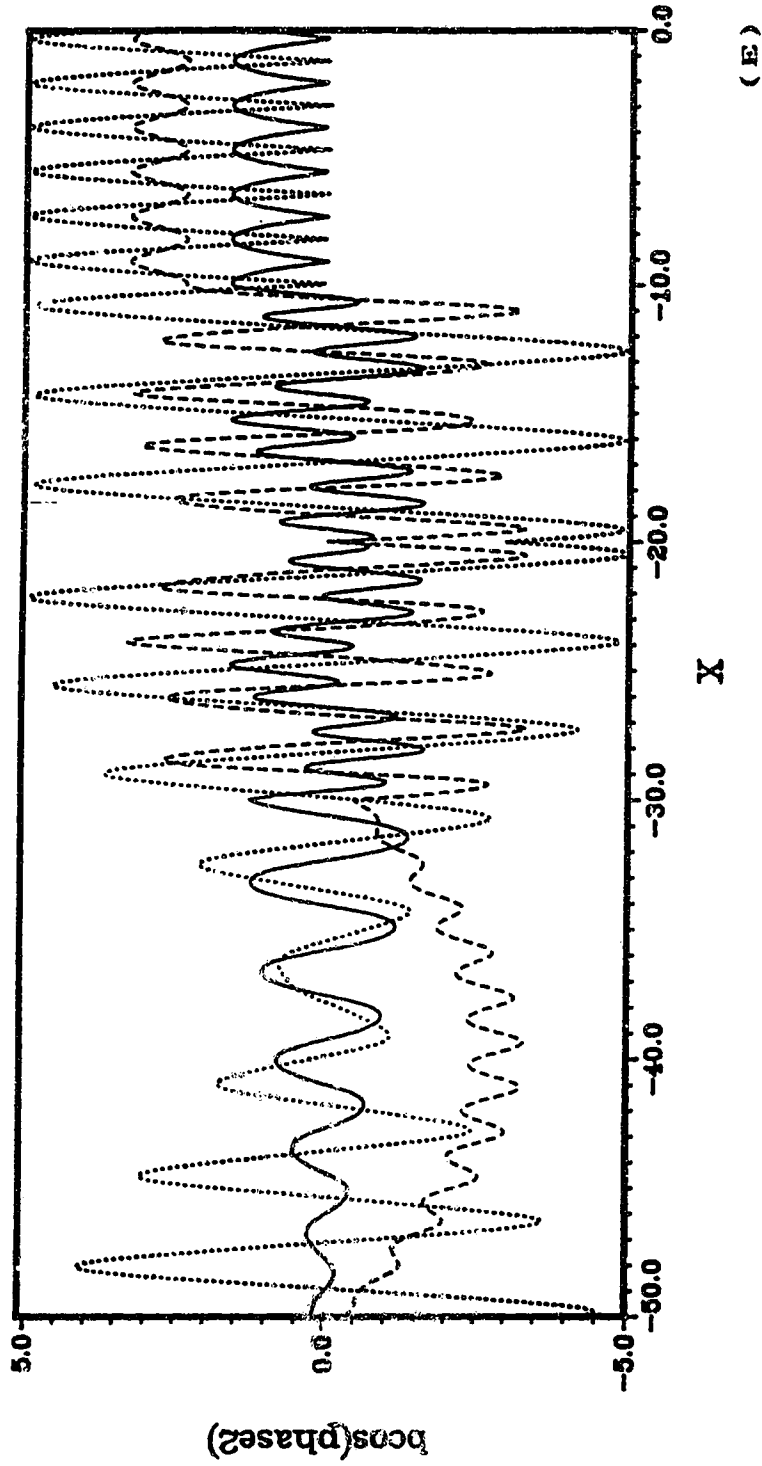


(B)



(c)





(E)

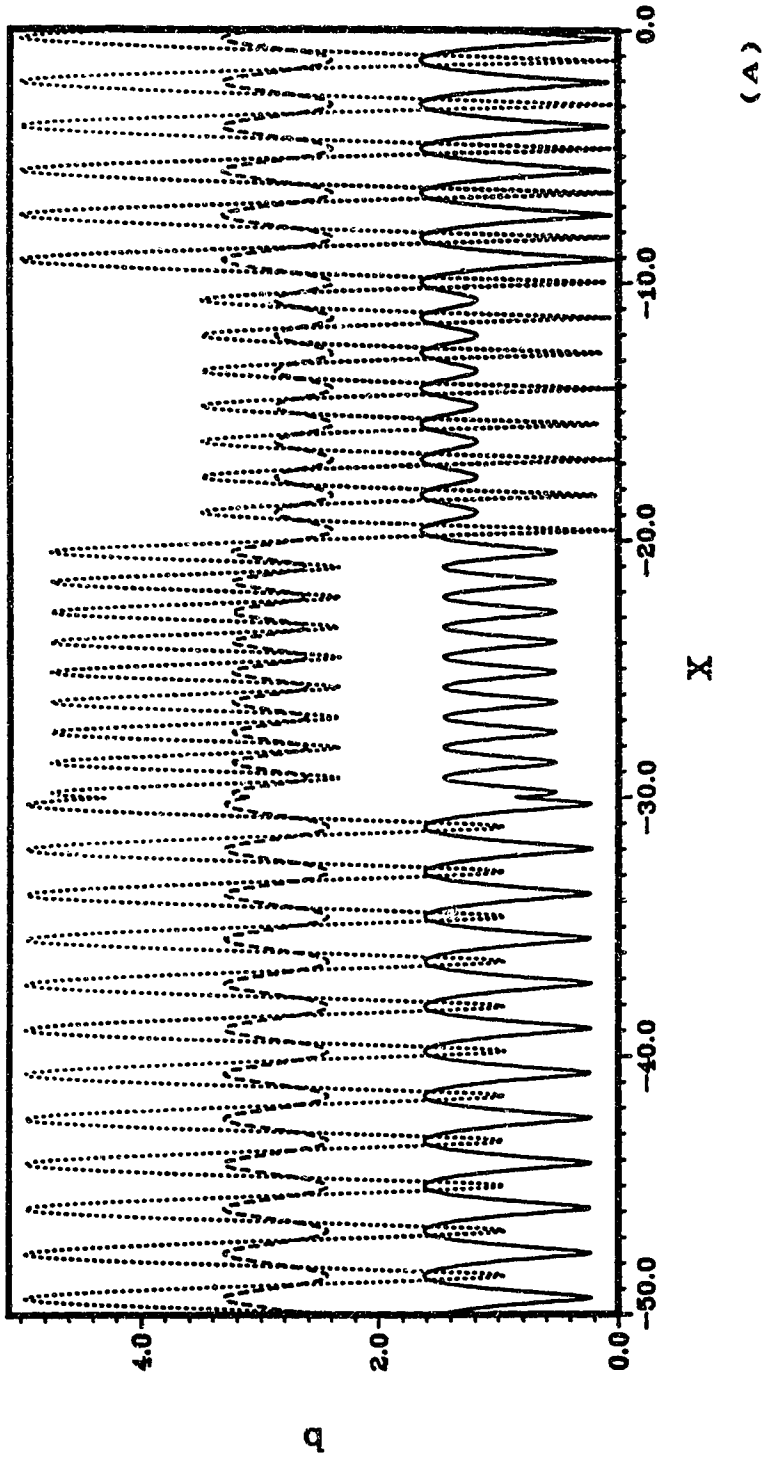
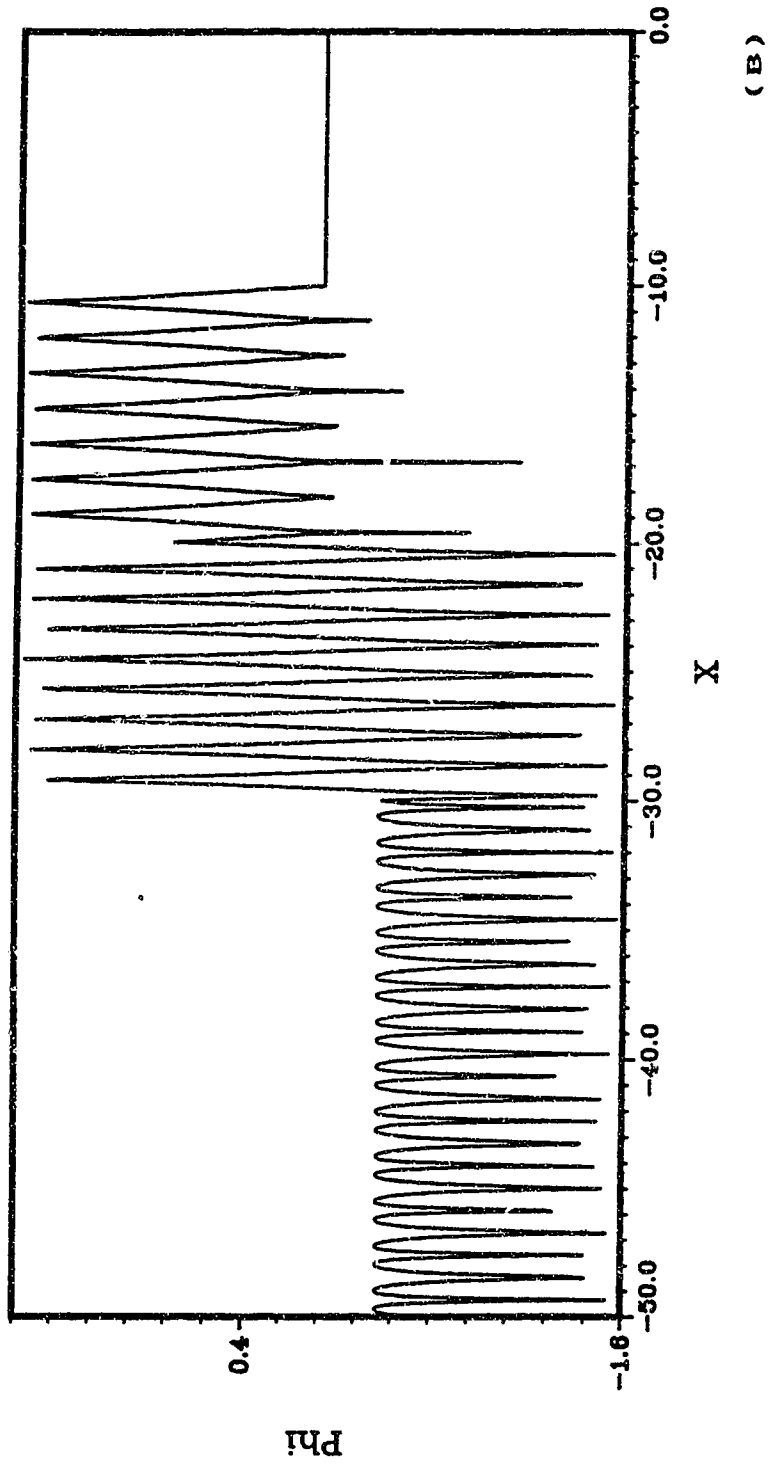
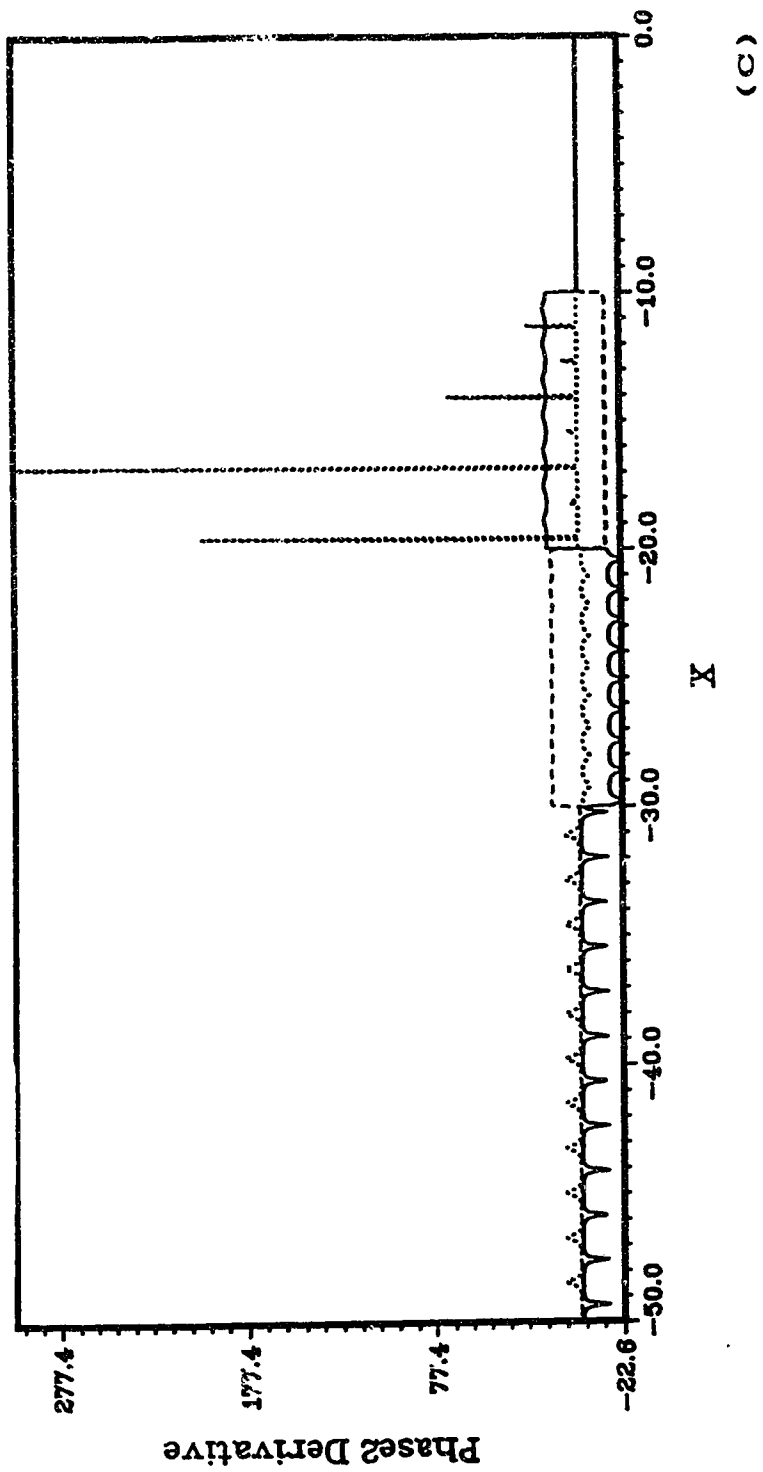


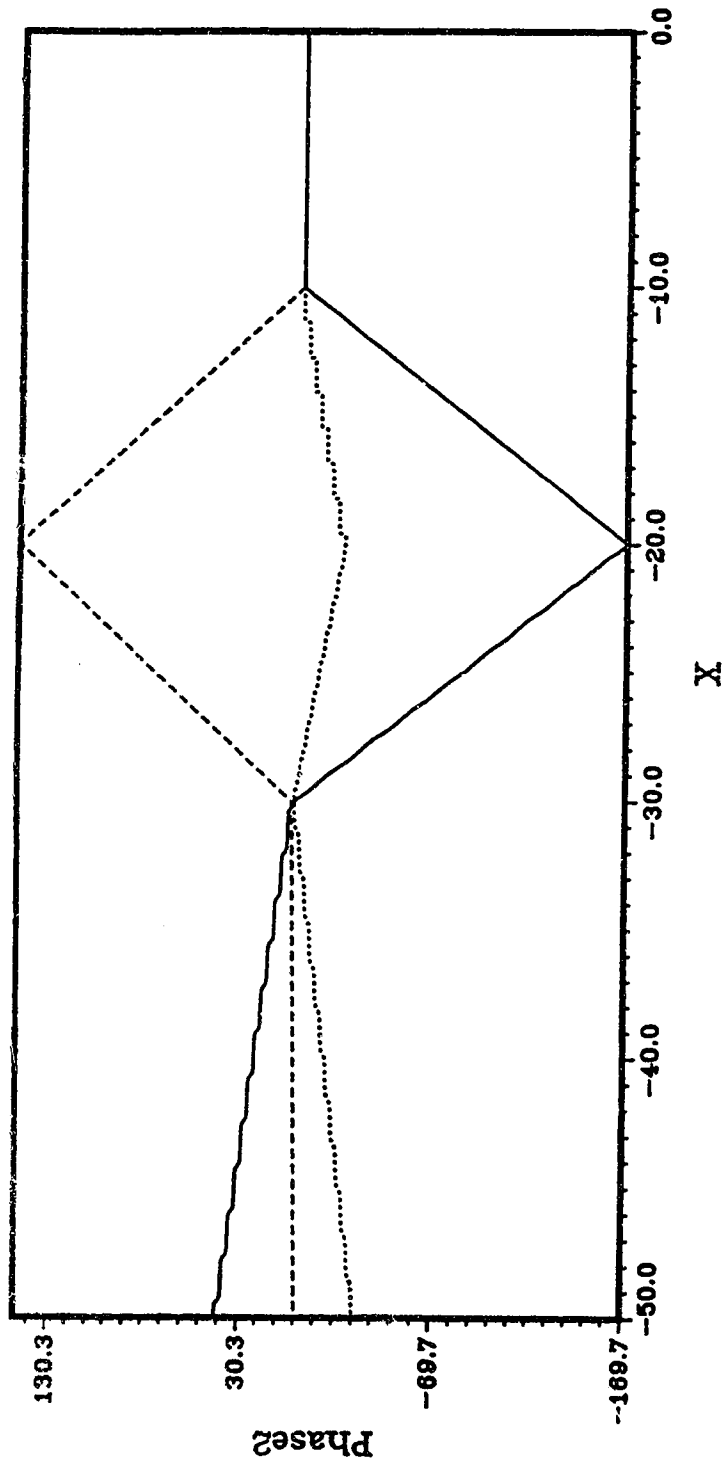
Fig. 12. Plots for initial amplitudes (5.3.4) and topography given by (5.2.1) and (5.3.1) with $H_0=50.0$.

- { A } b_i versus X
- { B } ϕ_i versus X
- { C } Phase2 Derivative versus X
- { D } Phase2 versus X
- { E } $b_i \cos(\phi_{\text{phase2}})$ versus X

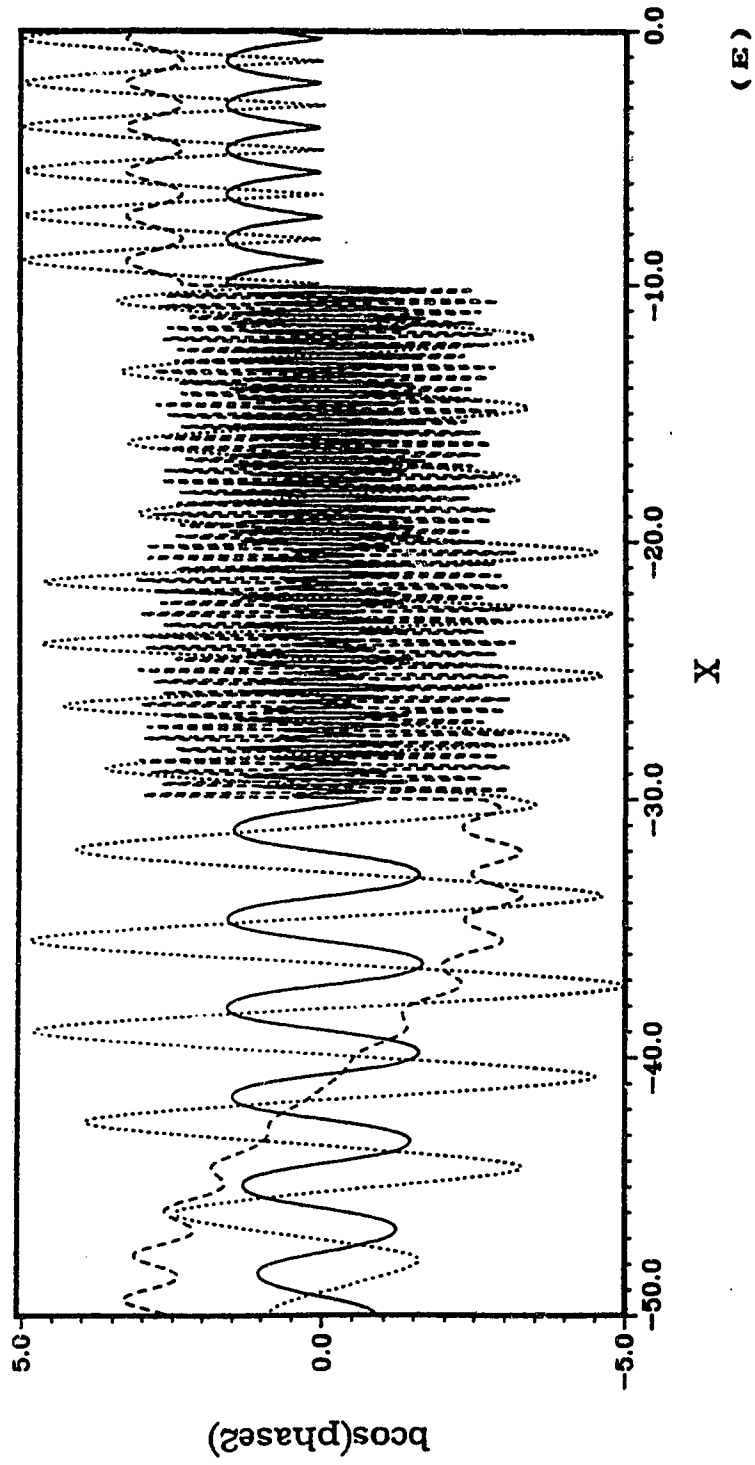
Wave 1, wave 2 and wave 3 are denoted by a thick curve, dashed curve and a dotted curve respectively.







(D)



5.4. Solutions to the Rossby Wave Triad over non Symmetric Piecewise Linear Topographic Configurations.

In this section we examine the effect of topographic configurations which are non-symmetric on the Rossby wave triad. The first case we shall examine is one which is similar to that in section 5.3. The geometry of this configuration may be visualized through Figure 2. We set

$$\left. \begin{array}{l} X_0 = 10 \\ X_1 = 20 \\ X_2 = 25 \\ H_0 = 10 \end{array} \right\} . \quad (5.4.1)$$

The second case we examine has equations of the form

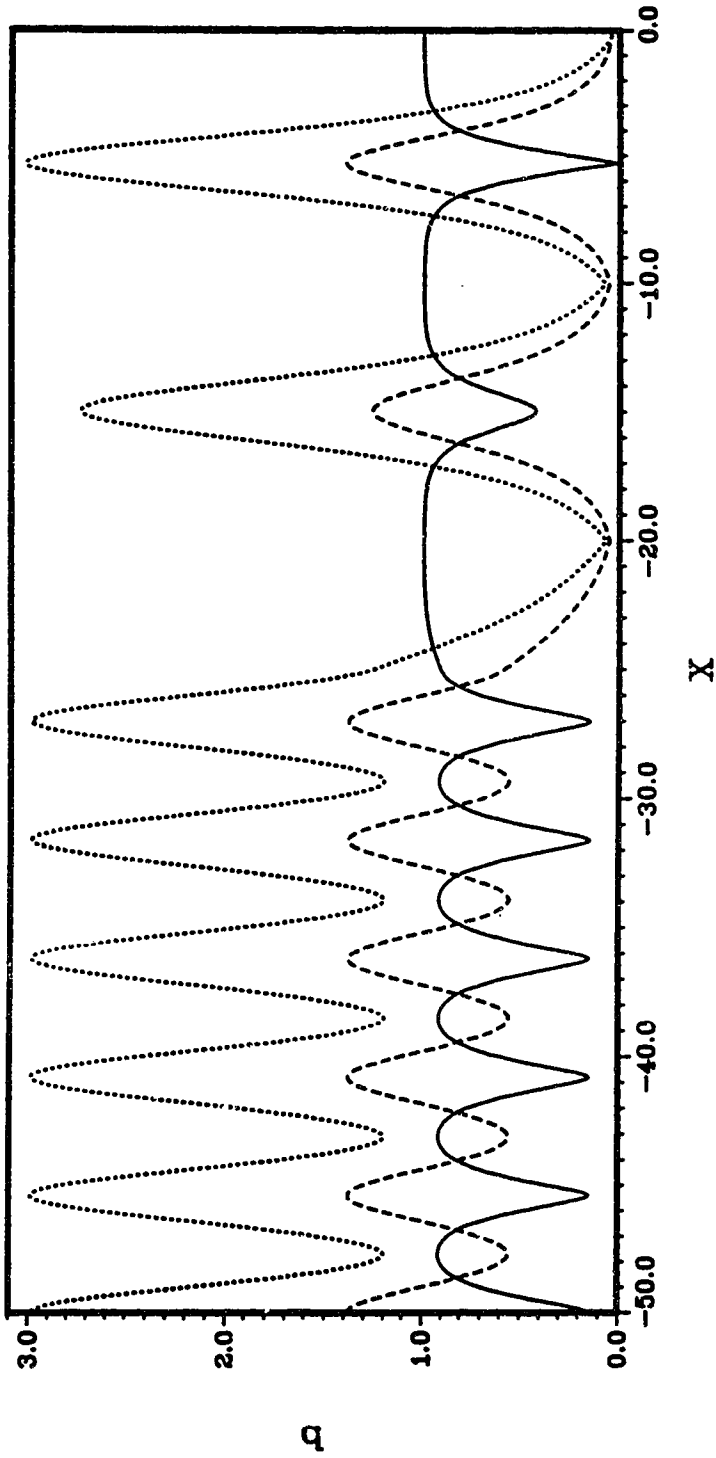
$$\left. \begin{array}{l} h'(X) = 0, X > X_0, X < X_1, \\ h'(X) = \frac{H_0(X - X_0)}{(X_1 - X_0)}, X_1 < X < X_0 \end{array} \right\} . \quad (5.4.2)$$

One can easily picture topography of this form by examining Figure 2. We set

$$\left. \begin{array}{l} X_0 = 10 \\ X_1 = 20 \\ H_0 = 10 \end{array} \right\} . \quad (5.4.3)$$

In both cases we choose initial amplitudes given by (5.3.2). Plots of the first case are given by Figure 13 and of the second case by Figure 14.

We may see by examining these plots that the effect of the topography on the triad is analogous to that in the symmetric case which was discussed in section 5.3. Therefore we shall not present a long review of these cases, but refer the reader to section 5.3

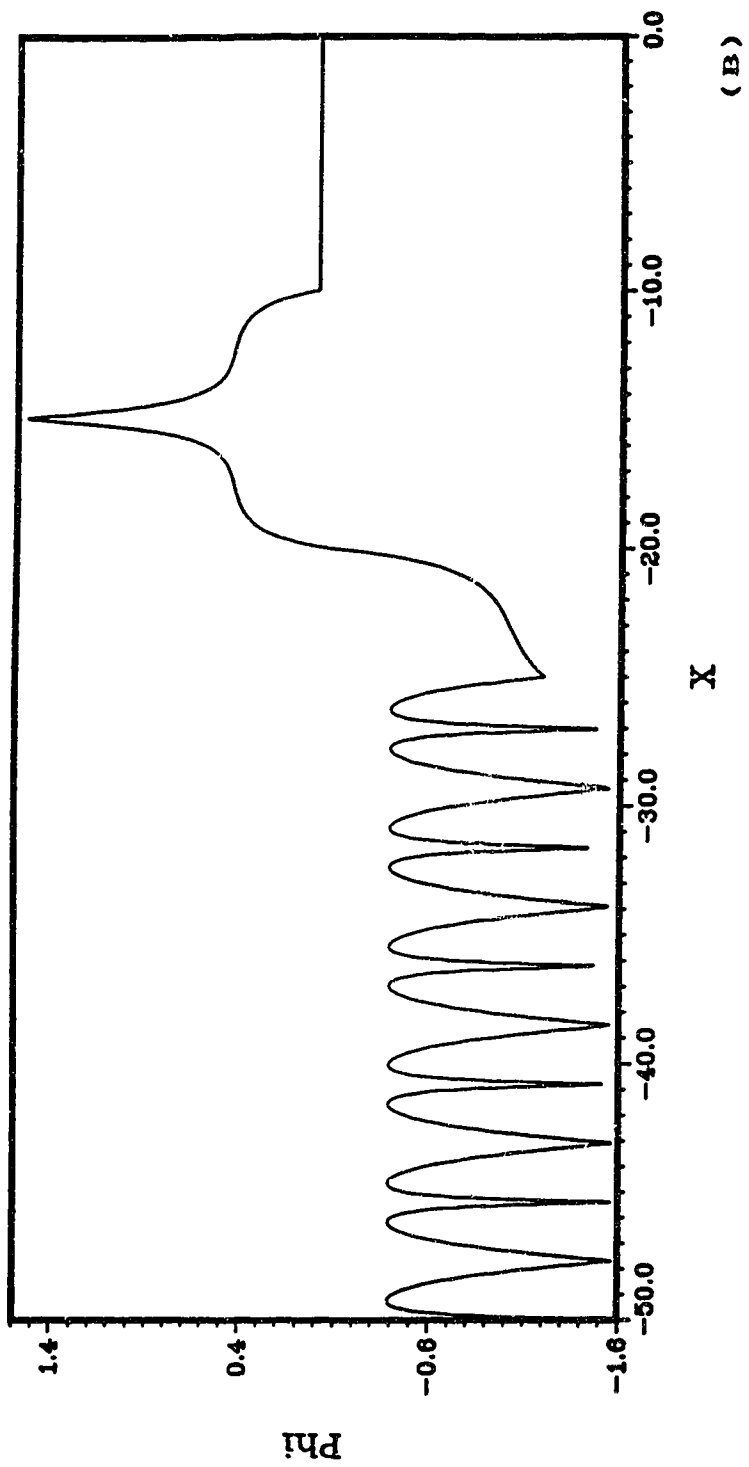


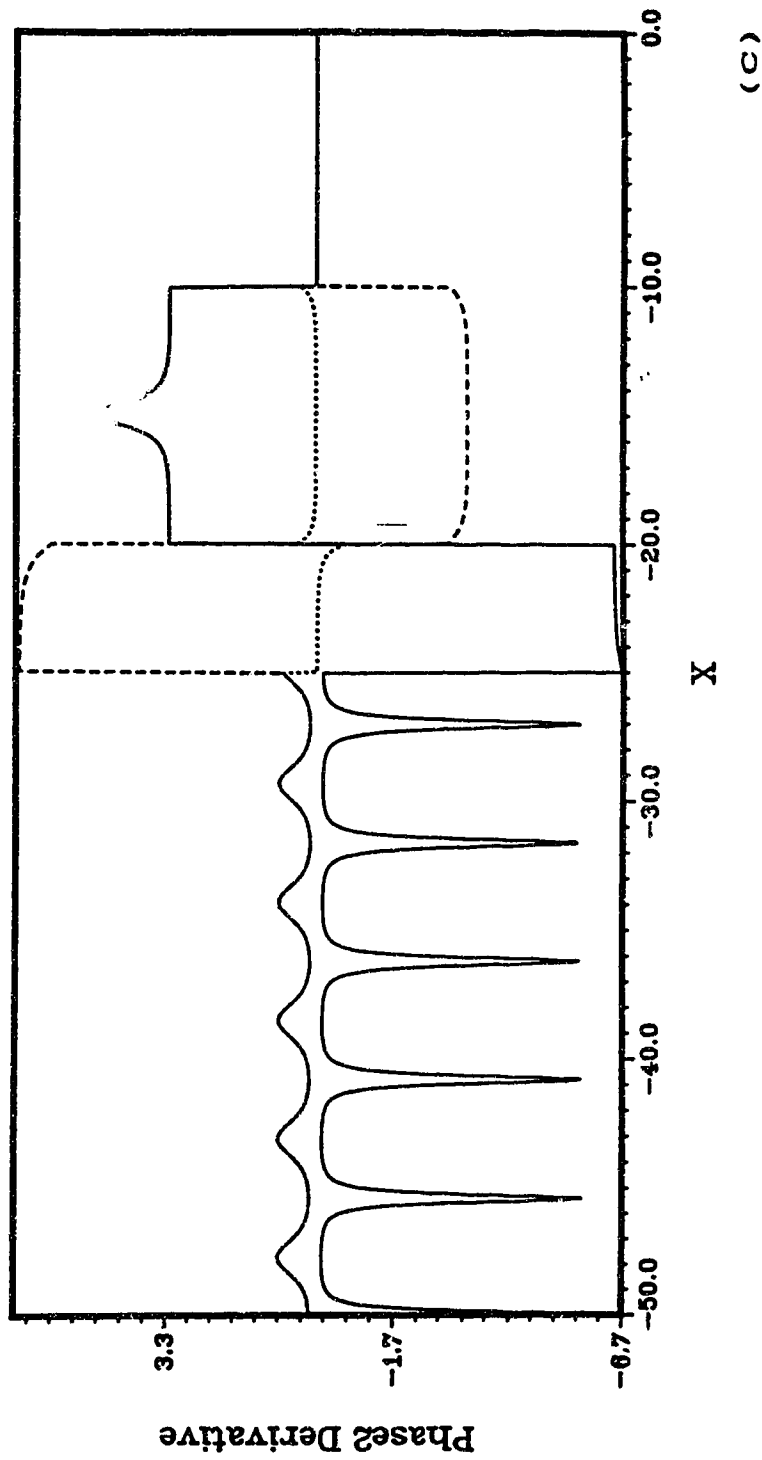
(A)

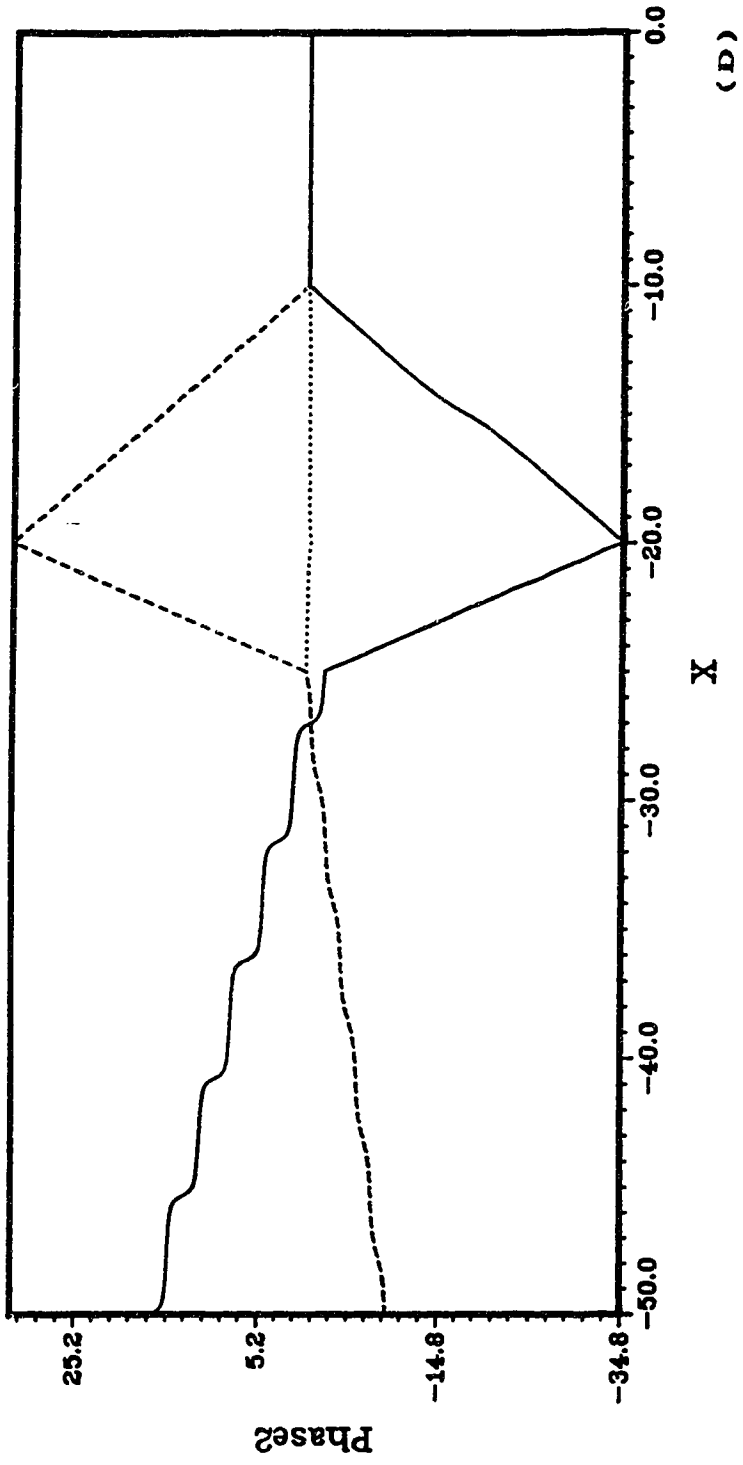
Fig. 13. Plots for initial amplitudes (5.3.2) and topography given by (5.2.1) and (5.4.1) with $H_0=10.0$.

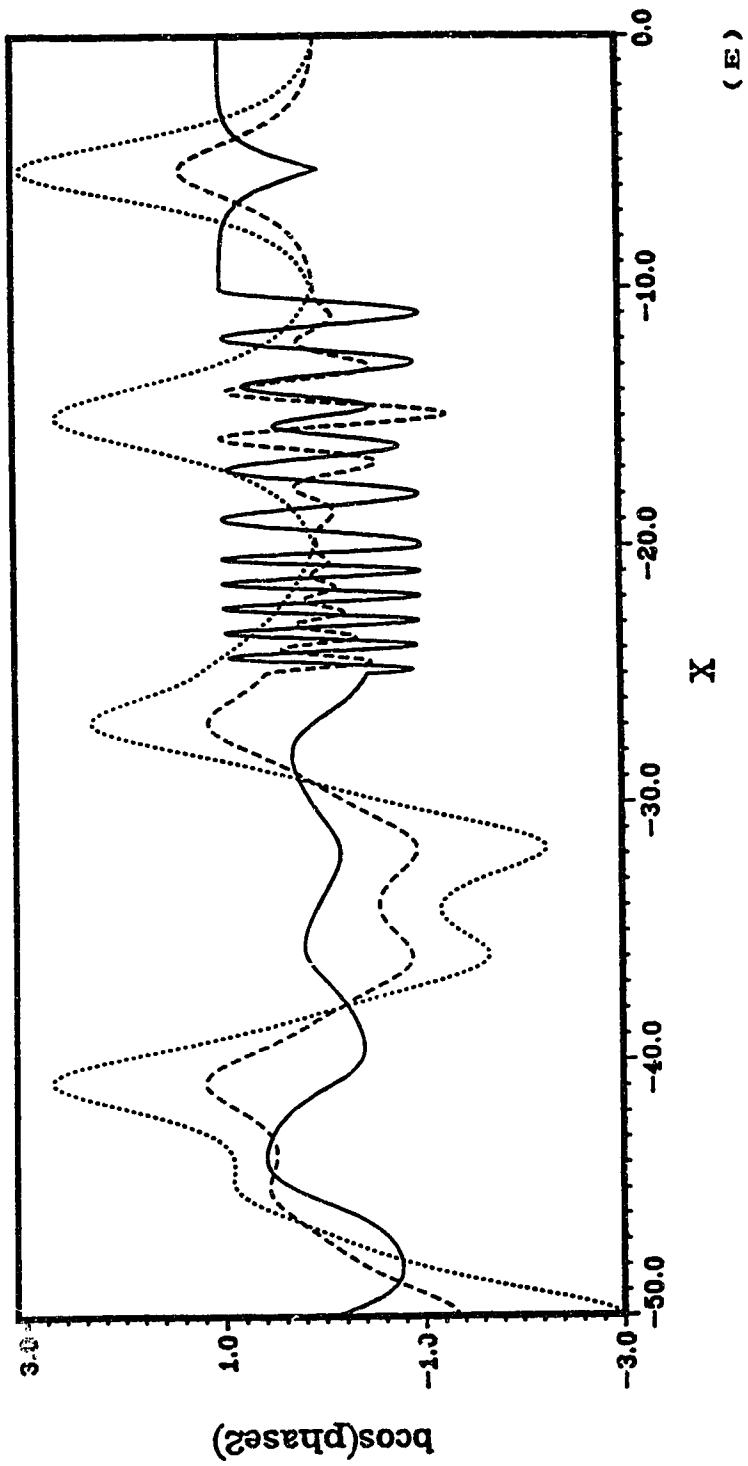
- (A) b_i versus X
- (B) Φ_i versus X
- (C) Phase2 Derivative versus X
- (D) Phase2 versus X
- (E) $b_i \cos(\text{phase2})$ versus X

Wave 1, wave 2 and wave 3 are denoted by a thick curve, dashed curve and a dotted curve respectively.









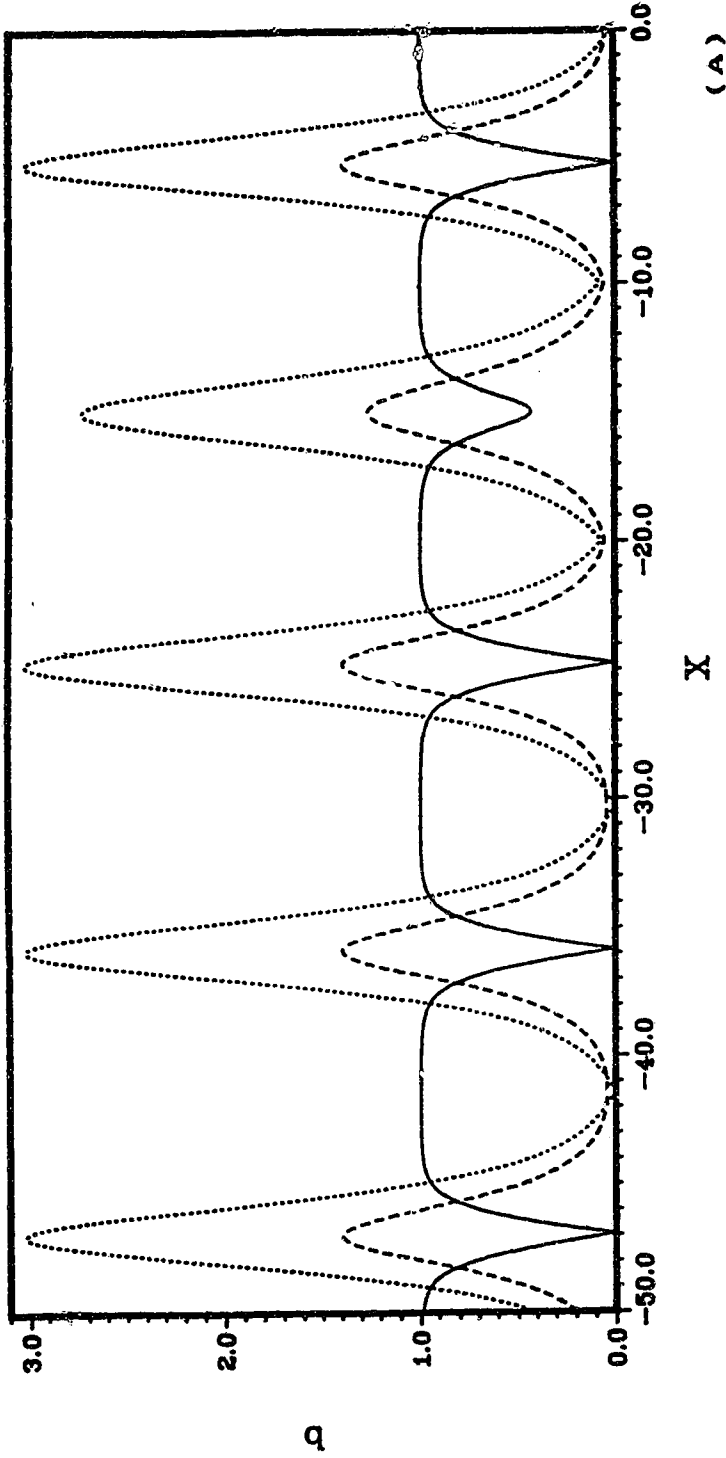
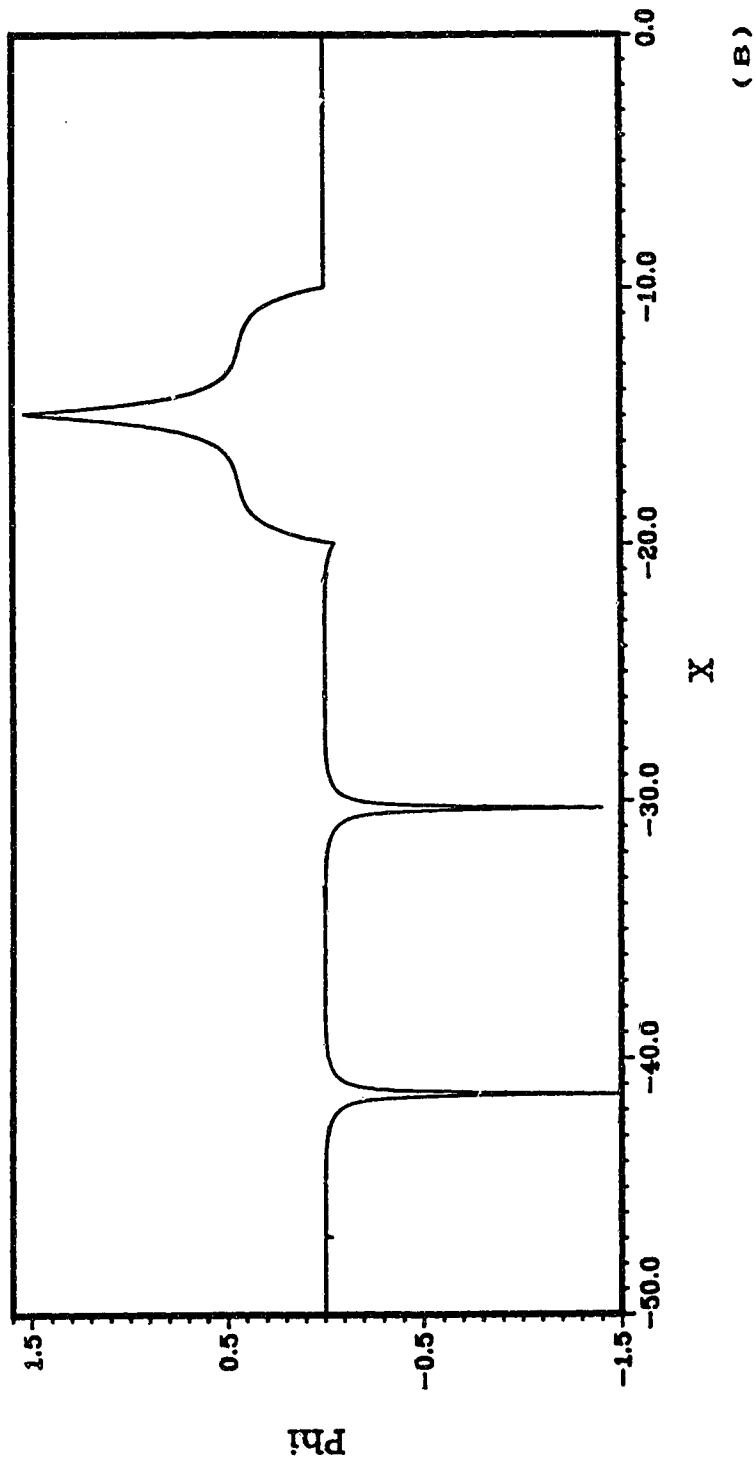
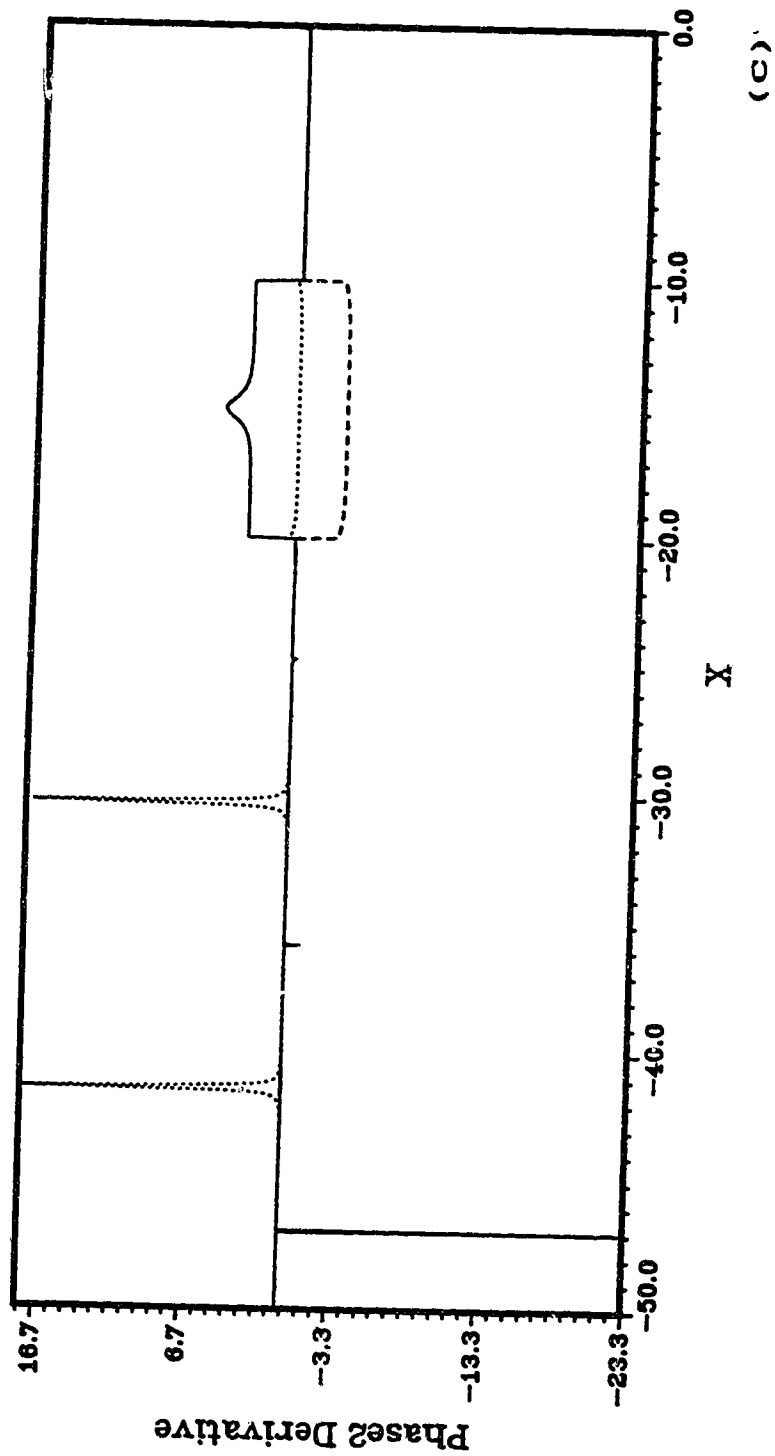


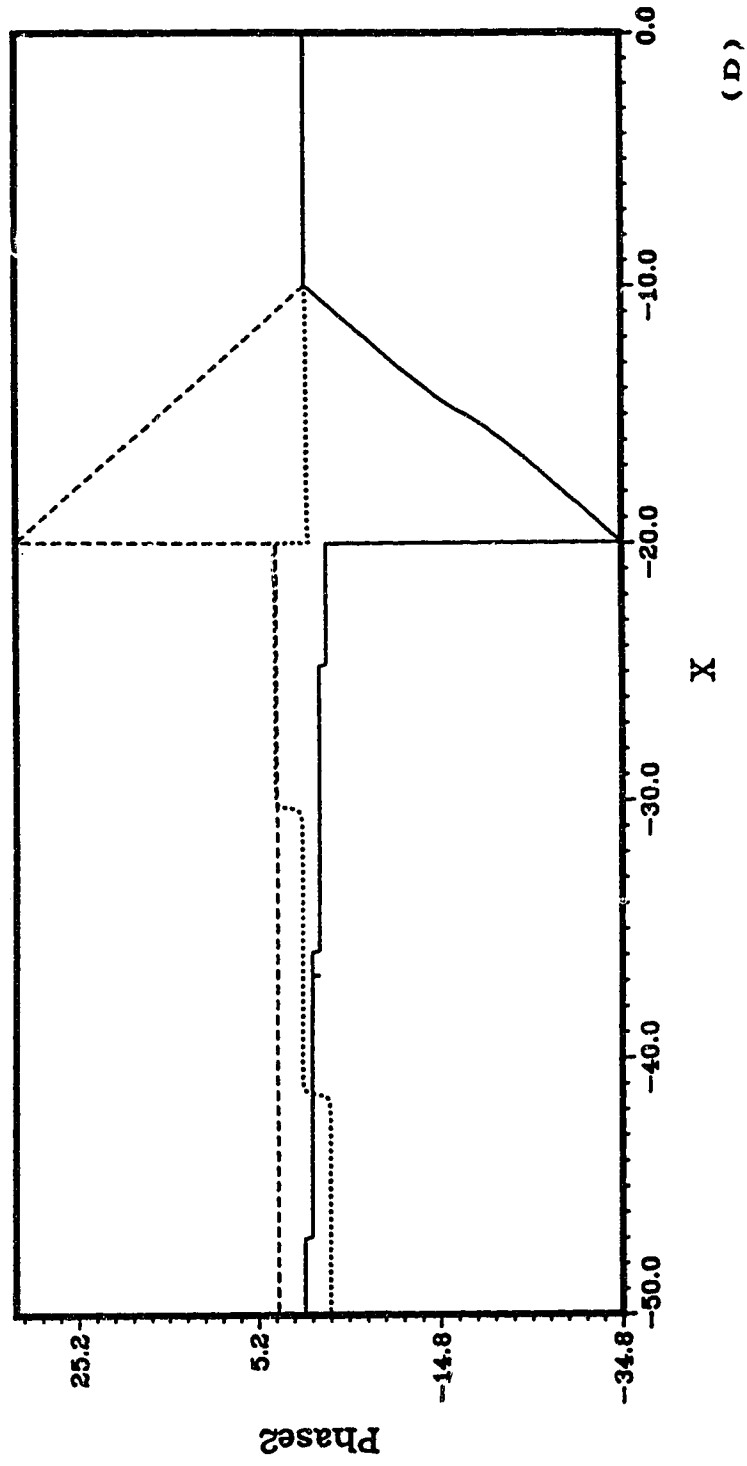
Fig. 14. Plots for initial amplitudes (5.3.2) and topography given by (5.4.2) and (5.4.3) with $H_0=10.0$.

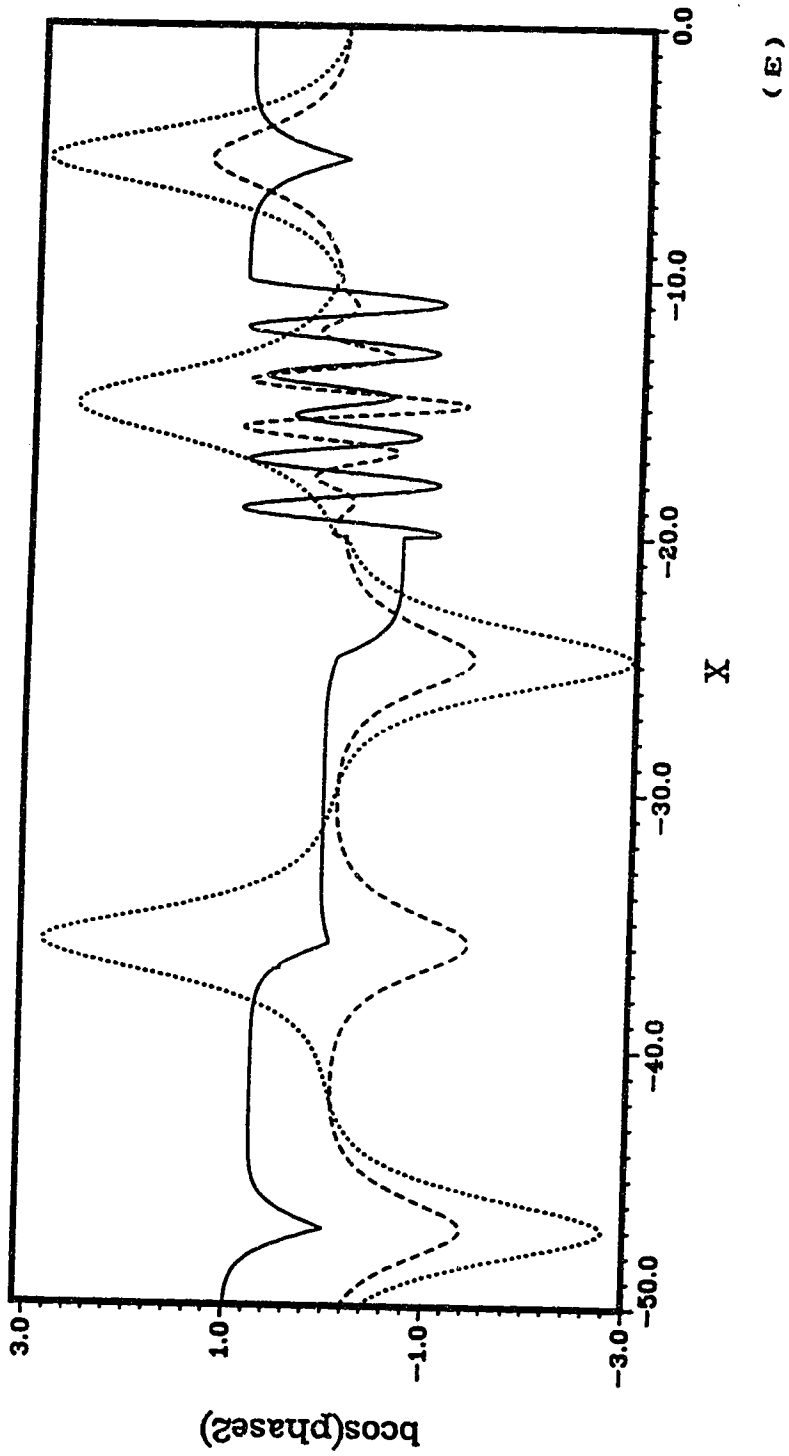
- (A) b_1 versus X
- (B) Φ versus X
- (C) Phase2 Derivative versus X
- (D) Phase2 versus X
- (E) $b_1 \cos(\text{phase2})$ versus X

Wave 1, wave 2 and wave 3 are denoted by a thick curve, dashed curve and a dotted curve respectively.









CHAPTER 6

CONCLUSIONS

We have derived an analytical asymptotic theory which describes the propagation of a Rossby wave triad under the influence of Ekman friction and finite-amplitude, but slowly-varying topographic gradients, which we have assumed to have the same small order of magnitude as the non-linear Jacobian terms in the quasi-geostrophic potential vorticity equation. For piecewise continuous linear topographic configurations, in the absence of friction, we have shown that the perturbed interaction equations may be solved exactly for the steady state problem.

We began by formulating the problem in terms of the shallow-water equations which included topographic and Ekman friction terms. In order to highlight the essential features of the triad interaction, we restricted the waves to propagate in an inviscid, homogeneous, hydrostatic and incompressible atmosphere. To determine analytically, the evolution of the triad as it propagated over topography, we examined the steady state solution in the absence of friction. Our principal conclusions are as follows:

- 1) In the absence of topographic forcing, the wave with the interaction coefficient which has a sign opposite to the other two, will always vary in the opposite direction to the other two, and in this way the wave energy will oscillate between the modes. This oscillation shows reversible behavior.
- 2) In the presence of topography, the waves behave as in 1, except the strength of the interaction is less, due to a de-phasing of the waves as they propagate over the topography. This de-phasing is still present after the waves have propagated over the topography, but the magnitude of the de-phasing is less.
- 3) The de-phasing is caused by a zonal wave number mismatch which is induced by the topography. The size of the zonal wave number mismatch and hence the magnitude of the de-phasing of the waves, is dependent on ϵ and

the slope of the topography.

The zonal wave number mismatch causes the conditions for resonance to cease to be fulfilled, thus the exchange of energy between the waves is diminished.

- 4) Different configurations of piecewise linear topography have analogous effects on the triad.

There are several areas in which the theory developed in this thesis may be improved. We have only presented a theory which represents the evolution in space for a stationary situation, and for this representation, we have limited ourselves to piecewise linear topographic configurations.

In a general description, however, the variation in both time and space must be considered, as well as general topographic configurations. Perhaps asymptotic solutions to the initial value problem with general topography can be solved by the inverse scattering method or another analytical approach. Analysis of our model or the initial value problem with the inclusion of some type of friction would provide a better description of the problem.

Eventually the non-linear effects will cause other waves to rise out of the background of imperceptible waves and share the energy of the initial waves. A look at third or fourth order terms and the effect of friction and topography would provide us with information on the flow of energy between the triad and other neighboring waves. Benny and Newell (1968) have shown, in the absence of topography and friction, that it is possible in the particular case when one of the members of the triad is the zonal flow, for neighboring waves to cause energy to be lost or gained by the zonal flow on longer time scales. The effects of topography and friction in this type of model would provide a description of the flow of energy between the triad and other neighboring waves. Finally, the most realistic situation would be to study a two-layer model of baroclinic instability. Meacham (1988) and Loesch (1974) have both studied this problem, however neither has attempted to examine how topographic forcing, as applied in

our model would affect their models. Meacham (1988) looked at instability and explosive growth of the triad in his model. Perhaps topographic forcing as we have defined it could cause the instability to be delayed or eliminated, because the exchange of energy between the waves may be inhibited by the topography as in our model.

Although the instability has been discussed in terms of a baroclinic model, there is no reason why instabilities cannot occur in cases of barotropic shear flow, and this type of model may be more tractable.

It would also be of interest to study the effects of thermal forcing on both the barotropic and baroclinic models.

BIBLIOGRAPHY

- Ablowitz, M.J. and H. Segur, 1981: Solitons and the inverse scattering transform. S.I.A.M., Philadelphia, Pennsylvania.
- Abramowitz, M. and J.A. Stegun, 1965: Handbook of Mathematical Functions. Dover, New York.
- Austin, J.F., 1980: The blocking of the middle latitude westerly winds by planetary waves. Q.J.R. Meteorol. Soc., 106, 327-350.
- Barnier, B., 1983: Energy transmission by barotropic Rossby waves across large-scale topography. J. Phys. Oceanogr., 14, 438-447.
- Bender, C.M. and S.A. Orszag, 1978: Advanced mathematical methods for scientists and engineers. McGraw-Hill, New York, 593 pp.
- Benny, D.J. and A.C. Newell, 1967: The propagation of non-linear envelopes. J. Math. and Phys., 46, 133pp.
- Benzi, R., B. Saltzman and A.C. Winn-Nielsen, 1986: Anomalous atmospheric flows and blockings. Adv. Geophys., 29, 459pp.
- Bretherton, F.P., 1964: Resonant interactions between waves: The case of discrete oscillations. J. of Fluid Mech., 20, 457-479.
- Chang, J., 1972: Atmospheric Circulation Systems and Climates. The Oriental Publishing Company, 328pp.
- Charney, J.G. and J.G. Devore, 1979: Multiple flow equilibria in the atmosphere and blocking. J. of Atmos. Sci., 36, 1205-1216.
- Charney, J.G. and D.M. Strauss, 1980: Form drag instability, multiple equilibria and propagating planetary waves in baroclinic, orographically forced planetary wave systems. J. of Atmos. Sci., 37, 1157-1176.
- Craik, A.D.D., 1985: Wave interactions and fluid flows. Cambridge University Press, Cambridge.
- Craik, A.D.D. and J.A. Adam, 1978: Evolution in space and time of resonant wave triads: I. The "pump-wave approximation". Proc. Roy. Soc. Land., A 363, 243-255.
- Dole, R.M. and N.D. Gordon, 1983: Persistent Anomalies of the extratropical northern hemisphere wintertime circulation: Geographical distribution and regional persistence characteristics. Mon. Wea. Rev., 111, 1567-1586.
- Drazin, P.G. 1970: Non-linear baroclinic instability of a continuous zonal flow. Q.J.R. Meteorol. Soc., 96, 667-676.
- Egger, J., 1978: Dynamics of blocking highs. J. of Atmos. Sci., 35, 1788-1801.
- Egger, J., 1979: Stability of blocking in barotropic channel flow. Beitr. Phys. Atmos., 52, 27-43.

Ghil, M. and S. Childress, 1987: Topics in Geophysical fluid dynamics: Atmospheric dynamics, dynamo theory, and climate dynamics. Springer-Verlag, 485pp.

Hart, J., 1979: Barotropic Quasi-geostrophic flow over mountains. *J. of Atmos. Sci.*, 36, 1736-1746.

Hsieh, W.W. and L.A. Mysak, 1980: Resonant interactions between shelf waves, with applications to the Oregon shelf. *J. of Phys. Ocean.*, 10, 1729-1741.

Kaup, D.J., A. Riemann and A. Bers, 1979: Space-time evolution of non-linear three-wave interactions: I. Interactions in a homogeneous medium. *Rev. Mod. Phys.*, 51, 275-310.

Kenyon, K., 1964: Non-linear Rossby waves: Student lectures, summer study program in geophysical fluid dynamics. Woods Hole Oceanographic Institution, vol. II, 69.

Knox, J.L., 1982: Atmospheric blocking in the northern hemisphere. Canadian Climate Centre, Report No. 82-2.

Loesch, A.Z., 1974: Resonant interactions between unstable and neutral baroclinic waves. Part I, *J. of Atmos. Sci.*, 31, 1177-1201.

Loesch, A.Z., 1974: Resonant interactions between unstable and neutral baroclinic waves, Part II, *J. of Atmos. Sci.*, 31, 1202-1217.

Longuet-Higgins, M.S. and A.E. Gill, 1967: Resonant interactions between planetary waves. *Proc. Roy. Soc.*, A229, 120pp.

Meacham, S., 1988; Non-modal baroclinic instability. *Dynamics of atmospheres and oceans*, 12, 19-45.

Mitchell, H.L. and J. Derome, 1985: Resonance of topographically forced waves in a quasi-geostrophic model. *J. of Atmos. Sci.*, 42, 1653-1666.

Miyakoda, K., C.T. Gordon, R. Caverly, W.F. Stern, J. Sirutis and W. Bourke, 1983: Simulation of a blocking event in January 1977. *Mon. Wea. Rev.*, 111, 846-869.

Newell, A.C., 1969: Rossby wave pocket interactions, *J. of Fluid Mech.*, vol. 35, Part 2, 255-271.

Pedlosky, J. 1981: Resonant topographic waves in barotropic and baroclinic flows. *J. of Atmos. Sci.*, 38, 2626-2641.

Pedlosky, J., 1970: Finite amplitude baroclinic waves. *J. of Atmos. Sci.*, 27, 15-30.

Pedlosky, J., 1979: Finite amplitude baroclinic waves in a continuous model of the atmosphere. *J. of Atmos. Sci.*, 36, 1908-1924.

Pedlosky, J., 1987: Geophysical fluid dynamics. Springer-Verlag, 624pp.

- Pierrehumbert, R.T. and P. Malguzzi, 1984: Forced coherent structures and local multiple equilibria in a barotropic atmosphere. *J. of Atmos. Sci.*, 41, 246-257.
- Riemann, A.H., A. Bers and D.J. Kaup, 1977: Nonlinear interactions of three wave packets in an inhomogeneous medium. *Phys. Rev. Lett.*, vol. 39, Number 5, 245-248.
- Rex, D.F., 1956: Blocking action in the middle troposphere and its effect on regional climate. *Tellus* 2, 196-211, 273-301.
- Rossby, C.G., 1939: Relation between variations in the intensity of the zonal circulation of the atmosphere and the displacement of the semi-permanent centers of action. *J. of Marine Research*, vol. 2, 38-55.
- Sanders, R.A., 1953: Blocking highs over the eastern North Atlantic Ocean and western Europe. *Mon. Wea. Rev.*, vol. 81, 67-73.
- Seymour, B.R., and M.P. Martell, 1974: Nonlinear geometrical acoustics. *Mechanics Today*, vol. 2.
- Swaters, G.E., 1988: Resonant three-wave interactions in non-linear hyper-elastic fluid filled tubes. *J. of Appl. Math. and Phys.*, vol. 39, 668-681.
- Thomson-Milne, L.M., 1950: Jacobian elliptic function tables. Dover Publications, Inc., 132 pp.
- Tremberth, K.E. and K.C. Mo., 1985: Blocking in the southern hemisphere. *Mon. Wea. Rev.*, 113, 3-21.
- Trevisan, A. and A. Buzzi, 1980: Stationary response of barotropic weekly nonlinear Rossby waves to quasi-resonant orographic forcing. *J. of Atmos. Sci.*, 37, 947-957.
- Tung, K.K. and R.S. Lindzen, 1979: A theory of stationary long waves: Part I. A simple theory of blocking. *Mon. Wea. Rev.*, 107, 714-734.
- Tung, K.K. and R.S. Lindzen, 1979: A theory of stationary long waves: Part II. Resonant Rossby waves in the presence of realistic vertical shears. *Mon. Wea. Rev.*, 107, 735-750.
- van Loon, H., 1956: Blocking action in the southern hemisphere. Part I. *NOTOS*, vol. 5, 171-175.
- Warn, T. and B. Brasnett, 1983: The amplification and capture of atmospheric solitons by topography: A theory of the onset of regional blocking. *J. of Atmos. Sci.*, 40, 28-38.
- Whitham, G.B., 1974: *Linear and nonlinear waves*. Wiley, New York, 636 pp.
- Weiland, J. and H. Wilhelmsson, 1977: Coherent non-linear interaction of waves in plasmas: International series in natural philosophy. vol. 88, Pergamon Press, Goteborg, Sweden, 350pp.

Appendix 1: Derivation of Equation (2.2.15)

Substitution of (2.2.10) into (2.2.14) produces the following $-J(\psi^0, \Delta\psi^0)$ will produce terms like (for A_1)

$$\left. \begin{aligned} & A_2^* A_3^* k_2 \ell_3 (-k_3^2 - \ell_3^2) \exp(-i(\theta_2 + \theta_3)) \\ & \quad + A_2^* A_3^* k_3 \ell_2 (-k_2^2 - \ell_2^2) \exp(-i(\theta_2 + \theta_3)) \\ & -A_2^* A_3^* k_3 \ell_2 (-k_3^2 - \ell_3^2) \exp(-i(\theta_2 + \theta_3)) \\ & \quad + A_2^* A_3^* k_2 \ell_3 (-k_2^2 - \ell_2^2) \exp(-i(\theta_2 + \theta_3)) \\ & + c.c. + \text{nonresonant terms,} \end{aligned} \right\} \quad (A.1.a)$$

which with the use of (2.2.13) maybe written

$$A_2^* A_3^* \exp(i\theta_1) z \cdot (\underline{K}_2 \times \underline{K}_3) (\underline{K}_2^2 - \underline{K}_3^2) + c.c. + \text{nonresonant terms} . \quad (A.1.b)$$

Similar terms are derived for A_2 and A_3

$$\left. \begin{aligned} \Delta\psi_T^{(0)} &= A_{jT} (-k_j^2 - \ell_j^2) \exp(i\theta_j) + c.c., \\ \psi_T^{(0)} &= A_{jT} \exp(i\theta_j) + c.c., \\ \psi_T^{(0)} &= A_{jX} k_j \omega_j \exp(i\theta_j) + c.c., \\ \psi_{iX}^{(0)} &= A_{jX} \exp(i\theta_j) + c.c., \\ \gamma(X) \psi_y^{(0)} &= A_j i \ell_j \exp(i\theta_u) \gamma(X) + c.c., \\ r \Delta\psi^{(0)} &= r A_j (-k_j^2 - \ell_j^2) \exp(i\theta_j) + c.c. \end{aligned} \right\} \quad (A.1.c)$$

The terms (A.1.b) and (A.1.c) are combined to form (2.2.15).

Appendix 2: Proof of (3.1.10a)

We begin with equation (3.1.10a)

$$z \cdot \underline{K}_2 \times \underline{K}_3 = z \cdot \underline{K}_3 \times \underline{K}_1 = z \cdot \underline{K}_1 \times \underline{K}_3 = d$$

If we take the first two terms of (3.1.10a)

$$z \cdot \underline{K}_2 \times \underline{K}_3 - z \cdot \underline{K}_3 \times \underline{K}_1 = 0 \quad (A.2.b)$$

and expand, we get

$$k_2 \ell_3 - k_3 \ell_2 - k_3 \ell_1 + k_1 \ell_3 = 0. \quad (A.2.b)$$

Simplifying (A.2.b) gives

$$\ell_3(k_1 + k_2) - k_2(\ell_2 + \ell_1) = 0. \quad (A.2.c)$$

If the conditions for resonance (2.2.13) are met, then (A.2.c) can be written

$$-\ell_3 k_3 + k_3 \ell_3 = 0. \quad (A.2.d)$$

Similar arguments apply to the other combinations of (k_j, ℓ_j) .

Appendix 3: Proof of (4.4.10)

We begin by taking the X derivative of (4.4.10) and we write it as follows

$$\begin{aligned}\Gamma_X &= b_{1X} b_2 b_3 \sin \Phi + b_{2X} \dot{b}_3 b_1 \sin \Phi + b_{3X} b_1 b_2 \sin \Phi \\ &\quad + \Phi_X b_1 b_2 b_3 \cos \Phi - s_1 (-\mu_0 \hat{c}) b_{1X} \quad \text{for } j = 1.\end{aligned}$$

Substituting (4.4.8) into the above equation yields

$$\begin{aligned}s_1 b_2^2 b_3^2 \sin \Phi \cos \Phi + s_2 b_1^2 b_3^2 \sin \Phi \cos \Phi + s_3 b_1^2 b_2^2 \sin \Phi \cos \Phi \\ + b_1 b_2 b_3 \cos \Phi \left[(-\mu_0 \hat{c}) - b_1 b_2 b_3 \left(\frac{s_1}{b_1^2} + \frac{s_2}{b_2^2} + \frac{s_3}{b_3^2} \right) \sin \Phi \right] \\ - (-\mu_0 \hat{c}) s_1^2 b_1 b_2 b_3 \cos \Phi \equiv 0.\end{aligned}$$

Since the derivative of Γ with respect to X equals to 0, Γ is a constant of the motion. Similar arguments apply for $j = 2, 3$.

APPENDIX 4; FORTRAN PROGRAM USED TO PLOT THE SOLUTION
 DERIVED IN SECTION 4.4 AND CHAPTER 5

```

-----
C
C   THIS PROGRAM CALCULATES THE SOLUTION TO THE ROSSBY WAVE
C   TRIAD OVER PIECEWISE LINEAR TOPOGRAPHY. THE FULL ANALYTICAL
C   SOLUTION BEING DERIVED IN SECTION 4.4.
C

PROGRAM TRIAD

C
C   VARIABLES ARE AS FOLLOWS:
C
C   A1,A2,A3... are the amplitudes.
C   A11,A21,A31... are the amplitudes times cos(phi_j).
C   A111,A211,A311... are the amplitudes times cos(phase2).
C   B1,B2,B3... are the interaction coefficients.
C   SN,CN,DN... are Jacobi elliptic functions.
C   SN2... has the value of Sn squared.
C   MU1,MU2,MU3... are topography terms.
C   GAMMA... is the constant of motion GAMMA.
C   ROOT(3)... holds the roots of p(x) in descending order.
C   K... is the modulus of the elliptic function used in THETA
C   calculation.
C   COMPIN... holds the values of the complete elliptic integral.
C   THETA1,THETA... is the initial calculation and final calculation
C   of THETA respectively.
C   KAPA2,PHI2,PHINT... are values we must input to calculate a
C   resonant triad.
C   M1,M2,M3,M10,M20,M30... are used to hold amplitude values
C   for use elsewhere in the program.
C   K1,K2,K3... are K wavenumbers 1,2,3 respectively.
C   L1,L2,L3... are L wavenumbers 1,2,3 respectively.
C   FIRST... is the lower limit of integration the numerical
C   routine uses to calculate the PHI's.
C   X... has the value of the distance.
C   X1,X2,X3,J4... are used to hold values of the distance for use
C   elsewhere in the program.
C   PH1,PH2,PH3... are values of the phases.
C   PH10,PH20,PH30... hold values of the phases for use elsewhere
C   in the program.
C   PH1X,PH2X,PH3X... are the derivatives of PHI1,PHI2,PHI3.
C   PH21,PH22,PH23... hold values of phase2.
C   PH21X,PH22X,PH23X... hold values of phase2 derivatives.
C   SP... is sin(PHI).
C   P... is PHI calculated from GAMMA.
C   RISE,RUN... divide to give the slope of the topography.
C   Y... holds the increment the amplitudes have changed.
C   H1... is the slope of the topography.
C   H...-1 times the slope of the topography times the topography
C   term (MU0).
C   U1,U... are the initial calculation and final argument for
C   the SN calculation respectively.
C   The rest of the variables are used as counters or to hold
C   error messages.
C

```

University of Alberta

```

COMMON /COM1/ H,GAMMA,ROOT(3),K,COMPIN,THETA,M10,M20,M30,
&B1,B2,B3
INTEGER EFF,EFF1,EFF2,EFF3,EFF4,IRULE
DOUBLE PRECISION A1,A2,A3,B1,B2,B3
DOUBLE PRECISION GAMMA,PHI,H,MUO,ROOT,K,THETA1,THETA,J1
DOUBLE PRECISION U1,Y,SN,CN,DN,SN2,M1,M2,M3,X,NN,P
DOUBLE PRECISION COMPIN,KAPA2,PHI2,PHINT,RISE,RUN
DOUBLE PRECISION M10,M20,M30,K1,K2,K3,L1,L2,L3,MU1,MU2,MU3,X1
DOUBLE PRECISION ERRABS,ERRREL,FIRST,ERREST
DOUBLE PRECISION PH1,PH2,PH3,J4
DOUBLE PRECISION A11,A111,PH10,PH20,PH30,PH21X,PH22X,PH23X
DOUBLE PRECISION A21,A211,PH1X,PH2X,PH3X,SP,PH21,PH22,PH23
DOUBLE PRECISION A31,A311,X2,X3,X4
EXTERNAL F1,F2,F3

C
C   SET VALUES FOR SHORT NUMERICAL ROUTINE TO CALCULATE PHASES
C
ERRABS=0.DO
ERRREL=0.0001DO
IRULE=2

C
C   CALCULATE VALUES FOR INTERACTION COEFFICIENTS AND TOPOGRAPHY
C   TERMS FROM WAVENUMBERS OF RESONANT TRIAD, WE MUST INPUT KAPA2
C   PHI2,PHINT. SEE LONGUET-HIGGINS AND GILL PAPER FOR MORE INFORMATION.
C
KAPA2=2.DO
PHI2=60.DO
PHINT=-140.DO
CALL WAVNUM(KAPA2,PHI2,PHINT,MUO,K1,K2,K3,
&L1,L2,L3,MU1,MU2,MU3,EFF4)
IF (EFF4.EQ. 1) GO TO 90
B1=-1.DO*B1

C
C   INPUT INITIAL AMPLITUDES
C
A1=???
A2=???
A3=???

C
C   PERFORM RENORMALIZATIONS
C
A1=A1*(1.DO/(DSQRT(B2*B3)))
A2=A2*(1.DO/(DSQRT(B3*B1)))
A3=A3*(1.DO/(DSQRT(B1*B2)))

C
C   STORE AMPLITUDES FOR USE IN SOLUTIONS
C
M10=A1
M20=A2
M30=A3

C
C   RE-RENORMALIZE THE AMPLITUDES
C
A1=A1*(DSQRT(B2*B3))
A2=A2*(DSQRT(B3*B1))
A3=A3*(DSQRT(B1*B2))
A11=A1
A21=A2
A31=A3
A111=A1

```

```

      A211=A2
      A311=A3
C
C      WRITE OUT INITIAL CONDITIONS
C
      J1=0.DO
      X=J1
      WRITE(3,60)X,A1,A2,A3
      WRITE(4,60)X,A11,A21,A31
      WRITE(7,60)X,A111,A211,A311
C
C      INITIALLY THE WAVES ARE EXCHANGING ENERGY WITH MAXIMUM EFFICIENCY
C
      PH1=0.DO
      PH2=0.DO
      PH3=0.DO
      PHI=0.DO
      PH21=0.DO
      PH22=0.DO
      PH23=0.DO
      PH21X=0.DO
      PH22X=0.DO
      PH23X=0.DO
      WRITE(66,60)X,PH21,PH22,PH23
      WRITE(67,60)X,PH21X,PH22X,PH23X
      WRITE(18,250)X,PHI

50     FORMAT(F7.3,1X,F11.8)
C
C      INITIALLY WE ARE IN A REGION OF NO TOPOGRAPHY (RISE=0)
C
      RUN=????
      RISE=????
      H1=RISE/RUN
      H=-1.DO*(RISE/RUN)*MUO
C
C      CALCULATE THE INITIAL CONSTANT OF MOTION
C
      GAMMA=M10*M20*M30*DSIN(PHI)-0.5DO*H*M20**2
C
C      CALCULATE DERIVATIVES OF PHI
C
      PH1X=0.DO
      PH2X=0.DO
      PH3X=0.DO
C
C      CALCULATE THE ROOTS OF THE CUBIC
C
      CALL CUBRT(EFF)
      IF (EFF .EQ. 1) THEN
        WRITE(6,5)
5      FORMAT( ' YOU HAVE COMPLEX ROOTS' )
        GO TO 99
      ENDIF
C
C      CALCULATE THE MODULUS OF THE ELLIPTIC FUNCTION
C

```

```

K=DSQRT((ROOT(1)-ROOT(2))/(ROOT(1)-ROOT(3)))
C
C   CALCULATE COMPLETE ELLIPTIC INTEGRAL
C
COMPIN=DELK1(K, EFF3)
IF (EFF3 .EQ. 0) THEN
  WRITE(6, 10) EFF3
10  FORMAT(' PROBLEM WITH COMPLETE ELLIP. INTG. ')
  GO TO 99
ENDIF

C
C   CALCULATE SN-1
C
THETA1=DASIN(DSQRT(ROOT(1)/(ROOT(1)-ROOT(2))))
THETA=DELLIF(K, THETA1, EFF1)
IF (EFF1 .EQ. 1 .OR. EFF1 .EQ. 2) THEN
  WRITE(6, 15) EFF1
15  FORMAT(' ERROR CALCULATING THETA', 1X, 'VALUE OF EFF1 IS', 1X, I2)
  GO TO 99
ENDIF

C
C   CALCULATE COMPLETE SOLUTION
C
WRITE(1, 60) X, PH1, PH2, PH3
WRITE(2, 60) X, PH1X, PH2X, PH3X
DO 20 I=1, 100
  J1=J1+1.00
  X1=(-1.00)*(J1/10.00)
  X=X1
  FIRST=0.00
  U1=(DSQRT(ROOT(1)-ROOT(3)))*(X1)+THETA

C
C   MAKE SURE THE ARGUMENT IS IN RANGE FOR SN CALCULATION
C
25  IF (U1 .GT. COMPIN) THEN
    U1 = U1-2.00*COMPIN
    GO TO 25
  ENDIF
  IF (U1 .LT. 0.00) THEN
    U1 = -1.00*U1
    GO TO 25
  ENDIF

C
C   CALCULATE SN SQUARED
C
CALL DJCBYF(U1, K, SN, CN, DN, EFF2, NN)
IF (EFF2 .EQ. 1 .OR. EFF2 .EQ. 2) THEN
  WRITE(6, 30) EFF2
30  FORMAT(' ERROR CALC. SN', 1X, 'VALUE OF EFF2 IS', 1X, I2)
  GO TO 99
ENDIF
SN2=SN*SN

C
C   CALCULATE Y
C
Y=(ROOT(2)-ROOT(1))*SN2+ROOT(1)

C
C   CALCULATE AMPLITUDES AND PHASE DERIVATIVES. THE M'S HOLD VALUES
C   OF THE AMPLITUDES USED TO CALC. ROOTS FOR NEXT TOPOGRAPHY AND TO
C   CALCULATE THE PHASE (PHI).

```



```

C
  A1=DSQRT(M10**2-Y)
  A2=DSQRT(M20**2+Y)
  A3=DSQRT(M30**2+Y)
  M1=A1
  M2=A2
  M3=A3
  P=DASIN((GAMMA+O.5DO*H*M2**2)/(M1*M2*M3))
  SP=(GAMMA+O.5DO*H*M2**2)/(M1*M2*M3)
  WRITE(18,250)X,P
  PH1X=(M1*M2*M3*SP)/(M1**2)
  PH2X=(-1.DO*M1*M2*M3*SP)/(M2**2)
  PH3X=(-1.DO*M1*M2*M3*SP)/(M3**2)
  WRITE(2,60)X,PH1X,PH2X,PH3X

C
C
C
  RE-RENORMALIZE THE AMPLITUDES

  A1=A1*(DSQRT(B2*B3))
  A2=A2*(DSQRT(B3*B1))
  A3=A3*(DSQRT(B1*B2))

C
C
C
  CALCULATE PHASES AND WAVES TIMES SLOW PHASE VARIATIONS

  CALL DQDAG(F1,FIRST,X1,ERRABS,ERRREL,IRULE,PH1,ERREST)
  CALL DQDAG(F2,FIRST,X1,ERRABS,ERRREL,IRULE,PH2,ERREST)
  CALL DQDAG(F3,FIRST,X1,ERRABS,ERRREL,IRULE,PH3,ERREST)
  WRITE(1,60)X,PH1,PH2,PH3
  A11=A1*DCOS(PH1)
  A21=A2*DCOS(PH2)
  A31=A3*DCOS(PH3)
  A111=A1*DCOS(PH1-H1*MU1*X)
  A211=A2*DCOS(PH2-H1*MU2*X)
  A311=A3*DCOS(PH3-H1*MU3*X)
  PH21=PH1-H1*MU1*X
  PH22=PH2-H1*MU2*X
  PH23=PH3-H1*MU3*X
  PH21X=PH1X-H1*MU1
  PH22X=PH2X-H1*MU2
  PH23X=PH3X-H1*MU3
  WRITE(66,60)X,PH21,PH22,PH23
  WRITE(67,60)X,PH21X,PH22X,PH23X

C
C
C
  WRITE OUT RESULTS

  WRITE(3,60)X,A1,A2,A3
  WRITE(4,60)X,A11,A21,A31
  WRITE(7,60)X,A111,A211,A311

20 CONTINUE
  M10=M1
  M20=M2
  M30=M3
  PH10=PH1
  PH20=PH2
  PH30=PH3

C
C
C
  WE NOW ARE IN A REGION OF TOPOGRAPHY (RISE=?)

  RUN=????
  RISE=????
  H1=-1.DO*(RISE/RUN)

```

```

H=(RISE/RUN)*MUO
C
C   CALCULATE THE NEW CONSTANT OF MOTION
C
GAMMA=M10*M20*M30*DSIN(P)-0.5DO*H*M20**2
C
C   CALCULATE THE ROOTS OF THE NEW CUBIC
C
CALL CUBRT(EFF)
IF (EFF .EQ. 1) THEN
  WRITE(6,5)
  GO TO 99
ENDIF

C
C   CALCULATE THE MODULUS OF THE ELLIPTIC FUNCTION
C
K=DSQRT((ROOT(1)-ROOT(2))/(ROOT(1)-ROOT(3)))
C
C   CALCULATE COMPLETE ELLIPTIC INTEGRAL
C
COMPIN=DELIK1(K,EFF3)
IF (EFF3 .EQ. 0) THEN
  WRITE(6,10)EFF3
  GO TO 99
ENDIF

C
C   CALCULATE SN-1
C
THETA1=DASIN(DSQRT(ROOT(1)/(ROOT(1)-ROOT(2))))
THETA=DELLIF(K,THETA1,EFF1)
IF (EFF1 .EQ. 1 .OR. EFF1 .EQ. 2) THEN
  WRITE(6,15)EFF1
  GO TO 99
ENDIF

C
C   CALCULATE COMPLETE SOLUTION
C
X2=X
J1=0.DO
DO 35 I=1,100
  J1=J1+1.DO
  X1=(-1.DO)*(J1/10.DO)
  X=X2+X1
  FIRST=0.DO
  U1=(DSQRT(ROOT(1)-ROOT(3)))*(X1)+THETA
C
C   MAKE SURE THE ARGUMENT IS IN RANGE FOR SN CALCULATION
C
26 IF (U1 .GT. COMPIN) THEN
  U1 = U1-2.DO*COMPIN
  GO TO 26
ENDIF
IF (U1 .LT. 0.DO) THEN
  U1 = -1.DO*U1
  GO TO 26
ENDIF

C
C   CALCULATE SN SQUARED AND Y
C
CALL DJCBYF(U1,K,SN,CN,DN,EFF2,NN)

```

```

IF (EFF2 .EQ. 1 .OR. EFF2 .EQ. 2) THEN
  WRITE(6,30)EFF2
  GO TO 99
ENDIF
SN2=SN*SN
Y=(ROOT(2)-ROOT(1))*SN2+ROOT(1)
C
C
C   CALCULATE AMPLITUDES AND PHASE DERIVATIVES
A1=DSQRT(M10**2-Y)
A2=DSQRT(M20**2+Y)
A3=DSQRT(M30**2+Y)
M1=A1
M2=A2
M3=A3
P=DASIN((GAMMA+O.5DO*H*M2**2)/(M1*M2*M3))
SP=(GAMMA+O.5DO*H*M2**2)/(M1*M2*M3)
WRITE(18,250)X,P
PH1X=(M1*M2**M3*SP)/(M1**2)
PH2X=(-1.DO*M1*M2*M3*SP)/(M2**2)
PH3X=(-1.DO*M1*M2*M3*SP)/(M3**2)
WRITE(2,60)X,PH1X,PH2X,PH3X
C
C
C   RE-NORMALIZE THE AMPLITUDES
A1=A1*(DSQRT(B2*B3))
A2=A2*(DSQRT(B3*B1))
A3=A3*(DSQRT(B1*B2))
C
C
C   CALCULATE PHASES AND WAVES TIMES SLOW PHASE VARIATIONS
CALL DQDAG(F1,FIRST,X1,ERRABS,ERRREL,IRULE,PH1,ERREST)
CALL DQDAG(F2,FIRST,X1,ERRABS,ERRREL,IRULE,PH2,ERREST)
CALL DQDAG(F3,FIRST,X1,ERRABS,ERRREL,IRULE,PH3,ERREST)
PH1=PH1+PH10
PH2=PH2+PH20
PH3=PH3+PH30
WRITE(1,60)X,PH1,PH2,PH3
A11=A1*DCOS(PH1)
A21=A2*DCOS(PH2)
A31=A3*DCOS(PH3)
A111=A1*DCOS(PH1-H1*MU1*X1)
A211=A2*DCOS(PH2-H1*MU2*X1)
A311=A3*DCOS(PH3-H1*MU3*X1)
PH21=PH1-H1*MU1*X1
PH22=PH2-H1*MU2*X1
PH23=PH3-H1*MU3*X1
PH21X=PH1X-H1*MU1
PH22X=PH2X-H1*MU2
PH23X=PH3X-H1*MU3
WRITE(66,60)X,PH21,PH22,PH23
WRITE(67,60)X,PH21X,PH22X,PH23X
C
C
C   WRITE OUT RESULTS
WRITE(3,60)X,A1,A2,A3
WRITE(4,60)X,A11,A21,A31
WRITE(7,60)X,A111,A211,A311
35 CONTINUE
M10=M1

```

```

M20=M2
M30=M3
PH10=PH1
PH20=PH2
PH30=PH3
C
C   WE NOW ARE IN ANOTHER REGION OF TOPOGRAPHY (RISE=?)
C
RUN=????
RISE=????
H1=RISE/RUN
H=(-1.DO)*(RISE/RUN)*MUO
C
C   CALCULATE THE NEW CONSTANT OF MOTION
C
GAMMA=M10*M20*M30*DSIN(P)-O.5DO*H*M20**2
C
C   CALCULATE THE ROOTS OF THE NEW CUBIC
C
CALL CUBRT(EFF)
IF (EFF .EQ. 1) THEN
  WRITE(6,5)
  GO TO 99
ENDIF
C
C   CALCULATE THE MODULUS OF THE ELLIPTIC FUNCTION
C
K=DSQRT((ROOT(1)-ROOT(2))/(ROOT(1)-ROOT(3)))
C
C   CALCULATE COMPLETE ELLIPTIC INTEGRAL
C
COMPIN=DELIK1(K,EFF3)
IF (EFF3 .EQ. 0) THEN
  WRITE(6,10)EFF3
  GO TO 99
ENDIF
C
C   CALCULATE SN-1
C
THETA1=DASIN(DSQRT(ROOT(1)/(ROOT(1)-ROOT(2))))
THETA=DELLIF(K,THETA1,EFF1)
IF (EFF1 .EQ. 1 .OR. EFF1 .EQ. 2) THEN
  WRITE(6,15)EFF1
  GO TO 99
ENDIF
C
C   CALCULATE COMPLETE SOLUTION
C
X3=X
J1=O.DO
DO 40 I=1,100
  J1=J1+1.DO
  X1=(-1.DO)*(J1/10.DO)
  X=X3+X1
  J4=(10.DO+X1)
  FIRST=O.DO
  U1=(DSQRT(ROOT(1)-ROOT(3)))*(X1)+THETA
C
C   MAKE SURE THE ARGUMENT IS IN RANGE FOR SN CALCULATION
C

```

```

27   IF (U1 .GT. COMPIN)THEN
      U1 = U1-2.DO*COMPIN
      GO TO 27
    ENDIF
    IF (U1 .LT. O.DO)THEN
      U1 = -1.DO*U1
      GO TO 27
    ENDIF

C
C   CALCULATE SN SQUARED AND Y
C
CALL DJCBYF(U1,K,SN,CN,DN,EFF2,NN)
IF (EFF2 .EQ. 1 .OR. EFF2 .EQ. 2) THEN
  WRITE(6,30)EFF2
  GO TO 99
ENDIF
SN2=SN*SN
Y=(ROOT(2)-ROOT(1))*SN2+ROOT(1)

C
C   CALCULATE AMPLITUDES AND PHASE DERIVATIVES
C
A1=DSQRT(M10**2-Y)
A2=DSQRT(M20**2+Y)
A3=DSQRT(M30**2+Y)
M1=A1
M2=A2
M3=A3
P=DASIN((GAMMA+O.5DO*H*M2**2)/(M1*M2*M3))
SP=(GAMMA+O.5DO*H*M2**2)/(M1*M2*M3)
WRITE(18,250)X,P
PH1X=(M1*M2*M3*SP)/(M1**2)
PH2X=(-1.DO*M1*M2*M3*SP)/(M2**2)
PH3X=(-1.DO*M1*M2*M3*SP)/(M3**2)
WRITE(2,60)X,PH1X,PH2X,PH3X

C
C   RE-NORMALIZE THE AMPLITUDES
C
A1=A1*(DSQRT(B2*B3))
A2=A2*(DSQRT(B3*B1))
A3=A3*(DSQRT(B1*B2))

C
C   CALCULATE PHASES AND WAVES TIMES SLOW PHASE VARIATIONS
C
CALL DQDAG(F1,FIRST,X1,ERRABS,ERRREL,IRULE,PH1,ERREST)
CALL DQDAG(F2,FIRST,X1,ERRABS,ERRREL,IRULE,PH2,ERREST)
CALL DQDAG(F3,FIRST,X1,ERRABS,ERRREL,IRULE,PH3,ERREST)
PH1=PH1+PH10
PH2=PH2+PH20
PH3=PH3+PH30
WRITE(1,60)X,PH1,PH2,PH3
A11=A1*DCOS(PH1)
A21=A2*DCOS(PH2)
A31=A3*DCOS(PH3)
A111=A1*DCOS(PH1-H1*MU1*J4)
A211=A2*DCOS(PH2-H1*MU2*J4)
A311=A3*DCOS(PH3-H1*MU3*J4)
PH21=PH1-H1*MU1*J4
PH22=PH2-H1*MU2*J4
PH23=PH3-H1*MU3*J4
PH21X=PH1X-H1*MU1

```

```

PH22X=PH2X-H1*MU2
PH23X=PH3X-H1*MU3
WRITE(66.60)X,PH21,PH22,PH23
WRITE(67.60)X,PH21X,PH22X,PH23X
C
C   WRITE OUT RESULTS
C
WRITE(3.60)X,A1,A2,A3
WRITE(4.60)X,A11,A21,A31
WRITE(7.60)X,A111,A211,A311
40 CONTINUE
M1O=M1
M2O=M2
M3O=M3
PH1O=PH1
PH2O=PH2
PH3O=PH3
COUNT=0.DO
C
C   WE NOW ARE IN A REGION OF NO TOPOGRAPHY (RISE=0)
C
RUN=????
RISE=????
H1=RISE/RUN
H=-1.DO*(RISE/RUN)*MUO
C
C   CALCULATE THE NEW CONSTANT OF MOTION
C
GAMMA=M1O*M2O*M3O*DSIN(P)-0.5DO*H*M2O**2
C
C   CALCULATE THE ROOTS OF THE NEW CUBIC
C
CALL CUBRT(EFF)
IF (EFF .EQ. 1) THEN
WRITE(6,5)
GO TO 99
ENDIF
C
C   CALCULATE THE MODULUS OF THE ELLIPTIC FUNCTION
C
K=DSORT((ROOT(1)-ROOT(2))/(ROOT(1)-ROOT(3)))
C
C   CALCULATE COMPLETE ELLIPTIC INTEGRAL
C
COMPIN=DELIK1(K,EFF3)
IF (EFF3 .EQ. 0)THEN
WRITE(6,10)EFF3
GO TO 99
ENDIF
C
C   CALCULATE SN-1
C
THETA1=DASIN(DSORT(ROOT(1)/(ROOT(1)-ROOT(2))))
THETA=DELLIF(K,THETA1,EFF1)
IF (EFF1 .EQ. 1 .OR. EFF1 .EQ. 2) THEN
WRITE(6,15)EFF1
GO TO 99
ENDIF
C
C   CALCULATE COMPLETE SOLUTION

```

```

C
X4=X
J1=0.DO
DO 45 I=1,200
  J1=J1+1.DO
  X1=(-1.DO)*(J1/10.DO)
  X=X4+X1
  FIRST=0.DO
  U1=(DSQRT(ROOT(1)-ROOT(3)))*(X1)+THETA
C
C   MAKE SURE THE ARGUMENT IS IN RANGE FOR SN CALCULATION
C
28  IF (U1 .GT. COMPIN)THEN
    U1 = U1-2.DO*COMPIN
    GO TO 28
  ENDIF
  IF (U1 .LT. 0.DO)THEN
    U1 = -1.DO*U1
    GO TO 28
  ENDIF
C
C   CALCULATE SN SQUARED AND Y
C
CALL DJCBYF(U1,K,SN,CN,DN,EFF2,NN)
IF (EFF2 .EQ. 1 .OR. EFF2 .EQ. 2) THEN
  WRITE(6,30)EFF2
  GO TO 99
ENDIF
SN2=SN*SN
Y=(ROOT(2)-ROOT(1))*SN2+ROOT(1)
C
C   CALCULATE AMPLITUDES AND PHASE DERIVATIVES
C
A1=DSQRT(M1O**2-Y)
A2=DSQRT(M2O**2+Y)
A3=DSQRT(M3O**2+Y)
M1=A1
M2=A2
M3=A3
P=DASIN((GAMMA+O.5DO*H*M2**2)/(M1*M2*M3))
SP=(GAMMA+O.5DO*H*M2**2)/(M1*M2*M3)
WRITE(18,250)X,P
PH1X=(M1*M2*M3*SP)/(M1**2)
PH2X=(-1.DO*M1*M2*M3*SP)/(M2**2)
PH3X=(-1.DO*M1*M2*M3*SP)/(M3**2)
C   WRITE(6,60)X,GAMMA,P,SP
C   WRITE(2,60)X,PH1X,PH2X,PH3X
C
C   RE-NORMALIZE THE AMPLITUDES
C
A1=A1*(DSQRT(B2*B3))
A2=A2*(DSQRT(B3*B1))
A3=A3*(DSQRT(B1*B2))
C
C   CALCULATE PHASES AND WAVES TIMES SLOW PHASE VARIATIONS
C
CALL DQDAG(F1,FIRST,X1,ERRABS,ERRREL,IRULE,PH1,ERREST)
CALL DQDAG(F2,FIRST,X1,ERRABS,ERRREL,IRULE,PH2,ERREST)
CALL DQDAG(F3,FIRST,X1,ERRABS,ERRREL,IRULE,PH3,ERREST)
PH1=PH1+PH1O

```

```

PH2=PH2+PH2O
PH3=PH3+PH3O
WRITE(1,60)X,PH1,PH2,PH3
A11=A1*DCOS(PH1)
A21=A2*DCOS(PH2)
A31=A3*DCOS(PH3)
A111=A1*DCOS(PH1-H1*MU1*X)
A211=A2*DCOS(PH2-H1*MU2*X)
A311=A3*DCOS(PH3-H1*MU3*X)
PH21=PH1-H1*MU1*X
PH22=PH2-H1*MU2*X
PH23=PH3-H1*MU3*X
PH21X=PH1X-H1*MU1
PH22X=PH2X-H1*MU2
PH23X=PH3X-H1*MU3
WRITE(66,60)X,PH21,PH22,PH23
WRITE(67,60)X,PH21X,PH22X,PH23X
C
C   WRITE OUT RESULTS
C
WRITE(3,60)X,A1,A2,A3
WRITE(4,60)X,A11,A21,A31
WRITE(7,60)X,A111,A211,A311
45 CONTINUE
M1O=M1
M2O=M2
M3O=M3
PH1O=PH1
PH2O=PH2
PH3O=PH3
C
60 FORMAT(F7.3,3(1X,F14.8))
C
99 STOP
END
C
SUBROUTINE WAVNUM(KAPA2,PHI2,PHINT,MUO,K1,K2,K3,
&L1,L2,L3,MU1,MU2,MU3,EFF4)
C
C   FIND A WAVE TRIPLET BASED ON LONGUET-HIGGINS AND GILL
C   PAPER (1967). USE THE WAVE TRIPLET TO CALCULATE
C   INTERACTION COEFFICIENTS AND TOPOGRAPHY TERMS.
C
INTEGER EFF4
COMMON /COM1/ H,GAMMA,ROOT(3),K,COMPIN,THETA,M1O,M2O,M3O,
&B1,B2,B3
DOUBLE PRECISION PI,KAPAO,KAPA2,KO,K1,K2,K3,LO,L1,L2,L3,A2
&,ALPHA,PHIPM,PHINT,PHI2,B,A,A1,C1,C2,C3,B1,B2,B3,W1,W2,W3,
&MUO,MU1,MU2,MU3,WO,H,GAMMA,ROOT,K,COMPIN,THETA,M1O,M2O,M3O
C
C   NOTE: PHI2 CANNOT BE EQUAL TO --(90) DEGREES.
C
PI= DACOS(-1.DO)
C
C   CONVERT PHI2 AND PHINT TO RADIANS
C
PHI2 = (PI*PHI2)/180.DO
PHINT = (PI*PHINT)/180.DO
C
C   CALCULATE P/ARAMETERS

```



```

C
  PHIPM = PHINT - PHI2
  A = (-1.DO)*((2.DO+2.DO*KAPA2**2)*DTAN(PHI2))
  A1 = 2.DO + KAPA2**2
  A2 = A/A1
  ALPHA = (0.500)*DATAN(A2)
  B = 4.DO+(2.DO+KAPA2**2)*DCOS(2.DO*(PHIPM-ALPHA))/DCOS(2.DO*AL
&PHA)
  KAPAO = DSQRT(-B+DSQRT(B**2+3.DO*(KAPA2**4+4.DO*KAPA2**2)))
C
C
  CALCULATE WAVENUMBERS
C
  KO = KAPAO*DCOS(PHINT)
  LO = KAPAO*DSIN(PHINT)
  K2 = KAPA2*DCOS(PHI2)
  L2 = KAPA2*DSIN(PHI2)
  K1 = (-0.500*K2) + (0.500*KO)
  L1 = (-0.500*L2) + (0.500*LO)
  K3 = (-0.500*K2) - (0.500*KO)
  L3 = (-0.500*L2) - (0.500*LO)
C
C
  CALCULATE GROUP VELOCITY OF EACH WAVE
C
  C1=(K1**2-L1**2-1.DO)/((K1**2+L1**2+1.DO)**2)
  C2=(K2**2-L2**2-1.DO)/((K2**2+L2**2+1.DO)**2)
  C3=(K3**2-L3**2-1.DO)/((K3**2+L3**2+1.DO)**2)
C
C
  CALCULATE FREQUENCY OF EACH WAVE
C
  W1=-K1/(K1**2+L1**2+1.DO)
  W2=-K2/(K2**2+L2**2+1.DO)
  W3=-K3/(K3**2+L3**2+1.DO)
C
C
  CALCULATE INTERACTION COEFFICIENT OF EACH WAVE
C
  B1=((K2*L3-K3*L2)*(K2**2+L2**2-K3**2-L3**2))/(K1**2+L1**2+
&1.DO)
  B2=((K3*L1-K1*L3)*(K3**2+L3**2-K1**2-L1**2))/(K2**2+L2**2+
&1.DO)
  B3=((K1*L2-K2*L1)*(K1**2+L1**2-K2**2-L2**2))/(K3**2+L3**2+
&1.DO)
  B1 = (-1.DO)*B1
  B2 = (-1.DO)*B2
  B3 = (-1.DO)*B3
  B1 = B1/C1
  B2 = B2/C2
  B3 = B3/C3
C
C
  CALCULATE TOPOGRAPHY TERMS
C
  MU1=L1/((K1**2+L1**2+1.DO)*C1)
  MU2=L2/((K2**2+L2**2+1.DO)*C2)
  MU3=L3/((K3**2+L3**2+1.DO)*C3)
  MUO=MU1+MU2+MU3
C
C
  DO SOME CHECKING TO INSURE WE HAVE A GOOD TRIAD
C
  EFF4=0
  WRITE(6,11)K1,L1,W1,B1,MUO,MU1
11  FORMAT(6(2X,F10.7))

```

```

      WRITE(6,21)K2,L2,W2,B2,MUO,MU2
21  FORMAT(6(2X,F10.7))
      WRITE(6,31)K3,L3,W3,B3,MUO,MU3
31  FORMAT(6(2X,F10.7))
      IF(B1 .GE. 0.DO)THEN
      WRITE(6,20)
20  FORMAT( 'B1 IS GREATER THAN OR EQUAL TO ZERO')
      EFF4=1
      RETURN
      ENDIF
      IF(B2 .LE. 0.DO .OR. B3 .LE. 0.DO)THEN
      EFF4=1
      WRITE(6,30)
30  FORMAT( 'B2 OR B3 IS LESS THAN OR EQUAL TO ZERO')
      RETURN
      ENDIF
      RETURN
      END

C
C
      SUBROUTINE CUBRT(EFF)
C
C      A SUBROUTINE TO CALCULATE CUBERROOTS
C
      COMMON /COM1/ H,GAMMA,ROOT(3),K,COMPIN,THETA,M10,M20,M30,
&B1,B2,B3
      INTEGER EFF
      DOUBLE PRECISION A,B,P,Q,R,TEST,M,THET,PI,S,H,GAMMA,ROOT,K
      DOUBLE PRECISION COMPIN,THETA,M10,M20,M30,B1,B2,B3

C
      S=-1.DO
      V1=M10**2
      V2=M20**2
      V3=M30**2

C
C      CALCULATE P,Q,R COEFFICIENTS FROM CUBIC IN THESIS
C
      P=-1.DO*(V1+S*V3+S*V2-(H**2/4.DO))
      Q=-1.DO*(V1*V3+V1*V2+S*V2**2*V3-GAMMA*H-(H**2/2.DO)*V2)
      R=GAMMA**2-V1*V2*V3+GAMMA*H*V2+(H**2/4.DO)*V2**2

C
C      BEGIN PROCESS OF CALCULATING ROOTS
C
      PI = DACOS(-1.DO)
      A = (3.DO*Q - P**2)/3.DO
      B = (2.DO*P**3 - 9.DO*P*Q + 27.DO*R)/27.DO
      TEST = (B**2)/4.DO + (A**3)/27.DO
      IF (TEST .GT. 0.DO) THEN
      EFF=1
      RETURN
      ENDIF
      M = 2.DO * DSQRT((-A)/3.DO)
      THET = (DACOS((3.DO*B)/(A*M)))/3.DO
      ROOT(1) = M*DCOS(THET) - P/3
      ROOT(2) = M*DCOS(THET + 2.DO*PI/3.DO) - P/3
      ROOT(3) = M*DCOS(THET + 4.DO*PI/3.DO) - P/3
      CALL SORT
      RETURN
      END
C

```

```

C
C      SUBROUTINE SORT
C
C      A SUBROUTINE TO SORT ROOTS IN DESCENDING ORDER
C
COMMON /COM1/ H,GAMMA,ROOT(3),K,COMPIN,THETA,M10,M20,M30,
&B1,B2,B3
DOUBLE PRECISION TEMP,H,GAMMA,ROOT,K,COMPIN,THETA
DOUBLE PRECISION B1,B2,B3,M10,M20,M30
INTEGER INDEX,COUNT
LOGICAL SORTED
COUNT = 3
SORTED = .FALSE.
32 IF (SORTED) GO TO 39
SORTED = .TRUE.
DO 34 INDEX=1,COUNT-1
  IF (ROOT(INDEX) .LT. ROOT(INDEX+1)) THEN
    TEMP = ROOT(INDEX)
    ROOT(INDEX) = ROOT(INDEX+1)
    ROOT(INDEX+1) = TEMP
    SORTED = .FALSE.
  ENDIF
34 CONTINUE
GO TO 32
39 CONTINUE
RETURN
END

C
C
C      DOUBLE PRECISION FUNCTION F1(X)
C
C      A FUNCTION TO BE NUMERICALLY INTEGRATED TO CALCULATE PHI 1
C
COMMON /COM1/ H,GAMMA,ROOT(3),K,COMPIN,THETA,M10,M20,M30,
&B1,B2,B3
DOUBLE PRECISION X,U1,Y,SN,DN,CN,SN2,A1,A2,A3,NN,PHASE
DOUBLE PRECISION H,GAMMA,ROOT,K,COMPIN,THETA,M10,M20,M30
DOUBLE PRECISION B1,B2,B3,SINP
INTEGER EFF2
U1=(DSQRT(ROOT(1)-ROOT(3)))*(X)+THETA

C
C      MAKE SURE THE ARGUMENT IS IN RANGE FOR SN CALCULATION
C
29 IF (U1 .GT. COMPIN)THEN
  U1 = U1-2.DO*COMPIN
  GO TO 29
ENDIF
IF (U1 .LT. 0.DO)THEN
  U1 = -1.DO*U1
  GO TO 29
ENDIF

C
C      CALCULATE SN SQUARED
C
CALL DJCBYF(U1,K,SN,CN,DN,EFF2,NN)
IF (EFF2 .EQ. 1 .OR. EFF2 .EQ. 2) THEN
  WRITE(6,30)EFF2
30 FORMAT(' ERROR CALC. SN IN F1',1X,'VALUE OF EFF2 IS',1X,12)
ENDIF
SN2=SN*SN

```

```

C
C   CALCULATE Y
C
Y=(ROOT(2)-ROOT(1))*SN2+ROOT(1)
C
C   CALCULATE AMPLITUDES AND PHASE. THE M'S HOLD VALUES OF THE
C   AMPLITUDES USED TO CALC. ROOTS FOR NEXT TOPOGRAPHY AND TO
C   CALCULATE THE PHASE
C
A1=DSQRT(M10**2-Y)
A2=DSQRT(M20**2+Y)
A3=DSQRT(M30**2+Y)
SINP=(GAMMA+O.5DO*H*A2**2)/(A1*A2*A3)
C
F1=(A1*A2*A3*SINP)/(A1**2)
RETURN
END
C
C
DOUBLE PRECISION FUNCTION F2(X)
C
C   A FUNCTION TO BE NUMERICALLY INTEGRATED TO CALCULATE PHI2
C
COMMON /COM1/ H,GAMMA,ROOT(3),K,COMPIN,THETA,M10,M20,M30,
&B1,B2,B3
DOUBLE PRECISION X,U1,Y,SN,DN,CN,SN2,A1,A2,A3,PHASE,NN
DOUBLE PRECISION H,GAMMA,ROOT,K,COMPIN,THETA,M10,M20,M30
DOUBLE PRECISION B1,B2,B3,SINP
INTEGER EFF2
U1=(DSQRT(ROOT(1)-ROOT(3)))*(X)+THETA
C
C   MAKE SURE THE ARGUMENT IS IN RANGE FOR SN CALCULATION
C
31 IF (U1 .GT. COMPIN)THEN
    U1 = U1-2.DO*COMPIN
    GO TO 31
ENDIF
IF (U1 .LT. O.DO)THEN
    U1 = -1.DO*U1
    GO TO 31
ENDIF
C
C   CALCULATE SN SQUARED
C
CALL DJCBYF(U1,K,SN,CN,DN,EFF2,NN)
IF (EFF2 .EQ. 1 .OR. EFF2 .EQ. 2) THEN
    WRITE(6,30)EFF2
30  FORMAT(' ERROR CALC. SN IN F2',1X,'VALUE OF EFF2 IS',1X,12)
ENDIF
SN2=SN*SN
C
C   CALCULATE Y
C
Y=(ROOT(2)-ROOT(1))*SN2+ROOT(1)
C
C   CALCULATE AMPLITUDES AND PHASE. THE M'S HOLD VALUES OF THE
C   AMPLITUDES USED TO CALC. ROOTS FOR NEXT TOPOGRAPHY AND TO
C   CALCULATE THE PHASE
C
A1=DSQRT(M10**2-Y)

```

```

      A2=DSQRT(M20**2+Y)
      A3=DSQRT(M30**2+Y)
      SINP=(GAMMA+O.5DO*H*A2**2)/(A1*A2*A3)
C
      F2=(-1.DO*A1*A2*A3*SINP)/(A2**2)
      RETURN
      END
C
C
      DOUBLE PRECISION FUNCTION F3(X)
C
C      A FUNCTION TO BE NUMERICALLY INTEGRATED TO CALCULATE PHI3
C
      COMMON /COM1/ H,GAMMA,ROOT(3),K,COMPIN,THETA,M10,M20,M30,
&B1,B2,B3
      DOUBLE PRECISION X,U1,Y,SN,DN,CN,SN2,A1,A2,A3,PHASE,NN
      DOUBLE PRECISION H,GAMMA,ROOT,K,COMPIN,THETA,M10,M20,M30
      DOUBLE PRECISION B1,B2,B3,SINP
      INTEGER EFF2
      U1=(DSQRT(ROOT(1)-ROOT(3)))*(X)+THETA
C
C      MAKE SURE THE ARGUMENT IS IN RANGE FOR SN CALCULATION
C
      32 IF (U1 .GT. COMPIN)THEN
          U1 = U1-2.DO*COMPIN
          GO TO 32
        ENDIF
      IF (U1 .LT. O.DO)THEN
          U1 = -1.DO*U1
          GO TO 32
        ENDIF
C
C      CALCULATE SN SQUARED
C
      CALL DJCBYF(U1,K,SN,CN,DN,EFF2,NN)
      IF (EFF2 .EQ. 1 .OR. EFF2 .EQ. 2) THEN
        WRITE(6,30)EFF2
      30 FORMAT(' ERROR CALC. SN IN F3',1X,'VALUE OF EFF2 IS',1X,12)
      ENDIF
      SN2=SN*SN
C
C      CALCULATE Y
C
      Y=(ROOT(2)-ROOT(1))*SN2+ROOT(1)
C
C      CALCULATE AMPLITUDES AND PHASE. THE M'S HOLD VALUES OF THE
      AMPLITUDES USED TO CALC. ROOTS FOR NEXT TOPOGRAPHY AND TO
      CALCULATE THE PHASE
C
      A1=DSQRT(M10**2-Y)
      A2=DSQRT(M20**2+Y)
      A3=DSQRT(M30**2+Y)
      SINP=(GAMMA+O.5DO*H*A2**2)/(A1*A2*A3)
C
      F3=(-1.DO*A1*A2*A3*SINP)/(A3**2)
      RETURN
      END

```